Characterization of insulin receptor and insulin like growth factor 1 receptor deficient mice

Inaugural-Dissertation

zur

Erlangung des Doktorgrades

Der Mathematisch -Naturwissenschaftlichen Fakultät

Der Universität zu Köln

vorgelegt von Fabian Schütte

aus Hattingen a.d. Ruhr

Köln 2012

Berichterstatter: Prof. Dr. Jens C. Brüning

Prof. Dr. F. Thomas Wunderlich

Tag der mündlichen Prüfung: 21.05.2012

Table of contents

Figure index

Table index

Abbreviations

°C	degrees Celsius
µ	micro
3’	three prime end of DNA sequences
5’	five prime end of DNA sequences
5’dNeo	truncated neomycin resistance gene
A	adenosine
ADP	adenosine diphosphate
AKT	proteinkinase B
ANOVA	analysis of variance
as	antisense
ATG	start codon
ATP	adenosine triphosphate
BAT	brown adipose tissue
BSA	bovine serum albumin
bp	base pair
C	cytosine
Caggs	chicken β-actin-promoter with cytomegalovirus enhancer
cDNA	complementary DNA
CO_2	carbon dioxide
Col1a1	collagen, type I, alpha 1
Cre	site specific recombinase from phage P1
Ct	cycle treshold
Da	Dalton
ddH2O	double destilled water
dsRNA	double stranded RNA
DMEM	Dulbecco's Modification of Eagle's Medium
DMSO	dimethylsulfoxide
DNA	desoxyribonucleic acid
DNase	desoxyribonuclease
dNTP	desoxyribonucleotide-triphosphate
dox	doxycycline
dsRNA	double stranded RNA
DTT	dithiothreitol
E.coli	Escherichia coli
e.g.	exempli gratia
EDTA	ethylendiamine tetraacetate
Egln1	EGL nine homolog 1

ELISA	enzyme-linked immunosorbent assay
ES cells	embryonic stem cells
EtBr	ethidium bromide
EtOH	ethanol
EWAT	epigonadal white adipose tissue
FCS	fetal calf serum
FFA	free fatty acid
Fig	figure
floxed	loxP flanked
Flp	flippase
FRT	flip-recombinase targets
g	gram
G	guanine
G418	geneticin
Glc-6-Pase	Glucose 6-phosphatase
Gab	growth factor receptor bound protein 2 associated binder
GDP	Guanosine-5'-diphosphate
GenTGS	Gesetz zur Regelung der Gentechnik
GIP	gastric inhibitory polypeptide
GLP-1	glucagon-like-peptide-1
GLUT2	glucose transporter type 2
GLUT4	glucose transporter type 4
GOI	gene of interest
Grb2	growth factor receptor bound protein 2
GTP	guanosine-5'-triphosphate
GTT	glucose tolerance test
h	hour
H&E	hematoxylin/eosin
HCl	hydrochloric acid
HEPES	N-2-hydroxyethylpiperazine-N'-2-ethansulfonic acid
Hp1bp3	heterochromatin protein1 binding protein3
Hprt	hypoxanthine-guanine phosphoribosyltransferase
HSL	hormone-sensitive lipase
HTGL	hepatic triglyceride lipase
Hyg	hygromycin resistance gene
Hz	Hertz
IGF1	insulin like growth factor 1
IGF1R	insulin like growth factor 1 receptor
IGFBP	insulin like growth factor 1 binding protein
IGFBP-rP	insulin like growth factor 1 binding protein related proteins
loxP	locus of crossover in P1
i.p.	intraperitoneal
IPS	impulse per second
IR	insulin receptor

IRS	insulin receptor substrate
ITT	insulin tolerance test
k	kilo
kb	kilobase pairs
KCl	potassium chloride
KD	knock down
KO	knockout
l	liter
LB	Lysogeny Broth
lacZ	gene encoding the enzyme beta-galactosidase
loxP	recognition sequence for Cre (locus of x-ing over phage P1)
LPL	lipoprotein lipase
m	milli
M	molar
MAPK	mitogen-activated protein kinase
MAP2K	mitogen-activated protein kinase kinase
MEM	Modified Eagle Media
$MgCl_2$	magnesium chloride
$MgSO_4$	magnesium sulfate
min	minute
miRNA	micro RNA
mRNA	messenger RNA
NaCl	sodium chloride
Na_2HPO_4	Sodium pyrophosphate
NaOH	sodium hydroxide
Neo	neomycin resistance gene
NMR	nuclear magnetic resonance
nt	nucleotide
OD	optical density
ORF	open reading frame
PAGE	polyacrylamid gel electrophoresis
pA	poly adenylation signal
PB	phosphate buffer
PBS	phosphate buffered saline
PCK1	Phosphoenolpyruvate carboxykinase 1
PCR	polymerase chain reaction
PGK	phosphoglycerate kinase
PI3K	phospatidylinisitol-3-kinase
PIP_2	phosphatinositol-4,5-bisphosphate
PIP_3	phosphatinositol-3,4,5-triphosphate
Pol II	RNA polymerase II
Pol III	RNA polymerase III
Puro	puromycin resistance gene
qPCR	quantitative realtime PCR

R26	Rosa26
RISC	RNA-induced silencing complex
Ras	rat sarcoma protein
RMCE	recombinase mediated cassette exchange
RNA	ribonucleic acid
RNAi	RNA interference
RNase	ribonuclease
rpm	revolutions per minute
RT	room temperature
s	sense
SA	splice acceptor site
SDS	sodiumdodecylsulfate
sec	second
SEM	standard error of the mean
Ser	serine
Shc	Src Homology 2-containing protein
shRNA	short hairpin RNA
siRNA	short interfering RNA
SOS	Son of Sevenless
SDS	saline-sodium citrate
T2DM	type 2 diabetes mellitus
TAE	Tris-acetic EDTA buffer
TBS	Tris buffered saline
tetO	tetracycline operator
tetR	tetracycline repressor
Tris	2-amino-2-(hydroxymethyl-)1,3-propandiole
Tyr	tyrosine
U	units
UTR	un-translated region
V	Volt
v/v	volume per volume
w/v	weight per volume
wt	wild type
Zsgreen	Zoanthus sp. green fluorescent protein

1 Introduction

1.1 Diabetes mellitus type 2

Diabetes mellitus comprises a group of chronic diseases, affecting about 346 million people worldwide. Over the last decades, the number of patients suffering from diabetes mellitus have drastically increased and are expected to tend to 440 million in the year 2030 (1). Diabetes mellitus is characterized by deregulation of glucose homeostasis. The hormone Insulin, released from pancreatic β-cells in response to food intake, plays a central role in the etiology of diabetes. Under non-pathogenic conditions, insulin maintains glucose homeostasis by stimulation of glucose uptake from the circulation into insulin target tissues (for review see (2)). Among the described forms of the disease type 2 diabetes mellitus (T2DM) is the most common, comprising about 90% of diabetes cases (3). T2DM is characterized by the development of insulin resistance in insulin target tissues as well as insulin secretory dysfunction (for review see (3-5)). The development of insulin resistance is a rather slow process, accompanied by an initial compensatory rising, but finally discontinued, insulin secretion (6). The incapability to respond to insulin results in hyperglycemia, i.e. elevated blood glucose levels, a characteristic indication of T2DM (for review see (7)). Further common symptoms are loss of weight, fatigue and polyuria (for review see (8,9)). Untreated T2DM may lead to serious acute complications, like diabetic ketoacidosis and diabetic hyperglycemic hyperosmolar coma, both leading to death (10-12). Long-term complications include the development of neuro-, angio-, nephro, and retinopathy and increased risk of cardiovascular diseases and strokes (10-12). The emergence of T2DM is strongly positively correlated with obesity and reduced physical activity, but genetic predispositions are assumed to be an important factor as well. (13-15). To date, the exact molecular mechanisms leading to the development of insulin resistance remain to be elucidated. Nonetheless, it has been suggested that both insulin resistance and β-cell dysfunction are induced by the enhanced release of free fatty acids (FFA) and pro-inflammatory mediators from the adipose tissue during the course of obesity (16-18). As diabetes emerges from a severe malfunction of

insulin signaling, detailed investigation of it´s function and interaction with related pathways is of central importance for a deeper understanding of this disease and subsequent improvement of treatment strategies.

1.2 The Insulin signaling system

1.2.1 Biological functions of the insulin signaling system

Signaling through insulin is considered to be the major regulatory mechanism of glucose and energy homeostasis. Insulin is a peptide hormone released by the β-cells of the pancreatic islets of Langerhans mainly in response to high levels of blood glucose, amino acids and lipids after food ingestion (19-23).

In its target tissues, particularly skeletal muscle, adipose tissue and liver, insulin regulates diverse processes involved in glucose uptake and metabolism. Broadly spoken, insulin is a signal to occupy externally supplied energy substrates instead of utilizing stored energy reserves. Insulin promotes the uptake of glucose in muscle and adipose tissue via translocation of the insulin responsive glucose transporter 4 (GLUT4) to the plasma membrane and stimulates glucose catabolism via glycolysis (24-26). Furthermore, insulin promotes the storage of substrates for energy metabolism by activating glycogen synthesis in liver, lipogenesis in adipose tissue and protein synthesis in muscle. On the other hand insulin inhibits the opponent processes, lipolysis, glycogenolysis and protein degradation (for review see (27)). Aside from its role in peripheral glucose homeostasis, insulin has been shown to reduce food intake via the central nervous system by acting on the hypothalamus (28-29). In addition to the acute effects of insulin on energy homestasis, it acts as a common growth factor by modulating mitosis and differentiation (for review see (27, 30)).

1.2.2 Insulin, structure and release

Insulin consists of two peptides, A- and B- chains, cleaved from a single precursor, proinsulin (31). Serum Insulin concentration is predominantly controlled through the release and not *de novo* synthesis of insulin (32-33). The most important acute signal leading to secretion of insulin from the β-cells is a rise in blood glucose level above a specific threshold (34, 35). β-cells absorb glucose via facilitated diffusion through glucose transporter GLUT2 (36, 37). Metabolism of absorbed glucose is subsequently leading to the release of insulin from secretory vesicles into the blood stream (for review see (38)). Beside glucose, increasing plasma levels of amino acids, lipids, Glucagon-like-peptide-1 (GLP-1) and Gastric inhibitory polypeptide (GIP), gastrointestinal hormones released after food intake (39, 40), and stimulation of the parasympathetic nervous system (for review see (41)) trigger the release of insulin.

1.2.3 Insulin receptor and post receptor signaling

The gateway to transmit the signal of circulating insulin into target tissue cells is the insulin receptor (IR). IR belongs to a subfamily of receptor tyrosine kinases and is expressed almost ubiquitously in mammalian tissues (42-47. The heterotetrameric transmembrane receptor is composed of two α/β-dimers connected by disulfide bridges (48, 49). The extracellular α-subunits constitute the ligand binding site whereas the β-subunits span the membrane and comprise the intrinsic tyrosine kinase activity in their intracellular portion (50-51). Upon binding of insulin, the α-subunit induces conformational changes of the β-subunit, leading to derepression of the tyrosine kinase activity. Trans-autophosphorylation at specific tyrosine residues (Tyr) provokes fully kinase activity and allows phosphorylation of cytoplasmic substrates binding the receptor (52-55). Most prominent among those is the family of insulin receptor substrates (IRS), IRS-1 to IRS-5. IRS-1 and IRS-2 seem to play the most crucial role. (56). Further substrates are Grb-2 associated binder (Gab), 14-3-3 proteins, SH2-containing protein (Shc) and others (57-59). These messengers distribute the signal from the IR into the

phospatidylinisitol-3-kinase (PI3K)/Akt and the mitogen-activated protein kinase (MAPK) pathway, as the major downstream pathways.

The PI3K/Akt pathway triggers the majority of acute responses to insulin on glucose and lipid metabolism, stimulating glucose uptake and the synthesis of glycogen, proteins and triglycerides as well as the expression of genes involved in glucose and lipid metabolism (60-62). PI3K is activated through binding to phosphorylated IRS and catalyses the transformation of the membrane lipid phosphatinositol-4,5-bisphosphate (PIP_2) to phosphatinositol-3,4,5-triphosphate (PIP_3) (60). The serine kinase AKT binds PIP_3 and thereby is collocated with the activating kinases phospoinositide-dependent protein kinase 1 (PDK1) (63, 64) and mammalian target of rapamycin complex 2 (mTORC2) (65, 66). Activated by those, AKT functions as a key regulator passing the signal to multiple downstream targets promoting glucose uptake, glycogen synthesis, protein synthesis and gene expression (for review see (27, 67, 68)) (Fig. 1).

In contrast to acute metabolic reactions, the MAPK pathway controls the mitogenic and differentiation response to insulin (for review see(30)). The signal of the activated IR is transmitted to the MAPK pathway through phosphorylated IRS and Shc by recruitment of growth factor receptor bound protein 2 (Grb2). Grb2 recruits Son of Sevenless (SOS). Colocalization of SOS and rat sarcoma protein (Ras) at the cell membrane leads to activation of Ras through exchange of Guanosine-5'-diphosphate(GDP) for Guanosine-5'-triphosphate (GTP) (69, 70). Activated Ras elicits a cascade of successive activating serine (Ser) phosphorylations of Raf, mitogen-activated protein kinase kinase (MAP2K) and finally mitogen-activated protein kinase (MAPK). Activated MAPK enters the nucleus and promotes the expression of several genes giving a positive signal to growth and differentiation (for review see (27, 30)) (Fig. 1).

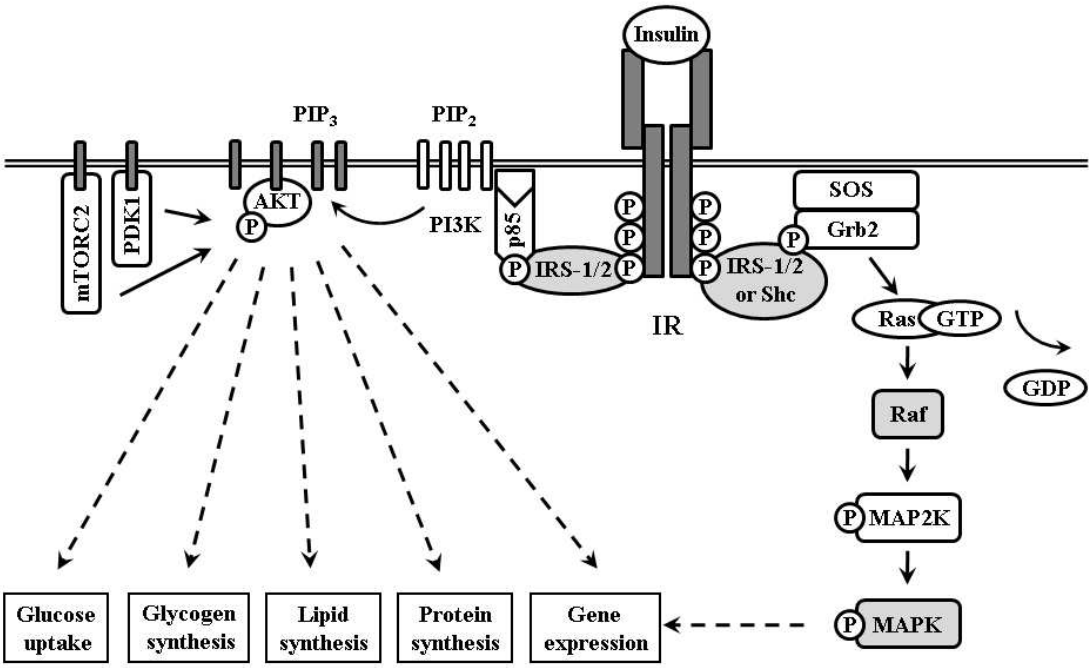

Fig. 1: Insulin receptor signal transduction via PI3K/Akt and MAPK pathway. Binding of insulin to the insulin receptor (IR) triggers the activation of it´s tyrosine kinase activity by autophosphorylation. The PI3K/Akt pathway is induced by insulin receptor substrate- 1 and 2 (IRS1/2) binding to the activated receptor and are phosphorylated by the IR itself. Phospatidylinisitol-3-kinase (PI3K) is activated by binding to phosphorylated IRS-1/2 and catalyses the transition of the membrane lipid phosphatinositol-4,5-bisphosphate (PIP_2) to phosphatinositol-3,4,5-triphosphate (PIP_3). Colocation of AKT kinase with it´s activating kinases phospoinositide-depent protein kinase 1 (PDK1) and mammalian target of rapamycin complex 2 (mTORC2) by their binding to PIP_3 is leading to it´s activation. Akt controls a wide range of biological functions by acting downstream targets promoting glucose uptake, glycogen synthesis, protein synthesis and gene expression. The MAPK pathway is activated by phosphorylation of IRS1/2 or SH2-containing protein (Shc) by the receptor. Recruitment of growth factor receptor bound protein 2 (Grb2) and Son of Sevenless (SOS) activates the GTPase rat sarcoma protein (Ras). Activated Ras induces a cascade of successive activating phosphorylations of Raf, mitogen-activated protein kinase kinase (MAP2K) and mitogen-activated protein kinase (MAPK). Activated MAPK promotes gene expression by acting on several transcription factors.

1.3 The insulin like growth factor 1 (IGF1) signaling system

1.3.1 Biological functions of the IGF1 signaling system

The insulin like growth factor (IGF1) is part of the somatotropic axis, one of the major endocrine systems regulating postnatal growth in mammals (71-73). IGF1 is mainly released by the liver in response to growth hormone (GH) secretion by the anterior pituitary gland (71, 74). Many of the somatic effects of GH are elicited by IGF1 as intermediary (71, 74). The IGF1 system is structurally closely related to the insulin system. The circulating hormone IGF1 and its cognate receptor, the IGF1 receptor (IGF1R), display high degrees of homology in sequence and structure with insulin and IR. Moreover, both systems trigger MAPK and PI3K/Akt pathways as their major intracellular downstream pathways (48, 75-77).

Despite the close relation between the two systems the well established biological effects of insulin and IGF1 signaling differ considerably. Whilst the major effects of insulin are thought to be regulation of energy homeostasis, IGF1 is mostly seen as an anabolic hormone and as a potent inhibitor of apoptosis (78-81). Deregulation of the IGF1 system is mainly correlated with the development of several types of cancer (for review see (82)). However, a growing numbers of studies suggest a role of IGF1 signaling in maintaining glucose homeostasis, a role to the IGF1 system in the development of diabetes mellitus (83-91).

1.3.2 IGF1, structure and release

Beside the liver as the major contributor, IGF1 is synthesized and released at a lower degree by almost any tissue in an autocrine and paracrine fashion (71, 74, 90). IGF1 is a single chain hormone, displaying a high level of homology with insulin, showing 48% amino acid identity, identical bonding by disulfide bridges and similar tertiary structure (75). In contrast to insulin, IGF1 does not circulate in a free, unbound form. About 99% of circulating IGF1 is bound to one of six IGF1 binding proteins

(IGFBP1-6) or to one of nine IGFBP related proteins (IGFBP-rP1-9) (91-94). IGFBPs play a critical role in IGF1 signaling by prolonging half-life of IGF1, regulating intra- and extravascular transport and affecting their affinity for receptor binding (92, 95, 96).

1.3.3 The IGF1 receptor and post receptor signaling

The IGF1R is expressed almost ubiquitously (97). As insulin and IGF1, IR and IGF1R display a high degree of homology, the same tertiary structure and do share the same mechanism of receptors activation and signal transduction. (48, 77, 98). Like IR, the IGF1R is a tetrameric receptor tyrosine kinase, composed of two extracellular α and two membrane spanning β subunits, bearing an intracellular tyrosine kinase domain (99-101). IGF1R and IR share approximately 70% amino acid homology, with 84 % as the highest degree in the tyrosine kinase domain (48, 102). Notably, IR and IGF1R display short highly heterogeneous sequences in their tyrosine kinase domains and further sequences of low homology in their carboxyl terminal domains (48). These differences may be in part responsible for distinctions in the downstream signaling and the biological effects of the both receptors.

The process of IGF1R activation is very similar to the previously described activation of IR. Hormone binding to the IGF1R activates its intrinsic tyrosine kinase activity gaining full activity after initial trans-phosphorylations (for review see (103)).
Activated IGF1R triggers diverse pathways by recruitment and phosphorylation of IRSs, Shc, Grb2 and 14-3-3 proteins (79-81, 104, 105). Among those, PI3K/Akt and MAPK pathway mediate most of IGF1´s effects and are the best investigated. The PI3K/Akt pathway is activated as previously described for IR signaling (Fig. 1). Anti-apoptotic and protein synthesis stimulating effects of IGF1 are mediated mainly via activation of Akt. Anti-apoptotic effects are induced by inhibitory phosphorylation of pro-apoptotic factors, as well as increased expression of anti-apoptotic proteins (103, 106-108). Furthermore Akt exerts a generally stimulating effect on protein synthesis (109). Activation of the MAPK pathway by IGF1R is associated with the effects of IGF1 on cellular proliferation

and differentiation by promoting expression of genes promoting mitosis (110, 111). Mechanisms of activation are the same for triggering MAPK via IR and IGF1R (Fig. 1).

The fact that insulin and IGF1 signaling cause such unequal biological effects by triggering the same major intracellular pathways appears conflicting. Selective outcome of insulin and IGF1 signals is assumed to depend on differences in the recruitment of intracellular docking proteins resulting from different substrate specificities, binding velocities, reaction times and activities (112, 114-116). In part, different ligand binding behavior might be explained by the mentioned sequence variations in the tyrosine kinase domains and the carboxyl terminal domains of IR and IGF1R (48).

1.3.4 Crosstalk events between insulin and IGF1 systems

Due to homology in amino acid sequence and in structure of the hormones and receptors interferences among insulin and IGF1 system occur. Insulin binds and activates IGF1R as well as IGF1 is capable of binding and activating IR (117). The binding affinities are indeed much lower than binding to their cognate receptors, making non physiological concentrations of hormones required to achieve receptor activation (91, 118, 119). Insulin binds to IGF1R with a 100-fold lower affinity than to IR (118). The binding affinity of IGF1 to IR is even 1.000-fold lower than the affinity of IGF1 to its cognate receptor (for review see (91, 119)). In this context, it is important that serum concentrations of IGF1 in human are 100-fold higher than concentrations of insulin (for review see (120)). More relevant than notional receptor binding seems to be the formation of functional hybrid receptors through the assembly of IR and IGF1R α/β-hemireceptors (121, 122). Hybrid receptors display low affinity to insulin, but high affinity to IGF1, at levels comparable to IGF1R (123-125). Until now, the biological response triggered by these hybrid receptors and their biological function remains unclear (for review see (126)).

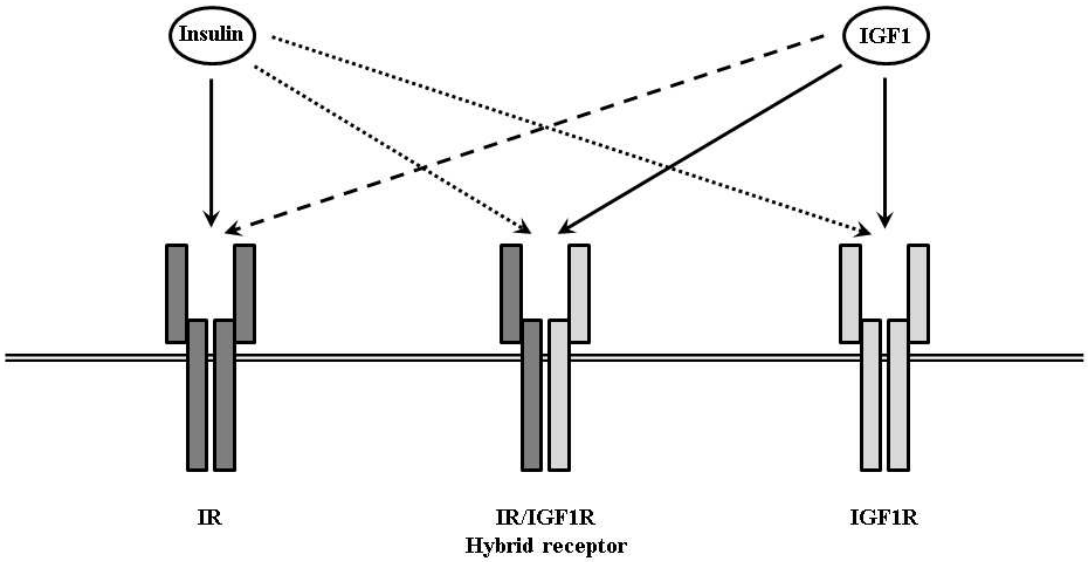

Fig. 2: Crosstalk between insulin and IGF1R systems. Close structural homology between receptors and hormones allows crosstalk between both systems through binding of insulin and IGF1 to non cognate receptors and the formation of hybrid receptors between IR and IGF1R hemireceptors. Insulin and IGF1 bind to each of these receptors, IRs, IGF1Rs and hybrid receptors, however with variable affinities. Insulin affinity to IGF1R and IR/IGF1R hybrid receptors is about 1,000-fold lower (dotted arrow) than to its cognate IR (solid arrow). IGF1 binds IGF1R and IR/IGF1R hybrid receptors with almost same affinity (solid arrow), whilst IR is bound with 100-fold lower affinity (dashed arrow).

1.3.5 The IGF1 system in the context of glucose metabolism

The close structural relation between insulin and IGF1 signaling systems suggest the possibility of redundant biological functions among IR and IGF1 system. As a matter of fact, there are increasing numbers of evidences from clinical trails as well as *in vitro* and *in vivo* studies suggesting a role of the IGF1 system in glucose homeostasis and the development of diabetes.

Reduced levels of circulating IGF1 are observed in patients suffering from T2DM (127). Furthermore, administration of IGF1 has shown to reduce serum glucose levels in healthy humans and individuals suffering from T2DM (128-131). However, the magnitude of these insulin-like effects of IGF1R is only 4-7 % of that of insulin (85, 87). Furthermore, improved insulin sensitivity was demonstrated after IGF1 administration in

several of these studies (88, 130, 131). As observed for IGF1 itself, reduced levels of IGFBPs are associated with hyperglycaemia (85). In particular, IGFBP1 may be relevant for the effects of IGF1 on glucose homeostasis, since treatment with IGFBP1 has shown to reduce serum glucose levels in humans (132, 133). Furthermore, mice overexpressing IGFBP3 display increased fasting serum glucose levels and impaired glucose tolerance (134, 135).

The role of IGF1R in this context has been demonstrated in mice overexpressing a dominant-negative IGF1R mutant in skeletal muscle, leading to functional inactivation of IGF1R and IGF1R/IR hybrid receptors and the development of a diabetes-like phenotype (87). In contrast, muscle specific inactivation of IR through it´s deletion or overexpression of a dominant-negative mutant in mice interestingly just cause a mild phenotype and allowed to maintain glucose homeostasis over months (42, 136). Further considerations about a role of IGF1R are given by *in vitro* studies in IR-deficient muscle cells and fibroblasts showing increased glucose uptake and glycogen synthesis after treatment with IGF1 or high concentrations of insulin (137, 138).

The effects of IGF1 on glucose clearance are predominately attributed to an IGF1 induced peripheral glucose uptake in skeletal muscle tissue (87, 89, 137-142). Glucose uptake in adipocytes after IGF1 stimulation has been described as well as decreased gluconeogenesis in hepatocytes (128, 141). However, both observations are controversially discussed.

Taken together, these studies indicate a potential role of the IGF1 system in the context of glucose homeostasis and the etiopathogenesis of diabetes, possibly by adopting functions of the IR or by influencing insulin signaling.

1.4 Technical background

1.4.1 Motivation for technical innovation

In this study the functional redundancy between IGF1R and IR in the context of glucose homeostasis has been examined. For this reason novel technical approaches have been developed, aiming to generate transgenic mice lacking the function of both receptors. The basic concepts for this development are two techniques, the recombinase-mediated cassette exchange (RMCE) and the use of RNA interference (RNAi). The combined application of these techniques is already successfully used to generate genetically engineered mice displaying a single gene inactivation (143, 144).

1.4.2 RNA interference (RNAi)

RNA interference (RNAi) is a eukaryotic mechanism of specific posttranscriptional gene regulation. Triggers of RNAi are 21 to 28 base pair (bp) long double stranded RNAs (dsRNAs) inducing degradation or translational inhibition of mRNAs bearing complementary sequences (145, 146). In vertebrates, natural occurring RNAi is induced by a non-coding RNA species designated as micro RNAs (miRNAs), cleaved out of complex hairpin structures and playing a crucial role in embryogenesis and tissue morphogenesis (147-153). This process employs a complex machinery of RNAses and multiproteincomplexes (153-157).

Several techniques have been developed to establish RNAi as an efficient tool for the down regulation of a specific gene of interest, designated as knock down (KD), suitable application for achievement of *in vivo* gene silencing in animal models (158). The most practical option to specifically induce a target gene KD in mice is the *in vivo* expression of artificial hairpin structures entering the endogenous RNAi pathway (159-163). Stable integration of expression vectors allows for a constitutive KD by constant production of hairpin RNAs (143, 160, 164). The most widely used method is the expression of so-called short hairpin RNAs (shRNAs). Those are composed of inverted repeats of a 19 to 29 nucleotide sequence, complementary to the target gene, connected

by a 6 to 9 nucleotide long spacer sequence. The shRNA transcript forms a hairpin by base pairing, constituting a substrate of the endogenous RNAi pathway and being processed to a RNA duplex triggering RNAi. Transcribed shRNA is exported actively from the nucleus into cytoplasm, where RNAse Dicer produces a duplex intermediate with characteristic 2nt 3´overhangs by removal of the loop sequence (154, 165, 166). This dsRNA is incorporated into the RNA-induced silencing complex (RISC), the effector of RNAi. Only one strain of the duplex remains in the Risc as a guide strand and mediates the specific binding of the complex to complementary target sites of mRNAs. Perfectly matching guide strands mediate endonuclear cleavage of bound mRNA by RISC (149, 150). RISC assembly shows a distinct strand bias favoring the incorporation of just one strand of the duplex, probable due to thermodynamic properties of the dsRNA intermediate (155, 156). Polymerase III (Pol III) depending promoters such as H1 and U6 are used for shRNA expression, providing strong and ubiquitous expression of short well defined transcripts without poly-A-tails (159, 160, 169, 170). To allow temporary control of shRNA expression inducible Pol III promoters have been developed by combining U6 and H1 with the tetracycline operator/repressor system (144, 171). The possibility to induce the KD upon administration of the inductor allows circumventing embryonic lethality by target genes loss of function, observed for about 30 % of murine genes. Predictable and reproducible KD efficiencies can be archived by targeted integrations of expression vectors in characterized and suitable loci. Rosa26 (R26) and hypoxanthine-guanine phosphoribosyltransferase (Hprt) loci have been used for this issue (143, 172, 173).

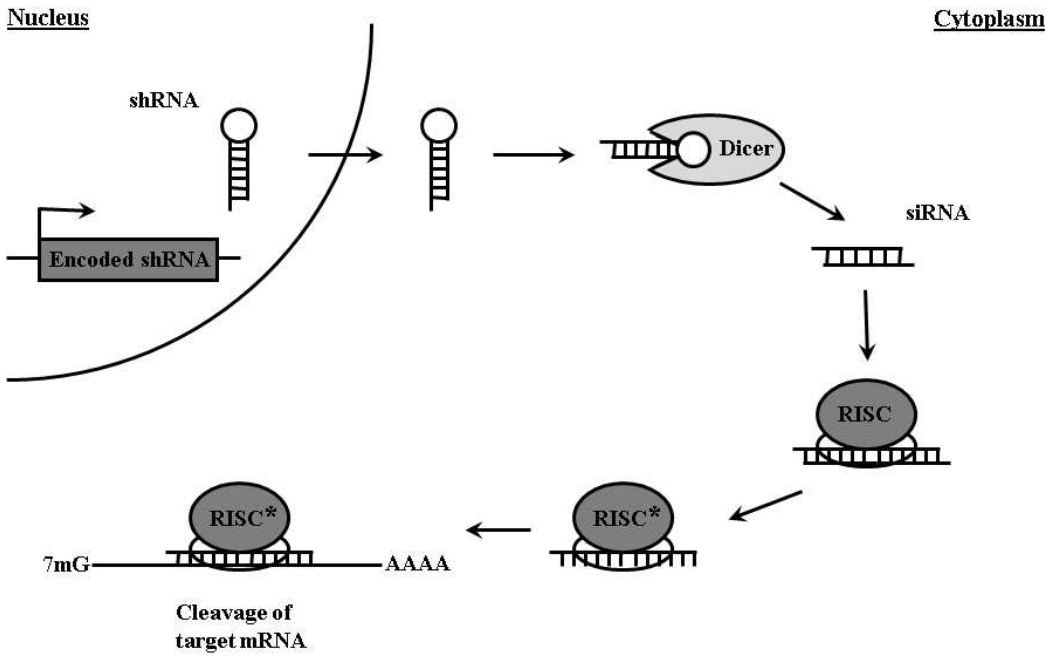

Fig. 3: RNAi induced by shRNA. The shRNA is expressed from a vector based or stably integrated template and enter the endogenous miRNA processing pathway. After export from nucleus into cytoplasm the loop structure is removed by Dicer thereby, producing the double strained siRNA. RISC incorporates and unwinds the double strain. One strain of the siRNA remains in the activated from of RISC (RISC*), guiding the complex to complementary binding sites of the target mRNA. Expression of the target gene is repressed by cleavage and subsequent degradation of bound mRNA.

Generation of loss of function mutants by using RNAi technology is directly competing with knockout (KO) mice achieving loss of function by partial or complete deletion of the gene of interest (GOI) by homologous recombination (158). Compared to KOs, there are several advantages of the RNAi technology, but disadvantages as well. First, a KD results in a reduction to 5 to 40 % of the original target mRNA level and not in a complete loss of function, as it is true for KOs (143, 174). In particular cases, a milder phenotype resulting from the remaining gene product offers a better-suited model for physiological conditions than a complete loss of function. On the other hand residual gene activities might complicate phenotype analysis in reverse genetic studies. A major advantage of RNAi is the short time needed for the generation of mouse KD mice. RNAi

alleles are acting in trans and thus do not have to be breed into homozygosity (143, 175). Furthermore, highly efficient recombinase based integration systems can be used for integration of shRNA expression vectors at predefined loci, since the mechanisms of RNAi are independent from the target gene´s genomic site and structure (143, 144). At last about 12 month are required to generate homozygote KO mice, whereas KD mice can be generated in just 7 month (143, 176). Problematic about artificial RNAi are potential off target effects, the unwanted KD of partially complementary mRNAs or unspecific effects due to immune stimulation (177-180). Options for the recognition of unspecific phenotypes originating from off target effects are given by control experiments using another shRNA sequence designed against the same target gene or co-expression of rescue mutants, designed target gene mutants bearing no target sequence of the used shRNA (181).

1.4.3 Recombinase mediated Cassette Exchange (RMCE)

The recombinase-mediated cassette exchange (RMCE) is a technique to perform the stable integration of transgenic elements by the exchange of a vector based donor cassette and a genomic acceptor cassette at previously prepared allele.

RMCE systems utilize the reaction catalyzed by sequence specific recombinases, FLP and Cre, in the first instance. These enzymes recombine DNA within their short recognition sites, the FLP recombinase recognition target (FRT) and the locus of crossover in P1 (loxP) of the Cre recombinase, at a very high frequency (182, 183). The basic principle of RMCE systems is the use of two couples of heterospecific recognition sites, e.g. a combination of loxP and FRT sites, or of wild type recognition site and an incompatible mutated sited (184-187). Two incompatible recognition sites in the same configuration flank donor and acceptor cassettes. In the presence of the corresponding recombinase just the compatible sites of vector and RMCE allele are recombined. Through this double reciprocal recombination, transposition of the cassettes between genome and vector is carried out (Fig. 4). The incompatible character of the available recognition sites prevents intramolecular reactions. Thus, even in the presence of the

recombinase, the exchanged cassette remains stably integrated. RMCE insertions occur at a very high frequency up to 95% in cultured murine embryonic stem (ES) cells (143, 188). Nevertheless, to achieve a genomic locus prepared for RMCE integration, targeting of this locus by classical integration techniques is required (143, 188, 189, 193). The RMCE technique is beneficial in the case of the need for repeated integration of different elements at the same loci, e.g. the expression of transgenic mRNAs, research on regulatory elements, creation of multiple mutant alleles or the expression of short RNAs for RNAi induction (143, 189, 190).

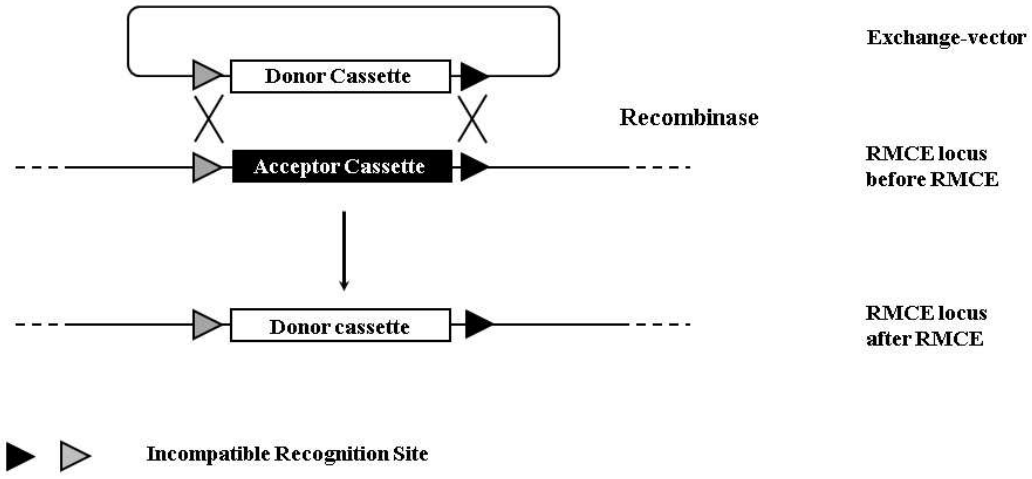

Fig. 4: Functionality of Recombinase mediated Cassette Exchange (RMCE). A RMCE is mediated through the enzyme catalyzed recombination of two heterospecific pairs of recognition sites. By this reaction the sequences bordered by this recognition sites, a genomic acceptor cassette and a vector based donor cassette, are transposed. Due to the incompatibility of the genomic recognition sites the exchanged cassette remains stable integrated, even in presence of recombinase.

The donor cassette integrates exclusive of prokaryotic backbone elements of the exchange vector, which are known for potential induction of epigenetic changes at the site of integration. The stable single copy integration in a predefined locus allows predictable and reproducible use of the given expression properties, the major advantage of the RMCE technique (144). Recently the potential to perform specific RMCE

reactions in two distinct genomic loci in parallel has been shown (191). Specificity for the individual loci has been archived by the use of four couples of heterospecific FRT variations.

Within this study a FLP based RMCE system situated in the rosa 26 (R26) locus served as a technical basis (143) (Fig. 5). The genomic part of this system is integrated into the first intron of the R26 gene, displaying ubiquitous transcriptional activity through all stages of mouse development (192). A phosphoglyceratkinase (PGK) promoter driven hygromycin resistance gene inside the acceptor cassette affords positive selection of R26(RMCE) bearing cells. Cassette exchange in R26 depends on the application of two hetereospecific pairs of wild type FRT sites and mutated recognition sites, designated as F3 sites (186). While a 2 bp variation within the recognition sequence inhibits the reaction between FRT and F3 sites completely, two F3 sites display the same self-recognition capacity as the wild type does (184). RMCE reaction is carried out through double reciprocal recombination of FRT and F3 pairs bordering acceptor and donor cassette in the same configuration, mediated by a co-expressed FLP recombinase. A marker system allows antibiotic selection by reconstitution of a non-functional neomycin resistance gene (5´dNeo), leaking start codon (ATG) and promoter, upon correct exchange. A splice acceptor site (SA) and an ATG facilitate expression of the truncated neomycin resistance gene (5´dNeo) on the exchange vector by employing the endogenous rosa26 promoter after cassette exchange. Functionality of 5´dNeo is exclusively restored by correct recombination of the F3 site, allowing geneticin (G418) selection after proper cassette exchange. In case of random integration events, transcription of 5´d Neo is prevented by a pA upstream of 5´d Neo on the exchange vector. The Hyg resistance gene gets lost in couse of RMCE reaction.

Stable single copy integration of shRNA or cDNA expression units in R26 takes advantage of the well characterized properties of this locus. Integration in R26 RMCE is highly efficient, with a frequency up to 95 % in murine ES cells, allowing rapid generate of transgenic mice with predictable and reproducible expression properties of inserted elements (143).

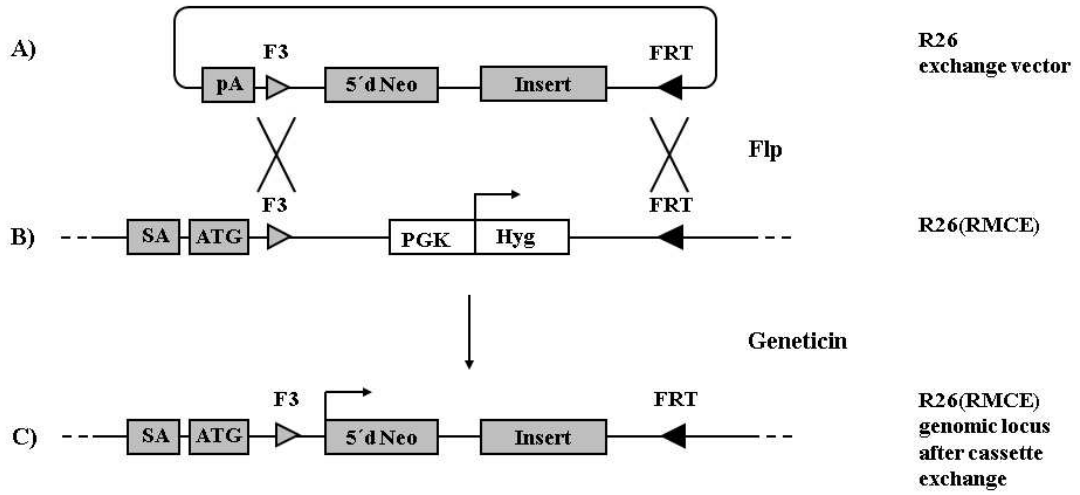

Fig. 5: Functionality of R26 RMCE system. A) The exchange vector contains in 5´-3´direction: polyadenylation signal (pA), F3 site, neomycin resistance gene leaking ATG and promoter (5´d Neo), insert, FRT site. **B)** The genomic part of R26(RMCE) contains following elements in 5´-3´direction: splice acceptor (SA), start codon (ATG), F3 site, phosphoglycerate kinase promoter (PGK), hygromycin resistance gene (Hyg), FRT site. Hyg allows antibiotic selection of R26(RMCE) cells. Stable expression of FLP avoids incomplete recombination events. **C)** SA and an ATG facilitate expression of 5´dNeo by employing the endogenous rosa26 promoter after cassette exchange, allowing G418 selection after correct cassette exchange. Hygromycin resistance gets lost upon RMCE.

1.5 Objectives

The aim of this study was to examine the functional redundancy between IGF1R and IR in the context of energy homeostasis. For this reason novel technical approaches have been developed, allowing the shRNA mediated KD of two independent target genes in transgenic mice. Two different strategies were pursued to reach this aim.

The first strategy was based on the generation of a murine ES cell line harbouring two irrespective RMCE acceptor cassettes at independent genomic loci. Such a cell line should enable the integration of two different shRNA expression cassettes in the two RMCE loci. As a second strategy two shRNA expression units were combined in a single RMCE donor cassette for integration into the R26 RMCE locus. This method was applied

for generation of a mouse model providing the concurrent KD of the insulin and the IGF1 receptor. These mice were physiologically characterized in terms of energy homeostasis.

2 Material and Methods

2.1 Chemicals and Enzymes

Chemicals and enzymes used in this work and the respective sources of supplies are indicated below, chemicals in table 1 and enzymes in table 2.

Chemical	**Supplier**
α-[32P]-dCTP	PerkinElmer Life Science, Cologne, Germany
β-mercaptoethanol	Fisher Scientific, Schwerte, Germany
10x PCR buffer	Invitrogen, Karlsruhe, Germany
20x saline-sodium citrate (SSC)	Invitrogen, Karsruhe, Germany
4-2-hydroxyethyl-1-piperazineethanesulfonic acid (HEPES)	Sigma Aldrich, Steinheim, Germany
Adenosintriphosphat (ATP), 10 mM	Invitrogen, Karlsruhe, Germany
Agarose ultra pure	Sigma Aldrich, Steinheim, Germany
Albumine from bovine serum	Sigma Aldrich, Steinheim, Germany
Ampicilin	VWR International, Langenfeld, Germany
Bovine Serum Albumin (BSA)	Santa Cruz Biotechnology, Santa Cruz, USA
Bromophenol blue	Merck, Darmstadt, Germany
Chloroform	Merck, Darmstadt, Germany
Complete protease inhibitor cocktail tablets	Roche Diagnostic, Mannheim, Germany
Desoxyribonukleotide triphosphate set (dNTP)	5 Prime, Hamburg, Germany
Dextran sulfat sodium salt	Sigma Aldrich, Steinheim, Germany
Dimethyl Sulfoxide (DMSO)	Sigma Aldrich, Steinheim, Germany
Dithiothreitol (DDT)	Sigma Aldrich, Steinheim, Germany
Dulbecco's Modification of Eagle's Medium (DMEM)	Fisher Scientific, Schwerte, Germany
Doxycycline hyclate	Sigma Aldrich, Steinheim, Germany

Ethanol absolute	Merck, Darmstadt, Germany
Ethidium bromide tablets	VWR International, Langenfeld, Germany
Ethylenediaminetetraacetic (EDTA)	Sigma Aldrich, Steinheim, Germany
Fetal calf serum (FCS)	PAN-Biotech, Aidenbach, Germany
Forward reaction buffer (x5)	Invitrogen, Karlsruhe, Germany
Fugene6 Transfection Reagent	Roche Diagnostics, Mannheim, Germany
G153 Developer	Agfa Healthcare, Mortsel, Belgium
G354 Fix	Agfa Healthcare, Mortsel, Belgium
Geneticin (G418)	Sigma Aldrich, Steinheim, Germany
Glucose 20%	Bela-pharm, Vechta, Germany
Glycerol	Merck, Darmstadt, Germany
Guanidine hydrochloride	AppliChem, Darmstadt, Germany
Hydrochloric acid (HCl)	Sigma Aldrich, Steinheim, Germany
Hygromycin B in PBS	Invitrogen, Karlsruhe, Germany
Insulin human	Novo Nordisk, Basvaerd, Denmark
Isopropanol	TH. Geyer & Co, Renningen, Germany
Kaliumchloride (KCl)	Sigma Aldrich, Steinheim, Germany
Lysogeny Broth (LB)	Sigma Aldrich, Steinheim, Germany
Magnesium chloride ($MgCl_2$)	Invitrogen, Karlsruhe, Germany
Magnesium sulfate ($MgSO_4$)	Invitrogen, Karlsruhe, Germany
Modified Eagle Media (MEM), non essential aminoacids	Invitrogen, Karlsruhe, Germany
N-Laurylsacrosinate	Sigma Aldrich, Steinheim, Germany
optiMEM I with Glutamax-I	Invitrogen, Karlsruhe, Germany
PCR reaction buffer HIFI (x10)	Invitrogen, Karlsruhe, Germany
PeqGOLD TriFast	Peqlab, Erlangen, Germany
Phenol-Chloroform-Isoamyl alcohol	Applied Biosystems, Darmstadt, Germany
Phosphatase inhibitor cocktail tablets, PhosSTOP	Roche Diagnostic, Mannheim, Germany
Phosphate buffered saline (PBS)	Invitrogen, Karlsruhe, Germany
Protein A Agarose	Millipore, Eschborn, Germany
Puromycin Dihydrochloride	Sigma Aldrich, Steinheim, Germany

QIAzol lysis reagent	Qiagen, Hilden, Germany
Reporter gene assay lysis buffer	Roche Diagnostic, Mannheim, Germany
Restriction enzymes and buffers P1	New England Biolabs, Frankfurt, Germany
Restriction enzymes and buffers P2	New England Biolabs, Frankfurt, Germany
Restriction enzymes and buffers P3	New England Biolabs, Frankfurt, Germany
Restriction enzymes and buffers P4	New England Biolabs, Frankfurt, Germany
RNAlater	Applied Biosystems, Darmstadt, Germany
Salmon sperm DNA solution ultra pure, sonificated	Fisher Scientific, Schwerte, Germany
Sodium chloride 0,9% (NaCl)	B. Braun, Melsungen, Germany
Sodium dodecyl sulfate (SDS)	Sigma Aldrich, Steinheim, Germany
Sodium hydroxide (NaOH)	VWR International, Langenfeld, Germany
Sodium pyrophosphate (Na_2HPO_4)	Sigma Aldrich, Steinheim, Germany
Sodium pyrovate ($C_3H_3NaO_3$)	Sigma Aldrich, Steinheim, Germany
Sucrose	Sigma Aldrich, Steinheim, Germany
Super Signal West Pico chemiluminescent substrate	Fisher Scientific, Schwerte, Germany
Tris/EDTA (TE) buffer, pH=7.0	Invitrogen, Karlsruhe, Germany
Tris acetate EDTA (TAE)	Fisher Scientific, Schwerte, Germany
Tris-glycine SDS running buffer	Invitrogen, Karlsruhe, Germany
Triton X-100	Sigma Aldrich, Steinheim, Germany
Trizma hydrochloride	Sigma Aldrich, Steinheim, Germany
Tween 20	Sigma Aldrich, Steinheim, Germany
Trypsin-EDTA (0.25%)	Gibco, Karlsruhe, Germany

Table 1: Chemicals used in this work.

Enzymes	**Supplier**
AflIII (5,000 U/ml)	New England Biolabs, Frankfurt, Germany
AscI (10,000 U/ml)	New England Biolabs, Frankfurt, Germany

BamHI (10,000 U/ml)	New England Biolabs, Frankfurt, Germany
BbsI (5,000 U/ml)	New England Biolabs, Frankfurt, Germany
BclI (15,000 U/ml)	New England Biolabs, Frankfurt, Germany
BsaBI (10,000 U/ml)	New England Biolabs, Frankfurt, Germany
BstBI (20,000 U/ml)	New England Biolabs, Frankfurt, Germany
ClaI (5,000 U/ml)	New England Biolabs, Frankfurt, Germany
DpnI (20,000 U/ml)	New England Biolabs, Frankfurt, Germany
EcoRI (10,000 U/ml)	New England Biolabs, Frankfurt, Germany
FseI (2,000 U/ml)	New England Biolabs, Frankfurt, Germany
High fidelity (HIFI) platinum taq polymerase (5 U/µl)	Invitrogen, Karlsruhe, Germany
HindIII (20,000 U/ml)	New England Biolabs, Frankfurt, Germany
HpaI (5,000 U/ml)	New England Biolabs, Frankfurt, Germany
KpnI (20,000 U/ml)	New England Biolabs, Frankfurt, Germany
MfeI (10,000 U/ml)	New England Biolabs, Frankfurt, Germany
MluI (10,000 U/ml)	New England Biolabs, Frankfurt, Germany
NarI (5,000 U/ml)	New England Biolabs, Frankfurt, Germany
NcoI (10,000 U/ml)	New England Biolabs, Frankfurt, Germany
NdeI (20,000 U/ml)	New England Biolabs, Frankfurt, Germany
NheI (10,000 U/ml)	New England Biolabs, Frankfurt, Germany
PacI (10,000 U/ml)	New England Biolabs, Frankfurt, Germany
PmeI (10,000 U/ml)	New England Biolabs, Frankfurt, Germany
Proteinase K (600 mAU/ml)	5 Prime , Hamburg, Germany
PstI (20,000 U/ml)	New England Biolabs, Frankfurt, Germany
PspXI (10,000 U/ml)	New England Biolabs, Frankfurt, Germany
SbfI (10,000 U/ml)	New England Biolabs, Frankfurt, Germany
SfiI (20,000 U/ml)	New England Biolabs, Frankfurt, Germany
SpeI (10,000 U/ml)	New England Biolabs, Frankfurt, Germany
SwaI (10,000 U/ml)	New England Biolabs, Frankfurt, Germany
Taq DNA Polymerase	Invitrogen, Karlsruhe, Germany
T4 DNA Polymerase	Invitrogen, Karlsruhe, Germany
T4 Kinase (10 U/µl)	Invitrogen, Karlsruhe, Germany

T4 Ligase H.C. (12 U/µl)	Invitrogen, Karlsruhe, Germany
XbaI (20,000 U/ml)	New England Biolabs, Frankfurt, Germany
XhoI (20,000 U/ml)	New England Biolabs, Frankfurt, Germany

Table 2: Enzymes used in this work.

2.2 Molecular Biological methods

2.2.1 General cloning cloning procedure

In general, digested plasmid DNA and annealed oligonucleotides were used for cloning DNA constructs. Vector DNA was digested by treatment of 2 µg DNA with 10 U of each applied restriction enzyme for 1.5 to 2 h. BSA and restriction enzymes and buffers were used according to manufacturer´s instructions. Digested DNA fragments were separated by size using electrophoretic separation in agarose gel (0.8 -1.5 % (w/v), agarose; 1 x TAE; 0.5 mg/ml ethidium bromide; 1 x TAE electrophoresis buffer) and isolated from gel using QIAquick Gel Extraction-Kit (Qiagen, Hilden, Germany), according to manufacturer's instructions. 100 µg vector DNA were used per ligation reaction in a molar vector to insert ratio of 3:1, for sticky end ligations, and 5:1 for blunt end ligations. For ligation with oligonucleotides 100 µg vector DNA was ligated with 4µl of diluted and annealed oligonucleotides, as described below under 2.2.2. DNA was incubated in a total reaction volume of 20 µl containing 4µl 5x Ligase Reaction Buffer (Invitrogen, Karlsruhe, Germany), 1 U T4 Ligase H.C. (Invitrogen, Karlsruhe, Germany) for 4 h at 16 °C. Ligation mixtures were transformed into MaxEfficiency DH5α chemical competent cells (Invitrogen, Karlsruhe, Germany), according to manufacturer´s introductions, spread on LB plates containing 100 µg/ml ampicillin and incubate overnight at 37 °C. Single colonies were analysed for correct ligation product by using CloneChecker™ System (Invitrogen, Karlsruhe, Germany) following users manual and subsequent analytic restriction digest, adjusted to the accordant cloning product.

2.2.2 Annealing of synthetic oligonucleotides for cloning

Oligonucleotides were used for several cloning steps. For each step two single strained oligonucleotides, sense (s) and antisense (as), were designed to be hybridizated into double strained DNA bearing overhangs compatible to the overhangs of vector fragment they are to be ligated to. Both oligonucleotides are phosphorylated by incubating 1 µg of each oligonucleotide with 5 µl 5x forward reaction buffer (Invitrogen, Karlsruhe, Germany), 2.5 µl 10 mM ATP (Invitrogen, Karlsruhe, Germany), 1 U T4 Kinase (Invitrogen, Karlsruhe, Germany) in a total volume of 25 µl at 37 °C for 30 min. Kinase was inactivated by subsequent incubation at 65 °C for 10 min. For annealing 14 µl of each kinasing mixture were pooled with 4 µl 5M NaCl, incubated at 65 °C for 15 min and subsequently cooled down slowly to room temperature. After adding 68 µl TE buffer this mixture is diluted 1:10 with ddH_2O. 4µl of diluted annealed oligonucleotides are used for ligation. All oligonucleotides used in this work were custom synthesized by metabion, Martinsried, Germany.

2.2.3 Blunting of sticky ended DNA

Blunting of sticky ends, created by restriction digest, was performed, if further procedure includes ligation with blunt ended fragments or abolishing of the restriction site by religation of blunted fragment. For blunting 4 µg vector DNA was digested in a Volume of 76 µl. After restriction digest 2 µl 10 mM dNTP mix, 20 µl 5 x T4 DNA Polymerase Buffer and 2 µl T4 DNA Polymerase (5 U/µl) were added and incubated at 11°C for 15 min. Fragment were separated in agarose gel electrophoresis and isolated from gel as described above under 2.2.1.

2.2.4 Cloning of single shRNA expression vectors (pR-shIGF1R1 – pR-shIGF1R6)

shRNA expression vectors were cloned using oligonucleotides constituted on basis of siRNAs designed by the algorithm BLOCK-iT™ RNAi Designer (Invitrogen, Karlsruhe, Germany). Used Sequences are displayed in table 3. The sense sequence, compatible to target mRNA, with an length of 19 to 21 nt siRNAs was embedded into an structure to allow transcripts formation of hairpin structure, termination of Pol III transcription and cloning of the oligonucleotide into pINV-7 (TaconicArtemis, Cologne, Germany), a standard vector for inducible RNAi and RMCE integration in R26. The siRNAs sense strand was connected to its fully complementary antisense strand by a loop sequence (TTCAAGAGA) and followed by five thymidines, a Pol III transcription termination site. Sense and antisense oligonucleotides (table 3) were designed to form overhangs compatible to BbsI/MluI digested pINV-7 (TaconicArtemis, Cologne, Germany) after annealing. Strands order relative to H1tetO promoter is sense strand followed by antisense strand. All oligonucleotides were purchased from metabion, Martinsried, Germany. Oligonucleotides were annealed, ligated to BbsI/MluI digested pINV-7 to yield pR-shIGF1R1 to pR-shIGF1R6. All Oligonucleotides were purchased from metabion, Martinsried, Germany.

shRNA	**Sequence of sense strand (5´-3´)**	**Oligonucleotides, name and sequence (5´-3´)**
shIGF1R1	GCAATCTGCTTATTAACATCCT	**oshIGF1R1_s:** CCCGCAATCTGCTTATTAACATCCTTCAAGAG AGGATGTTAATAAGCAGATTGCTTTTTA
		oshIGF1R1_as: CGCGTAAAAAGCAATCTGCTTATTAACATCC TCTCTTGAAGGATGTTAATAAGCAGATTGC
shIGF1R2	GGAAGAACCGAATCATCATAA	**oshIGF1R2_s:** TCCCGGAAGAACCGAATCATCATAATTCAAG AGATTATGATGATTCGGTTCTTCCTTTTTA
		oshIGF1R2_as: CGCGTAAAAAGGAAGAACCGAATCATCATA ATCTCTTGAATTATGATGATTCGGTTCTTCC

shIGF1R3	GCACAACTACTGCTCCAAAGA	**oshIGF1R3_s:** TCCCGCACAACTACTGCTCCAAAGATTCAAG AGATCTTTGGAGCAGTAGTTGTGCTTTTTA
		oshIGF1R3_as: CGCGTAAAAAGCACAACTACTGCTCCAAAGA TCTCTTGAATCTTTGGAGCAGTAGTTGTGC
shIGF1R4	GGACAGATCCTGTGTTCTTCT	**oshIGF1R4_s:** TCCCGGACAGATCCTGTGTTCTTCTTTCAAGA GAAGAAGAACACAGGATCTGTCCTTTTTGGT AC
		oshIGF1R4_as: CGCGGTACCAAAAAGGACAGATCCTGTGTTC TTCTTCTCTTGAAAGAAGAACACAGGATCTG TCC
shIGF1R5	CATCAGGATTGAGAAGA	**oshIGF1R5_s:** TCCCCCATCAGGATTGAGAAGATTCAAGAGA TCTTCTCAATCCTGATGGTTTTTA
		oshIGF1R5_as: CGCGTAAAAACCATCAGGATTGAGAAGATCT CTTGAATCTTCTCAATCCTGATGG
shIGF1R6	GCACCATCCTGAAGGGCAA	**oshIGF1R6_s:** TCCCGCACCATCCTGAAGGGCAATTCAAGAG ATTGCCCTTCAGGATGGTGCTTTTTA
		oshIGF1R6_as: CGCGTAAAAAGCACCATCCTGAAGGGCAATC TCTTGAATTGCCCTTCAGGATGGTGC

Table 3: Tested shRNAs against IGF1R, sequences and oligonucleotides. Sense strands of used shRNAs were designed by the algorithm BLOCK-iT™ RNAi Designer (Invitrogen, Karlsruhe, Germany) and embedded into a standard shRNA structure to enable cloning of the shRNA by using oligonucleotides into the expression vector pINV-7 (TaconicArtemis), transcripts formation of hairpin structure and termination of Pol III transcription. Sequences are displayed in 5´-3´direction and are designated "sense" when complementary to target mRNA. All oligonucleotides were purchased from metabion, Martinsried, Germany.

2.2.5 Cloning of expression vectors for two shRNAs (pshIGF1R2_shIR5 and pshIR5_shIGF1R2)

For cloning of double KD Vectors MluI restriction site was abolished from the vectors pINV-7_shIR5 (144), bearing a shRNA directed against IR, and pshIGF1R2 by MluI digestion followed by blunting and religation. Vectors without MluI restriction site were designated as pshIR5_dMluI and pshIGF1R2_dMluI. For cloning of pshIR5_shIGF1R2 the 8703 bp fragment of NheI/SpeI digested pshIGF1R2 was ligated to the 450 bp fragment of NheI/SwaI digested pshIR5_dMluI. For cloning of pshIGF1R2_shIR5 the 8703 bp fragment of NheI/SpeI digested pINV-7_shIR5 (144) was ligated to the 450 bp fragment of NheI/SwaI digested pshIGF1R2_dMluI.

2.2.6 RecE/RecT based (ET)-cloning

The arms of homology of Col1a1 needed for targeting vectors were subcloned from bacterial artificial chromosomes (BACs) bearing strain RPCIB731P14208Q (imaGenes, Nottingham) using ET-cloning, as described by Muyrers *et al*.. Two vectors were generated containing 3´ and 5´arm of homology. To obtain each PCR product for transformation in BAC cells containing pSC101-BAD-gbaA-tet (193) two consecutive PCR reactions were performed. In the first PCR step the primer couples designated as "inside" with pACYC177 (193) as template were used. The reactions were performed in a total volume of 50 µl, containing 2 ng pACYC177 (193), 0.5 µM of each "inside" primer, sense and antisense, 0.3 mM dNTP Mix, 2 mM $MgSO_4$, 1 x PCR reaction buffer (HIFI) and 5 U HIFI platinum Taq polymerase (Invitrogen, Karlsruhe, Germany). Standard PCR program starts with 5 min of denaturation at 95°C, followed by 25 cycles of denaturation at 95°C for 30 sec, annealing at 58 °C for 30 sec and elongation at 72 °C for 2.5 min and a final elongation step at 72 °C for 10 min. PCR products were purified using QIAquick Gel Extractions-Kit (Qiagen, Hilden, Germany), according to manufacturer's instructions for PCR-fragment purification. For elimination of template DNA products were digested with DpnI for at least 3 hours and subsequently purified using QIAquick Gel Extractions-Kit (Qiagen, Hilden, Germany), as described under 2.2.1. The second PCR step was

performed using the primer couples designated as “outside” with 5 µl of the respective PCR product obtained from step one as template. Reaction mixture and PCR program were the same as described above for the first PCR step.

Primer couples “inside” and “outside” used to gain PCR products for ET-cloning of 3´ arm of homology as well as 5´ arm of homology are stated in table 4. Prior to transfection PCR products were purified using MSB® Vario Cleanup Kit (Invitek, Berlin, Germany), following manufacturer´s protocol 2. Both arms of homology for targeting of Col1a1 locus were subcloned from BAC to the vectors pCol1a1_3´arm, containing the 3´arm arm of homology, and pCol1a1_5´arm, containing the 5´arm of homology.

Arm of homology	**Primer name**	**Primer sequence (5´-3´)**
3´arm	**3´_s-inside**	AGGTGGGGAGAGGCCAGCTACCCCTCCATGTGTGACCAAG GAGCAACCTGGCAATTGGAGTTTTCGTTCCACTGAGCGTC
	3´_as-inside	GTCTACAGAGTGAGTTCCAGGACAGCCAGGGCTACACAGA GAAACCCTGTCTCTGATCAATGCTCTGCCAGTGTTACAACC
	3´_s-outside	TGTGACACCCCAGCATTAGAAGGCCCCTTCTATACTAAATT ATGGTTTCTTTGGGCTAGAGGTGGGGAGAGGCCAGCTACC CC
	3´_as-outside	AATCCCAGCACTTGGGAGGCAGAGGCAGGCGGATTTCAGA GTTTGAGGCCAGCCTGGTCTACAGAGTGAGTTCCAGGACA G
5´arm	**5´_s-inside**	GCCCTCAAAGGGATTCAAGCAGCAGAAACAGGGACTGAGA CATGGAGGAGTTTAAACGCAATTGGAGTTTTCGTTCCACT
	5´_as-inside	CAGCTTCATATGGCAGGACCTGCCTTCCCTGCAGAGCCCCA CCTGAGCTTGCTGATCAATGCTCTGCCAGTGTTACAACC
	5´_s-outside	TCTCCATGCTGACGACCTGAGGCCTGGGAGGTGTTGCCCAT GGATCCTGGGAGGTTCATGAGCCCTCAAAGGGATTCAAG
	5´_as-outside	GGGAGATGAACCAATGACACCTTCCCTCCCTCCTGGTCCCT TGAACTTCCTGGGTCACCAGCTTCATATGGCAGGACCTGC

Table 4: Primers used in ET-cloning. Primers used in ET-cloning to gain arms of homology for targeting of Col1a1 locus. Primer couples designated as ”inside” are used for a first PCR step with pACYC177

(193) as template. Primer couples designated as "outside" are used for the second PCR step with the Product of step one as template. Primer sequences are displayed in 5´-3´direction. All primers were purchased from metabion, Martinsried, Germany.

2.2.7 Cloning of pCol1a1T(RMCE_2Neo)

The targeting vector, pCol1a1T(RMCE_2Neo), for insertion of RMCE_2Neo in the locus of Col1a1 was cloned in 25 steps, as described below. All oligonucletides used for cloning these vectors are stated in table 5. For cloning of the first intermediate pColT1.1 the 3371 bp fragment of XhoI/KpnI digested pBasic48 (TaconicArtemis, Cologne, Germany) was ligated to the annealed oligonucleotides oColT1.1_s and oColT1.1_as. SbfI digested pColT1.1 was ligated to the 1823 bp fragment of SbfI digested pINV-7 (TaconicArtemis, Cologne, Germany) to generate pColT1.2. For cloning of pColT1.3 the vector pBasic46 (TaconicArtemis, Cologne, Germany) was XhoI/KpnI digested and ligated to annealed oligonucleotides oColT1.3_s and oColT1.3_as to gain pColT1.3. The 3190 bp fragment of PstI/MluI digested pColT1.3 was ligated to the 5562 bp fragment of PstI/AscI digested pCAGGS-I-lacZ-pA (TaconicArtemis, Cologne, Germany) to generate pColT1.4. pColT1.4 was Nhe/KpnI digested and the resulting 5629 bp fragment was ligated to the 5001 bp fragment of Nhe/KpnI digested pColT1.2 to give pColT1.5. For cloning of pColT2.1 the plasmid pBasic45 (TaconicArtemis) was XhoI/KpnI digested and ligated to the annealed oligonucleotides oColT2.1_s and oColT2.1_as. The vector was ClaI/NheI digested and the resulting 2719 bp fragment was ligated to the 1989 bp fragment of ClaI/NheI digested pTT84 (TaconicArtemis, Cologne, Germany) to gain pColT2.2. In the next step the 4697 bp fragment XhoI/SalI digested pColT2.2 was ligated to the 4038 bp fragment of XhoI/SalI digested pTT71-hGH (TaconicArtemis, Cologne, Germany) to obtain pColT2.3. For cloning of pColT2.4 the plasmid pBasic45 (TaconicArtemis, Cologne, Germany) was BamHI/AflIII digested and ligated to the annealed oligonucleotides oColT2.4_s and oColT2.4_as. pColT2.4 was HpaI/FseI digested and ligated to the 2082 bp fragment of BsaBI/FseI digested pTT84-new (TaconicArtemis, Cologne, Germany). pColT2.5 was generated by ligation of the 4782 bp fragment of AscI/AflIII digested

ColT2.4 to the 3536 bp fragment of AscI/AflIII digested pColT2.3. pColT2.5 was AscI digested and ligated to the 7496 bp fragment of AscI digested pColT1.5 to obtain pColT2.6. For cloning of the intermediate pColT3.1 the 2789 bp fragment of BsaBI/KpnI digested pBasic45 (TaconicArtemis, Cologne, Germany) was ligated to the annealed oligonucleotides oColT3.1_s and oColT3.1_as. pColT3.1 was EcoRI/KpnI digested and ligated to annealed oligonucleotides oColT3.2_s and oColT3.2_as to gain pColT3.2. The 3000 bp fragment of SfiI/KpnI digested pColT3.2 was ligated to the 1051 bp fragment of SfiI/KpnI digested pINV-6 (TaconicArtemis, Cologne, Germany) to generate pColT3.3. pColT3.4 was obtained by ligation of NarI/MfeI digested pColT3.3 to 3870 fragment of BstBI/MfeI digested pCol1a1_3´arm. For cloning of pColT3.5 the 7898 bp fragment MluI of digested pColT3.4 was ligated to the 7496 bp fragment of AscI digested pCol2.6. For cloning of pColT4.1 pBasic45 (TaconicArtemis, Cologne, Germany) was XhoI/KpnI digested and ligated to the annealed oligonucleotides oColT4.1_s and oColT4.1_as. pColT4.2 was generated by ligation of the 3165 bp fragment of PacI/KpnI digested pColT4.1 with the annealed oligonucleotides oColT4.2_s and oColT4.2_as. The 3230 bp fragment of SfiI/FseI digested pColT4.2 was ligated to the 1051 bp fragment of SfiI/FseI digested pINV-6 (TaconicArtemis, Cologne, Germany) to generate pColT4.3. This plasmid was ClaI/NcoI digested and the resulting 4268 bp fragment was ligated to the 822 fragment of ClaI/NcoI digested pINV-7 (TaconicArtemis, Cologne, Germany) to gain pColT4.4. pColT4.5 was generated by T4 blunting the AscI restriction site of pColT4.4 and religation of the generated fragment. For cloning of pColT4.6 the vector pColT4.5 was MluI digested, the resulting fragment was blunted and ligated to the 1319 bp fragment of SfiI/NdeI digested pINV-6 (TaconicArtemis, Cologne, Germany). pColT4.7 was obtained by ligation of PmeI/BclI digested pColT4.6 to 10441 bp fragment of PmeI/BclI digested pCol1a1_5´arm. For generating the final targeting vector pCol1a1T(RMCE_2Neo) pColT4.7 was MluI/BstBI digested and the resulting 13454 bp fragment was ligated to the 12509 bp fragment of AscI/BstBI digested ColT2.6.

oligonucleotide	**Sequence (5´-3´)**
oColT1.1_s	TCGAGGCGCGCCAGTATAACTTCGTATAGCATACATTATACGAAGTTAT AGTCCTGCAGGGCTAGCACGCGTGGTAC
oColT1.1_as	CACGCGTGCTAGCCCTGCAGGACTATAACTTCGTATAATGTATGCTATA CGAAGTTATACTGGCGCGCC
oColT1.3_s	TCGAGGCTAGCAGATAACTTCGTATAGCATACATTATACGAAGTTATAG TCTGCAGCTGACGCGTGGCGCGCCGGTAC
oColT1.3_as	CGGCGCGCCACGCGTCAGCTGCAGACTATAACTTCGTATAATGTATGCT ATACGAAGTTATCTGCTAGCC
oColT2.1_s	GATCCGGCGCGCCGCTAGCACGTGATCGATACTCGAGGTACCGTCGACG AATTCTTAAGTGTACA
oColT2.1_as	CATGTGTACACTTAAGAATTCGTCGACGGTACCTCGAGTATCGATCACG TGCTAGCGGCGCGCCG
oColT2.4_s	GATCCCGCGGCCGCGAGCTCGTTTAAACGGCCGGCCACGTGGTTAACGG CGCGCCATCGATA
oColT2.4_as	CATGTATCGATGGCGCGCCGTTAACCACGTGGCCGGCCGTTTAAACGAG CTCGCGGCCGCGG
oColT3.1_s	TTCGAACCATGGCCCGGGCGGCGCCATGGCAATTGGCCATAGCGGCCTA GGCCGGCCGAATTCGGTAC
oColT3.1_as	CGAATTCGGCCGGCCTAGGCCGCTATGGCCAATTGCCATGGCGCCGCCC GGGCCATGGTTCGAA
oColT3.2_s	AATTCAGAAGTTCCTATTCCGAAGTTCCTATTCTTCAAAAGGTATAGGA ACTTCTTAAGACGCGTCAGCTGGCGCGCCGGTAC
oColT3.2_as	CGGCGCGCCAGCTGACGCGTCTTAAGAAGTTCCTATACCTTTTGAAGAA TAGGAACTTCGGAATAGGAACTTCTG
oColT4.1_s	TCGAGGTTTAAACGGCCATAGCGGCCTAGGCCGGCCATCGATTTAATTA AGGTAC
oColT4.1_as	CTTAATTAAATCGATGGCCGGCCTAGGCCGCTATGGCCGTTTAAACC
oColT4.2_s	CTGATCAGTTAACGCGTGAAGTTCCTATACTTTCTAGAGAATAGGAACT TCGGAATAGGAACTTCTCCATGGTTAAT
oColT4.2_as	TAACCATGGAGAAGTTCCTATTCCGAAGTTCCTATTCTCTAGAAAGTAT AGGAACTTCACGCGTTAACTGATCAGGTAC

Table 5: Oligonucleotides used for cloning pCol1a1T(RMCE_2Neo). Corresponding sense and antisense oligonucleotides were phosphorylated and annealed as described under 2.2.2. All oligonucleotides were purchased from metabion, Martinsried, Germany. Sequences are displayed in 5´-3´direction.

2.2.8 Cloning of a basic exchange vector for RMCE-2 and pC-shIR5

As an exchange vector for RMCE-2 a basic shRNA expression vector, pColEx5 was cloned. All oligonucleotides used for cloning pColEx5 are stated in table 6. For cloning of the first intermediate pColEx1 the 2958 bp fragment of AscI/KpnI digested pBasic45 (TaconicArtemis, Cologne, Germany) was ligated to the annealed oligonucleotides oColEx1_s and oColEx1_as. pColEx1 was FseI/XhoI digested and the resulting 3029 bp fragment was ligated to a 1837 bp fragment resulting from FseI/XhoI digestion of pTT84 (TaconicArtemis, Cologne, Germany) to generate pEx2. AscI digested pINV-7 (TaconicArtemis, Cologne, Germany) was ligated to the annealed oligonucleotides oColEx2_s and oColEx2_as to yield pColEx3. pColEx3 was FseI digested and ligated to the annealed oligonucleotides oColEx4_s and oColEx4_as to obtain pColEx4. For cloning of the final exchange vector pColEx5 the 4846 bp fragment of FseI/AscI digested pColEx2 was ligated to the 3186 bp resulting from FseI/AscI digestion of pColEx4.

oligonucleotide	**Sequence (5´-3´)**
oColEx1_s	CGCGCCGGCCGGCCCTCGAGCGAAGTTCCTATACTTTCTAGAGAATAGG AACTTCGGAATAGGAACTTCGGTAC
oColEx1_as	CGAAGTTCCTATTCCGAAGTTCCTATTCTCTAGAAAGTATAGGAACTTC GCTCGAGGGCCGGCCGG
oColEx2_s	CGCGCCTAGGCTAGCCATGGTGATCA
oColEx2_as	CGCGTGATCACCATGGCTAGCCTAGG

oColEx4_s	CCTAGGTACCATATGACCGG
oColEx4_as	TCATATGGTACCTAGGCCGG

Table 6: Oligonucleotides used for cloning basic RMCE-2 exchange vector. Corresponding sense and antisense oligonucleotides were phosphorylated and annealed as described under 2.2.1. All oligonucleotides were purchased from metabion, Martinsried, Germany. Sequences are displayed in 5´-3´direction.

The shRNA expression vector pColEx_shIR5 was generated by ligating BbsI/MluI digested pColEx5 to annealed oligonucleotides oshIR5_s and oshIR5_as (144).

2.2.9 Cloning of pColVaLo_shEgln1

The targeting vector, pColVaLo_shEgln1, for insertion of VaLo_shEgln1 in the locus of Col1a1 was cloned in 9 steps, as described below. All oligonucleotides used in this cloning procedure are stated in table 7. First the FseI site in pINV-7 (TaconicArtemis, Cologne, Germany) was eliminated by digesting the vector with FseI, blunting the resulting fragment followed by its religation to gain pVaLo1. In a second step the NheI and SpeI sites in pVaLo1 were removed by digesting with both Enzymes and religation of the resulting 8669 bp fragment. The resulting vector pVaLo2 was KpnI/AscI digested and ligated to the annealed oligonucleotides oVaLo3_s and oVaLo3_as to gain pVaLo3. pVaLo3 was PspXI/SfiI digested and ligated to the annealed oligonucleotides oVaLo4_s and oVaLo4_as to generate pVaLo4. For cloning of pVaLo5, pVaLo4 was SpeI digested and ligated to the 1884 bp fragment of NheI digested pColT1.2. pVaLo6 was cloned by ligation of NheI/HpaI digested pVaLo5 with the 888 bp fragment of XbaI/SwaI digested pINV-6 (TaconicArtemis, Cologne, Germany). pVaLo_shEgln1 was gained from ligation of MfeI/MluI digested pVaLo5 to the 412 bp fragment of MfeI/MluI digested pINV-7_shEgln1(TaconicArtemis, Cologne, Germany). The vector pCol_5´-3´arms was generated by ligation of PmeI/BclI digested

pCol1a1_3´arm with the 7141 bp fragment of PmeI/BclI digested pCol1a1_5´arm. The final vector pColVaLo_shEgln1 was cloned by ligation of FseI/MluI digested pCol_5´-3´arms to the 7056 bp fragment of FseI/AscI digested pVaLo_shEgln1.

oligonucleotide	**Sequence (5´-3´)**
oVaLo3_s	CGCGTGGTACCGAATTCGTTAACGCTAGCGGCCGGCCATGTAC
oVaLo3_as	ACATGGCCGGCCGCTAGCGTTAACGAATTCGGTACCA
oVaLo4_s	TCGACATGGCGCGCCGCTCGAGGATCACGTGACTAGTGGCCATAG
oVaLo4_as	TGGCCACTAGTCACGTGATCCTCGAGCGGCGCGCCATGT

Table 7: Oligonucleotides used for cloning pColVaLo_shEgln1. Corresponding sense and antisense oligonucleotides were phosphorylated and annealed as described under 2.2.1. All oligonucleotides were purchased from metabion, Martinsried, Germany. Sequences are displayed in 5´-3´direction.

2.2.10 Isolation of Genomic DNA

To obtain genomic DNA from cultured cells murine embryonic stem cells were incubated in lysis buffer (10 mM Tris-HCl (pH 7.5), 10 mM EDTA, and 10 mM NaCl, 5% (w/v) N-Laurylsacrosinate, 0.5 mg/ml proteinase K) at 60°C overnight. DNA was precipitated by adding double amount of 100% ethanol, absolute, and incubation for 1 h at 4°C. When performing DNA-isolation from 6-well cultured cells, DNA- precipitate was transferred into a new vial and washed twice with 70% (v/v) ethanol. After air drying at room temperature (RT) for 15 minutes, DNA was and resolved in 200 µl TE buffer (10 mM Tris-HCl (pH 7.5), 1 mM EDTA (pH 8.0)). When performing DNA-isolation from 96-well cultured cells, DNA- precipitate was washed and dissolved on 96-well plate. After precipitation liquid was discharged and DNA precipitate was washed twice with 70% (v/v) ethanol. After air drying at room temperature (RT) for 15 minutes DNA was directly resolved

in digest reaction mix for southern blot analysis. For genomic DNA isolation from mouse tail biopsies, samples were incubated overnight in lysis buffer (100 mM Tris-HCl (pH 8.5), 5 mM EDTA, 0.2% (w/v) SDS, 0.2 M NaCl, 200 µg/ml proteinase K) in a thermomixer (Eppendorf, Hamburg, Germany) at 55°C and 1100 rpm. Samples were centrifuged to discard debris and supernatant was transferred into a new vial. DNA-precipitation was then performed by addition of an equivalent amount of isopropanol. After centrifugation and washing twice with 70% (v/v) ethanol, the DNA pellet was dried at room temperature for 15 minutes and resolved in 400 µl in ddH_2O.

2.2.11Polymerase Chain Reaction (PCR) for genotyping of transgenic mice

The PCR method (160, 161) was used to genotype generated mice for the presence of transgenic elements using customized primers listed in table 8. Reactions were performed in a thermocycler MultiCycler PTC 225 Tetrad (Bio-Rad Laboratories, CA, USA). All PCRs were performed in a total volume of 50 µl, containing a minimum of 50 ng genomic template DNA, 0.5 µM of each primer, sense and antisense, 0.3 mM dNTP Mix, 2 mM $MgCl_2$, 1 x PCR buffer and 5 units/µl Taq DNA Polymerase (Invitrogen, Karlsruhe, Germany). Standard PCR program starts with 5 minutes (min) of denaturation at 95°C, followed by 35 cycles of denaturation at 95°C for 30 seconds (sec), annealing at 56 °C for 30 sec and elongation at 72°C for 1 min and a final elongation step at 72°C for 10 min. Amplified DNA fragments were detected via electrophoretic separation in agarose gel (1,,5 % (w/v), agarose; 1 x TAE; 0.5 mg/ml ethidium bromide; 1 x TAE electrophoresis buffer). Expected amplicon sizes are listed in table 8.

Detected alleles	Primer	Amplicons
- R26(shIGF1R1-6) - R26(shIR5) - Col1a1(VaLo_shEgln1)	1165_s: CCATGGAATTCGAACGCTGACGTC	Targeted allele: 365 bp Wt allele: no amplicon
	1165_as: TATGGGCTATGAACTAATGACCC	
- R26(shIR5_shIGF1R2)	1734_s: GTTGGGTCCACTCAGTAGATGCC	Targeted allele: 1050 bp Wt allele: no amplicon
	1734_as: GGAACATACGTCATTATTGACGTC	

Table 8: Primer used in genotyping and amplicon length. Transgenic mice were genotyped via PCR. Primers used for amplification and the expected amplicon sizes for targeted alleles are shown. Primer sequences are displayed in 5´-3´direction and are designated "sense" when coinciding with transcriptional direction. All primers were purchased from metabion, Martinsried, Germany.

2.2.12 Southern Blotting

Southern Blots were used to detect targeting of Cola1 locus, Cre-mediated deletion of the neomycin resistance gene from Col1a1(RMCE_2Neo) as well as RMCE-integration in Cola1(RMCE) and R26(RMCE). Probes and enzymes used for the particular detections are listed in table 9. 10 µg of genomic DNA were digested overnight using 40 U of enzyme, respectively to the detection to be performed. After separating fragments by size via electrophoresis in a 0.8 % (w/v) agarose gel at 90 V DNA was transferred to a Hybond^{TM} –XL nylon membrane (GE Healthcare, Freiburg Germany) by alkaline capillary transfer (194). Blotted DNA was crosslinked to the membrane by

baking at 80 °C for 1 h after washing two times with 2x SSC. Membrane was pre-hybridized in hybridization solution (1 M NaCl, 50 mM Tris-HCl (pH 7.5), 10 % (w/v) dextran sulfat, 0.1 % (w/v) SDS, 250 µg/ml sonicated salmon sperm) at 65 °C overnight in rotating hybridization tubes. Probes were generated by PCR or by digestion of plasmid DNA as stated in table 9 and labelled with α- ^{32}P-dCTP (PerkinElmer Life Science, Cologne, Germany) using Amersham Readyprime II Random Prime Labelling System (GE Healthcare, Freiburg Germany) following users manual. For hybridization labelled probes were added to pre-hybridization solution and incubated overnight at 65 °C in rotating hybridization tubes. Unspecifically bound probes were removed by washing hybridizes membrane initially twice with 2 x SSC/ 0.1 % (w/v) SDS under gentle shaking for 10-20 min, followed by one washing step in 0.2 x SSC/ 0.1 % (w/v) SDS until radiation of membrane is reduced to a value under 20 impulses per second (IPS). Washed membranes were sealed with plastic foil and exposed to autoradiography film Kodak BioMax MS; Sigma Aldrich, Deisenhof, Germany) at -80 °C for 3 days. Films were developed using automatic developer processing machine Curix60 (Agfa Health Care GmbH, Mortsel, Belgium).

Probe	**Size**	**Origin**
Rosa3´	386 bp	Digest of vector JS43 (TaconicArtemis, Cologne, Germany) with HindIII
Rosa5´	533 bp	PCR on vector JS32 (TaconicArtemis, Cologne, Germany) using R62s (AAGGATACTGGGGCATACG) and R64as (CTTCTCAGCTACCTTTACACACC)
internal_Neo	519 bp	Digest of vector KD602 (TaconicArtemis, Cologne, Germany) with HindIII and EcoRI
internal_Puro	292 bp	Digest of vector pMultilink Puro (TaconicArtemis, Cologne, Germany) with SpeI and XhoI
Col3´	451 bp	PCR on BAC (RPCIB731P14208Q, imaGenes, Nottingham) using

		ocol11(GGTCAGGATCTGACAGGTC) and ocol12 (GTCAGGGAGTGTCTCATCTGGC)
Col 5´	346 bp	PCR on BAC (RPCIB731P14208Q, imaGenes, Nottingham, UK) using Cola 5´_s (CCTCTTGCTGCTGCTCCCTCC) and Cola 5´_as (CCACCGTTATAGACCTACTCTTC)

Table 9: Probes used in Southern Blot analysis. Probes used for validation of RMCE integrations in R26(RMCE), Cola1(RMCE-2), for targeting of Cola1 locus with Col1a1(RMCE-2Neo), Cre-mediated deletion of Neo from Col1a1(RMCE-2Neo) and targeting of Cola1 locus with Col1a1(VaLo_shEgln1). Primer sequences are displayed in 5´-3´direction. All primers were purchased from metabion, Martinsried, Germany.

2.2.13 RNA Extraction and Quantitative Realtime-PCR (qPCR)

Realtime-PCR was applied to determine mRNA levels of IR, IGF1R and Egln1. Total RNA was extracted from murine ES-cells and tissue samples using Qiagen RNeasy Plus Mini Kit (Qiagen, Hilden, Germany) according to manufacturer´s introductions. 1 µg mRNA per sample was reversely transcribed using High Capacity cDNA Reverse Transcription Kit (Applied Biosystems, Darmstadt, Germany) following users manual. Quantification was performed by using gene specific TaqMan® Gene Expression Assays (Applied Biosystems, Darmstadt, Germany) and ABI Prism 7900HTFast real-time PCR System (Applied Biosystems, Darmstadt, Germany).Gene Expression Assays and Accession Numbers of the National Centre of Biotechnology Information (NCBI) used for assay selection are stated in table 10. Samples were adjusted for total RNA content to levels of heterochromatin protein 1 binding protein 3 (Hp1bp3). Relative cDNA amounts were quantified using Sequence Detector System (SDS) software version 2.1 (ABI). Threshold cycle (Ct) values were automatically converted to fold range RQ value ((RQ) = $2^{-\Delta\Delta Ct}$).

mRNA	Accession Number of reference sequence	Assay
IGF1R	NM_010513.2	Mm00802831_m1
IR	NM_010568.2	Mm01211881_m1
Egln1	NM_053207.2	Mm00459770_m1
tetR	DQ_414432	Mm01211881_m1
Hp1bp3	NM_010470.1	Mm00802807_m1

Table 10: TaqMan® Gene Expression Assays and NCBI – Accession Numbers. Assays used for quantification of IGF1R, IR and Hp1bp3 mRNA levels were purchased from Applied Biosystems, Darmstadt, Germany.

2.2.14 DNA-Sequencing

DNA-sequencing reactions were performed used Big Dye Termination v3.1 Cycle Sequencing System Kits (Applied Biosystems, Darmstadt, Germany). 400 ng DNA were used in a reaction mix containing 1.0 µl, 2.5 x Ready Reaction Premix (2.5x), 3.0 µl 5 x BigDye, Sequencing Buffer, 2.0 pmol/µl sense as well as antisense primer in a total volume of 10 µl. Amplification was performed following the program of 20 sec at 95 °C, 20 sec at 55 °C, 2 min at 60 °C for 25 cycles. Fluorescent-labelled fragment were purified by using Sephadex TM G-50 Medium (GE Healthcare Bio-science, Freiburg, Germany). DNA- sequence was automatically determined using ABI Prism 3130xl genetic Analyser. Evaluation of sequencing data was performed using Sequencher 4.9 (Gene Codes Corporation, Ann Arbor, USA) software.

2.2.15 DNA and RNA Quantification

Nucleic acid concentrations were determined by measurement of absorption at 260 nm using NanoDrop® ND-1000 UV-Vis Spectrometer (Peqlab, Erlangen, Germany). Quality of purified nucleic acid was estimated by 260/280 nm absorbance ratio.

2.3 Biochemistry

2.3.1 Protein Extraction

Total Protein was extracted from snap-frozen tissue samples. Tissues were disrupted in 3 ml lysis buffer (50mM HEPES (pH 7.4); 1% Triton X-100 (v/v); 50 mM NaCl; 10mM EDTA; 0.1% (w/v) SDS; Protease Inhibitor Cocktail Tablets mini (Roche Diagnostic, Mannheim, Germany), 1 tablet to 10ml; phosphataseinhibitorcocktail1 (Roche Diagnostic, Mannheim, Germany)100µl to 10ml) per mg sample and homogenized using TissueLyser II (Qiagen, Hilden, Germany) for 2 min at 30 Hz with 5 mm stainless steel beads (Qiagen, Hilden, Germany). Cell debris were removed by centrifugation at 13.000 rpm for 1 h at 4 °C. Lysed adipose tissues were centrifuged twice to get rid of formed fat layer. Supernatant was transferred to fresh vial.

2.3.2 Protein Quantification

Protein concentrations were determined using bicinchoninic acid (BCA) protein assay using Pierce BCA protein assay kit (Fisher Scientific, Schwerte, Germany) following manufacturer´s protocol.

2.3.3 Western Blotting

Protein extracts were diluted to a concentration of 2.5 mg/ml in organ lysis and 4 x SDS sample buffer (250 mM Tris-HCl (pH 6.8), 200 mM DTT, 8% (w/v) SDS, 40%

(v/v) glycerol, and 0.04% (w/v) bromophenol blue), incubated for a minimum time of 5 min at 95 °C. Samples were stored at -80 °C when not used immediately.

Protein extracts were separated by sodium dodecyl sulfate polyacrylamide gel electrophoresis (SDS-PAGE) on 4-12 % Novex® Tris-Glycine polyacrylamide gel (Invitrogen, Karlsruhe, Germany) in 1 x SDS running buffer. 50 -100 µg protein of each sample were applied to SDS gel. Unraveled protein were transferred to nitrocellose membranes (Invitrogen, Karlsruhe, Germany) using the iBlot® Dry Blotting System (Invitrogen, Karlsruhe, Germany). Membranes were blocked by incubating in 5 % (w/v) BSA in 1 x TBS, 0.1 % (v/v) Tween20 for 1 h rotating at room temperature. Target protein specific primary antibody were applied to the membrane in freshly prepared blocking solution, diluted as stated by manufacturer, and incubated overnight at 4 °C on a rotating device. After hybridization membranes were washed three times with 1 x TBS/0.01% (v/v) Tween20 for 5 min. Hybridization and washing procedure was repeated with Anti rabbit IG-HRP linked #7074 (Cell signaling Technology, Beverly, USA), used as secondary antibody. Membranes were incubated in ECL Western Blotting Substrate (VWR International, Langenfeld, Germany) for 15 min, sealed with plastic foil and exposed to chemiluminescence films (Kodak BioMax MS; Sigma-Aldrich Chemie GmbH, Deisenhof, Germany) and developed using an automatic developer processing machine Curix60 (Agfa Health Care GmbH, Mortsel, Belgium). For adjustment to total protein levels membranes were stripped by Incubating for 0.5-1 h at 56 °C in stripping buffer (100mM Mercaptoethanol, 2 % SDS and 62.5 mM Tris-HCl at pH 6.7) and blotting procedure was repeated with α-tubulin (DMA1) mouse mAb #3873 (Cell signaling Technology, Beverly, USA) in case of IR and IGF1R detection. Phospho-Akt and Phospho-GSK3 levels were adjusted to total Akt or total GSK3 levels, respectively. Used Antibodies are displayed below in table 11.

Target protein	Antibody
IGF1R	IGF-I Receptor β (111A9) Rabbit mAb #3018
IR	Insulin Receptor β (4B8) Rabbit mAb #3025
α-tubulin	α-Tubulin (DM1A) Mouse mAb #3873
Phospho-Akt	Phospho-Akt (Ser473) Antibody #9271
Total Akt	Akt (pan) (11E7) Rabbit mAb #4685
Phospho-GSK3	Phospho-GSK-3β (Ser9) (5B3) Rabbit mAb #9323
Total GSK3	GSK-3β (27C10) Rabbit mAb #9315

Table 11: Antibodies used for Western blot. Antibodies used for detection of IGF1R and IR expression levels as well as for the phosphorylation status of Akt and GSK3. All antibodies were purchased from Cell Signalling Technology, Beverly, USA.

2.3.4 Enzyme-linked Immunosorbent Assay (ELISA)

Serum Insulin levels were determined using Rat insulin ELISA Kit, #90010 (Crystal Chem., Downer Grove, IL, USA) and Mouse Insulin Standard 2ng # 90020 / INSSM021(Crystal Chem., Downer Grove, IL, USA), according to manufacturer´s guidelines. Serum IGF1 concentrations were detected using Quantikine Mouse/Rat IGF-I Immunoassay # MG100 (R&D systems, Wiesbaden, Germany)

2.3.5 Histological analysis

Pancreatic tissue samples were dissected, fixed overnight in 4% (w/v) PFA (Sigma Aldrich, Steinheim, Germany) and subsequently embedded for paraffin sections. Sections of 7 µm were deparaffinised and stained in hematoxylin and eosin. H&E (Sigma

Aldrich, Steinheim, Germany) staining was performed following standard protocols. Optical examination was performed using AxioVisio 4.2 (Carl Zeiss MicroImagin, Oberkochen, Germany)

2.4 Cell culture

2.4.1 Murine embryonic stem cell lines

Embryonic stem cell lines used in this thesis are C57BL/6NTac(TaconicArtemis, Cologne, Germany), a Taconic substrain of C57BL/6 hybrid line and B6/RMCE (TaconicArtemis, Cologne, Germany) C57BL/6NTac implying the previously described RMCE system at the R26 locus (Fig. 5) including zsGreen, and promoter hygromycin resistance gene.

2.4.2 Embryonic stem cell culture

Murine Es stem cells were cultured on a layer of mitomycin C treated primary feeder fibroblasts. Dulbecco's Modified Eagle Medium (DMEM) containing 20% fetal calf serum (FCS), 1 x non essential amino acids (MEM), 2 mM L-glutamine, 1 mM sodium pyruvate, 20 mM HEPES (pH 7.4), 0.1 mM 2-β-mercaptoethanol, 2000 U/ml LIF was used as culture medium. In case of the cell line B6/RMCE (TaconicArtemis) 150 μg/ml hygromycin was added to the medium whilst C57BL/6NTac (TaconicArtemis) cells were cultured without addition of antibiotics. ES cells were grown in 10 cm dishes, 6-well or 96-well culture plates (Falcon, Bedford, USA) and kept at 37 °C under humid atmosphere (95 %) with 7.5 % CO_2. ES cell colonies were splitted every 1-3 days. Culture plates were washed once with PBS and treated with trypsin at 37°C until cells detached from the plate surface. Cells were resuspended in an appropriate volume of media and splitted (usually 1:3 – 1:6) onto fresh feeder dishes.

For long term storage ES-cells were frozen in cryovials (Nunc, Wiesbaden, Germany) with 10% DMSO at -80°C and transferred into liquid nitrogen.

2.4.3 Transfection of ES cells with RMCE exchange vectors

2 x 10^5 ES cells were plated on a 6 well plate one day before transfection. For formation of transfection complex 6 µl Fugene6 Transfection Reagent was mixed with 100 µl serum free medium optiMEM I with Glutamax-I and incubated for 5 min at room temperature. 2 µg of circular exchange vector DNA (c=0.5 µg/µl) and 2 µg (c=0.5µg/µl) pCAGGS-flpe-ires-puro (125, 177) were added to 100 µl of the Fugene6/OptiMEM mixture and incubated for 45 min at room temperature. Subsequently this mixture was added drop wise to the medium of cultured cells and mixed by gentle circuiting movement. Medium of the transfected cells was changed one day after transfection. For simultaneous transfection of RMCE exchange vectors of R26 and Col1a1 RMCE systems same amount of each vector was used, as described above. From day 2 on, the medium was changed daily to medium containing either 200 µg/ml Geneticin (G418) after transfection with R26 exchange vectors, 1.5 µg/ml puromycin after transfection with Cola1 exchange vectors, or both antibiotics in same concentrations after transfection with exchange vectors of both RMCE-systems. Seven days after transfection, single clones were isolated by standard procedures as described (125, 178). Correct integration was subsequently validated by Southern Blot analysis.

2.4.4 Electroporation of ES cells with targeting vectors

For integration via homologues integration 100 µg of targeting vector were linearised by digestion with a single cutting restriction endonuclease in a total volume of 400 µl. Subsequently linearized vector DNA was purified by phenol-chloroform extraction. Reaction solution was mixed well with 400 µl Phenol-chloroform-isoamylalcohol, 25:24:1 in a Phase-Lock tube (5 Prime, Hamburg, Germany) and centrifuged for 5 min at 10.000 rpm. Supernatant was mixed with 400 µl chloroform-

isoamylalcohol, 24:1 in a new Phase-Lock tube (5 Prime, Hamburg, Germany) and centrifuged as described above. 1/10 Volume NaOAc pH 5.2 and 2 Volumes of Ethanol absolute were added to the supernatant and centrifuge at 13.000 rpm for 30 min at room temperature. DNA-pellet was washed in 1 ml 70% Ethanol, air dried and redissolved in TE buffer to a final concentration of 1ug/µl. $1x10^7$ PBS washed cells were resuspended in 700 µl Transfection buffer (20 mM HEPES (pH 7.0), 137 mM NaCl, 15 mM KCl, 0.7 mM Na_2HPO_4, 6mM Glucose, 0.1mM β- mercaptoethanol) and transferred to 30 µg linearized targeting vector DNA in a volume of 100 µl. This suspension was incubated for 5 min at room temperature in an electroporation cuvette (Biorad, Hercules, USA), prior to electroporation cells in a Biorad Gene Pulser (Biorad, Hercules, USA) at 500 µF and 240 V. Time constant values in the range of 6.0 - 8.0 ms were accepted. After incubating the electroporated cells for 5 min at room temperature suspension was transferred to 3.5 ml prewarmed Dulbecco's Modified Eagle Medium (DMEM) containing 20% fetal calf serum (FCS), 1 x non essential amino acids (MEM), 2 mM L-glutamine, 1 mM sodium pyruvate, 20 mM HEPES, 0.1 mM β-mercaptoethanol, 2000 U/ml LIF and $2.5x10^6$ (1 ml) cells were plated per 10 cm dish containing selection resistant feeder. Cells were cultured for 48 hours before start of selection with 200 µg/ml geneticin (G418) after electroporation with VaLo_shEgln1 and Col1a1(RMCE-2Neo) constructs

2.4.5 Doxycycline (dox) treatment of ES cells

Single ES cell clones were cultivated in ES cell medium, as described under 2.4.2, containing 1 µg/ml doxycycline (Sigma Aldrich, Steinheim, Germany) for 72 hours.

2.4.6 Cre- mediated in virto deletion

Floxed neomycin resistance gene was deleted from Col1a1(RMCE-2Neo) bearing cells by Cre-mediated in vitro deletion. Cre expression vector pHW1 (TaconicArtemis,

Cologne, Germany) was transfected by electroporation in circular form after purification by phenol-chloroform extraction as described under 2.4.3. 20 µg purified expression vector DNA were electroporated to $5x10^6$ PBS washed cells using Amaxa Cell Line Nucleofector™ KitR (Amaxa Biosystems, Cologne, Germany) following users manuals protocol A13. Total cells were plated on 10 cm dish containing selection resistant feeder. Cells were trypsinized one day after electroporation and $1x10^3$ to $1x10^4$ Cells were plated on 10 cm dish containing selection resistant feeder. Cells were incubated for 7 days selecting with 150 µg/ml hygromycin.

2.5 Mouse experiments

2.5.1 Animal care

General animal handling was performed as described by Hogan and Silver (167, 168). Mice were kept in a pathogen free facility at TaconicArtemis GmbH, Cologne, Germany in isolated ventilated cages TecniplastTM (Tecniplast Deutschland GmbH, Hohenpeißenberg, Germany) providing a High-Efficiency Particulate Air (HEPA) filter supply (Tecniplast Deutschland GmbH, Germany) and exhaust air (99.97 %). Mice were housed at 21°C +/- 1°C on a 12 h light / 12 h dark cycle with the light on from 7 a.m. to 7 p.m. Animals were fed *ad libitum* with Ssniff PS M-Z; S8289-Po12 (Ssniff Spezialdiäten GmbH, Soest, Germany) either as normal chow or with addition of 1 g/kg dox, for dox-induction. Withdrawn of food was only required prior accomplishment of glucose tolerance test for 16 h. All animals had access to water *ad libitum*. At the end of the study period, animals were sacrificed by CO_2 anaesthesia or cervical dislocation. All work was performed in accordance with the "Gesetz zur Regelung der Gentechnik" (GenTGS) October 2001 (German Biologic Act) and the Tierschutzgesetz 1998 (German Animal Welfare Act). Animal procedures and euthanasia were approved by the local government authorities (Bezirksregierung Köln) and were in accordance with National Institutes of Health guidelines.

2.5.2 Generation of transgenic mice

C57BL/6NTac mouse strains were obtained from Taconic. Chimeric mice were generated at TaconicArtemis GmbH by injection of trypsinized recombinant ES cell clones into diploid blastocystes and implanted into the uterus of pseudopregnant mice. Male chimeras were mated to C57BL/6NTac females to gain fully derived ES mice.

2.5.3 Body weight

Body weight was monitored daily from the first day of dox-induction for one week and subsequently in weekly interval for 7 more weeks.

2.5.4 Blood collection for determination of blood glucose levels and recovery of Serum

Whole venous blood was collected daily 2 h after beginning of light phase from the first day of Dox-induction for one week and subsequently in weekly interval for 7 more weeks by submandibular puncture of the *vena facialis*. Volumes of taken blood samples were 20 µl in daily and up to 100 µl in weekly collections. Fasted blood glucose values were measured using an automatic glucose monitor (Ascensia ELITE, Bayer Vital, Leverkusen, Germany). Serum was obtained after incubating blood for 30 min on ice and precipitation of cellular blood components by centrifugation for 15 min, at 13.000 rpm and 4°C.

2.5.5 Glucose and insulin tolerance test

For glucose tolerance tests (GTT), mice were fasted by withdraw of food overnight for 16 h. After determination of fasted blood glucose levels, each animal received 10 ml/kg body weight of 20 % glucose solution applied via an intraperitoneal injection. Blood glucose was determined in whole venous blood obtained after tail cut at 15, 30, 60 and 120 min after injection.

Insulin tolerance tests (ITT) was performed in random fed animal injected intraperitoneal with a 0.75 U/ml insulin solution (0.75 U/kg body weight) after determination of random fed blood glucose concentration. Blood glucose levels were estimated as described above 15, 30 and 60 min after injection.

2.5.6 Food intake

Daily food intake was measured over a period of 7 days for mice in groups of up to 2 animals per cage and calculated as the average intake per mice and day of chow over the time stated.

2.5.7 In vivo nuclear magnetic resonance measurement of fat content

Whole body fat content was determined in vivo by nuclear magnetic resonance using Minispec mq7.5 NMR analyzer (Brucker Optics, Ettlingen, Germany). Whole body fat mass is obtained as percentage of bodyweight.

2.5.8 Stimulation of Insulin cascade

For detection of Stimulation of Insulin cascade mice were fasted for 6 h and received 0.75 U/ml insulin solution (0.75 U/kg body weight) via intraperitoneal injection 30 min prior to dissection of tissue samples. Phosphorylation status of Akt at Ser473 and GSK3 at Ser9 was detected using Western blot.

2.6 Statistical Methods

2.6.1 Standard Deviation

Variability within data sets was estimated by their calculating standard deviation (σ).

$$\sigma = \sqrt{\frac{1}{N}\sum_{i=1}^{N}(\chi_i - \mu)^2} \quad \text{, where } \mu = \frac{1}{N}\sum_{i=1}^{N}\chi_i$$

2.6.2 Two-Tailed Unpaired Students T Test

Data sets were analyzed for statistical significance using a two-tailed unpaired student's T test.

$$T = \frac{\overline{\chi}_1 - \overline{\chi}_2}{SE(\overline{\chi}_1 - \overline{\chi}_2)} \quad \text{, where } SE(\overline{\chi}_1 - \overline{\chi}_2) = s_p\sqrt{\frac{1}{n_1} + \frac{1}{n_2}}$$

$$\text{and} \quad s_p = \sqrt{\frac{(n_1 - 1)s_1^2 + (n_2 - 1)s_2^2}{n_1 + n_2 - 2}}$$

p values where taken from tables of t-distribution comparing values of T to $t_{n1+n2\ -2}$ distribution. All p values below 0.05 were considered to be significant.

2.6.3 Analysis of variance (ANOVA) and Bonferroni post-test

Analysis of variance (ANOVA) and Bonferroni post-test were calculated using GraphPad Prism Version 4.0 by GraphPad Software Inc.

3 Results

3.1 Technical Development

3.1.1 Screen for efficient shRNAs directed against IGF1R

Two different strategies were tested for the simultaneous silencing of two target genes in transgenic mice. The first strategy is based on the generation of a murine ES cell line bearing two independent RMCE acceptor cassettes at distinct genomic loci. Such a cell line enables the specific integration of two different shRNA expression cassettes at the prepared RMCE alleles. As a second strategy, two shRNA expression units were combined in a single exchange cassette for integration into the R26 RMCE allele.
After evaluation, the method was applied for the generation of a mouse model providing the concurrent KD of the insulin and the IGF1 receptor. For silencing of IR, a previously described shRNA (shIR5) was used. Strong KD triggered by shIR5 has been demonstrated in ES cells as well as *in vivo* (126, 179). An shRNA sequence for efficient and specific silencing of IGF1R needed to be identified.

For silencing of IR a previously described shRNA (shIR5) was used. Strong KD triggered by shIR5 has been demonstrated in ES cells as well as *in vivo* (126, 179). To define a potent trigger for silencing of IGF1R, six shRNAs of different sequence were designed using the invitrogen algorithm BLOCK-iT™ RNAi Designer. Those were inserted into R26 RMCE exchange vectors for shRNA expression, yielding pR-shIGF1R1 to pR-shIGF1R6. Single copies of each vector were stably integrated into the murine ES cell line B6/RMCE by employing the R26 RMCE system (126). Correct RMCE was confirmed by Southern blot analysis (Fig. 6A). Expected signal sizes are 4.3 kb for R26 wt allele, 3.8 kb for R26(RMCE) allele before exchange and 6.2 kb for R26(RMCE) allele after exchange. The employed shRNA expression system allows tet-repressor (tetR)-mediated temporal control of RNAi. Transcription of the shRNA is blocked in absence of dox by binding of co-expressed tetR to the tet-operator (tetO), inserted in H1tetO (Fig. 6B). Upon administration of dox tetR detaches from H1tetO and

allows Pol III-dependent transcription of the encoded shRNA (Fig. 6C). Efficiency of IGF1R silencing was analyzed in ES cells via qPCR after doxycyclin induction in two clones per shRNA (Fig. 6D). Values are displayed as percentage of IGF1R expression in untreated cells of each clone. KD efficiencies were ranging between 13 % and about 50 % remaining IGF1R mRNA levels, as average of both clones. The most potent effect was observed for shIGF1R2 at 13 % residual IGF1R expression, which was therefore selected for further procedure.

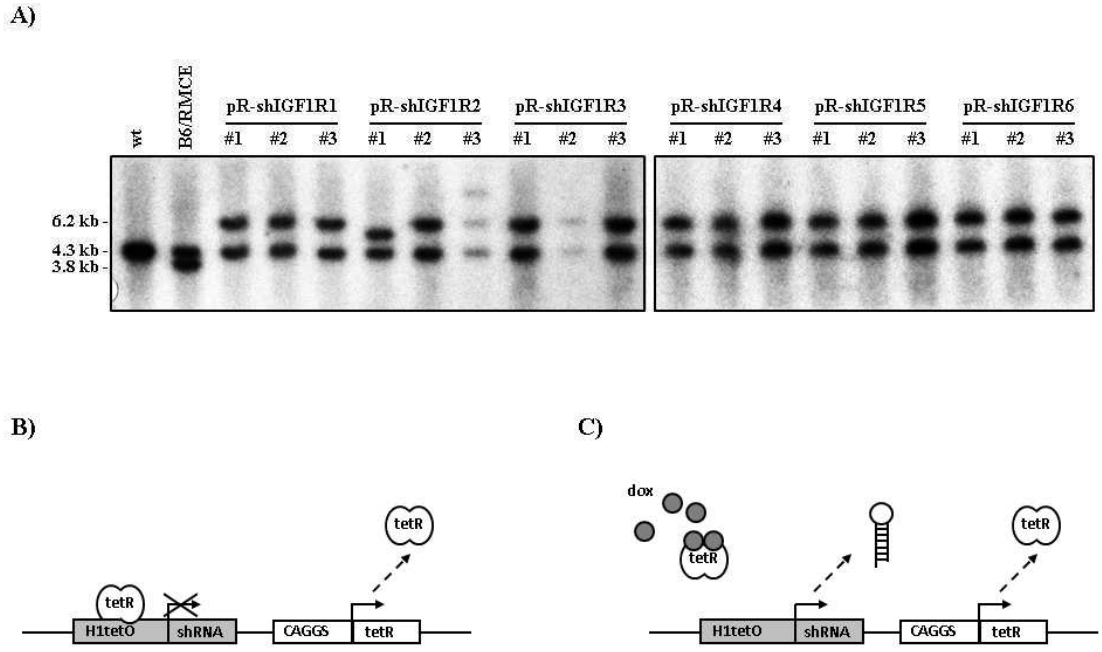

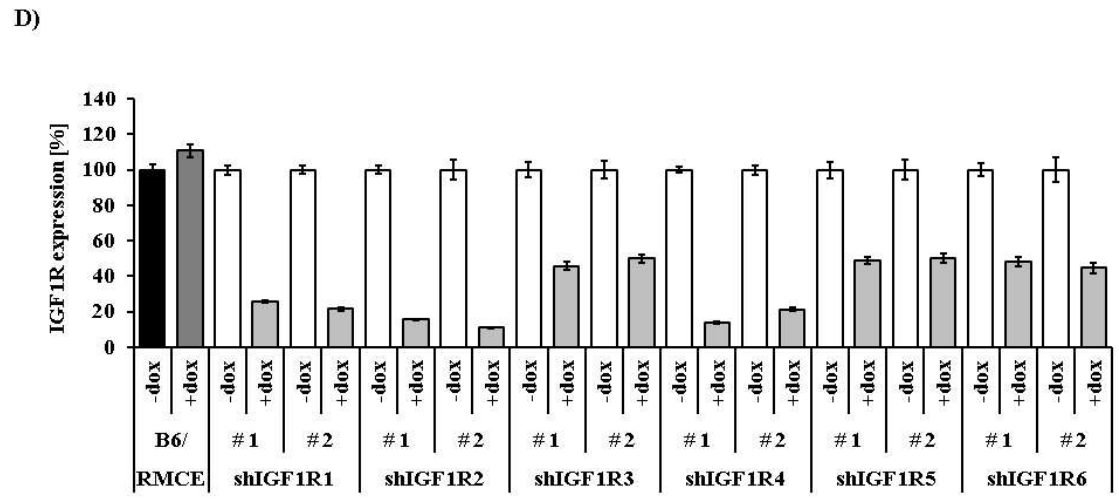

Fig. 6: Screen for efficient shRNAs against IGF1R. Six shRNAs, shIGF1R1 to shIGF1R6, were tested for their KD efficiency in murine ES cells. Single copies of shRNA expression vectors, pR-shIGF1R1 to pR-shIGF1R6 were stably integrated in B6/RMCE employing the R26 based RMCE system. **A)** Southern blot was used to control 3 clones per vector for correct integration. Expected sizes for R26 wt allele, R26(RMCE) allele before and after exchanged were 4.3 kb, 3.8 kb and 6.2 kb, respectively. The used shRNA expression system allowed tetR-mediated temporal control of RNAi, depicted in a schematic view. **B)** Transcription is blocked in the absence of dox by binding of the co-expressed tetR to H1tetO. **C)** Upon administration of dox tetR detaches from the promoter allowing transcription of the shRNA. **D)** mRNA expression rates of IGF1R were measured under conditions of induced (+dox, light grey bars) and not induced (-dox, white bars) shRNA expression in duplicates of two clone per shRNA. Induced (+dox, dark grey bar) and not induced (-dox, black bars) B6/RMCE cells were applied as negative control. Expression in not induced cells was set as 100 % for each clone. Values are mean ± SEM.

3.1.2 Generation of murine ES cell line bearing two RMCE alleles (first strategy)

This strategy is based on the generation of a murine ES cell line harbouring two alleles prepared for RMCE integration, to allow the simultaneous and specific integration of two inserts via cassette exchange, hereafter designated as double RMCE (dRMCE).
A established singular RMCE system, mediating integration into the in the Rosa 26 locus, served as a technical basis for this approach (125).

As a first step a second RMCE system (RMCE-2) had to be designed, whose architecture rules out interactions with the R26 system to allow the employment of both approaches in one cell line. RMCE-2 was designed by example of the R26 RMCE system in terms of the used RMCE-strategy, recombinase and marker-system. Functionality of

RMCE-2 is based on FLP mediated recombination of two pairs of FRT and F5 sites. The employed F5 site is a functional FRT mutant displaying no interaction to FRT and F3 sites (168). A β-galactosidase gene (lacZ) in the acceptor cassette allows verification of cells bearing a prepared RMCE-2 locus by β-galactosidase staining. Permanent antibiotic selection had to be omitted because the three resistance markers, well established for the adopted cell line, are elsewhere used in R26 RMCE and RMCE-2. In presence of Flp recombinase donor and acceptor cassette are exchanged between vector and genome through recombination of FRT and F5 pairs (Fig. 7C). Correct recombination of the FRT site sets a truncated, non functional, puromycin resistance gene (5´dPuro) in the donor cassette into the frame of an ATG at the genomic RMCE-2 site and facilitates it's expression by employing a PGK-promoter. Transcription of 5´ dPuro after unspecific integration events is blocked by a polyadenylation signal (pA) in the exchange vector. Thus, clones positive for exchange in RMCE-2 can be selected by puromycin treatment of transfected cells.

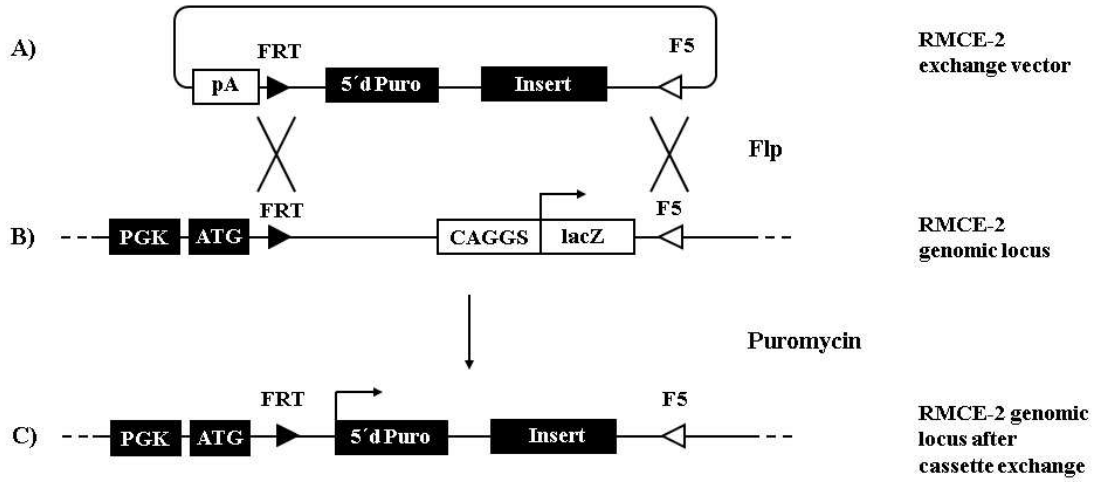

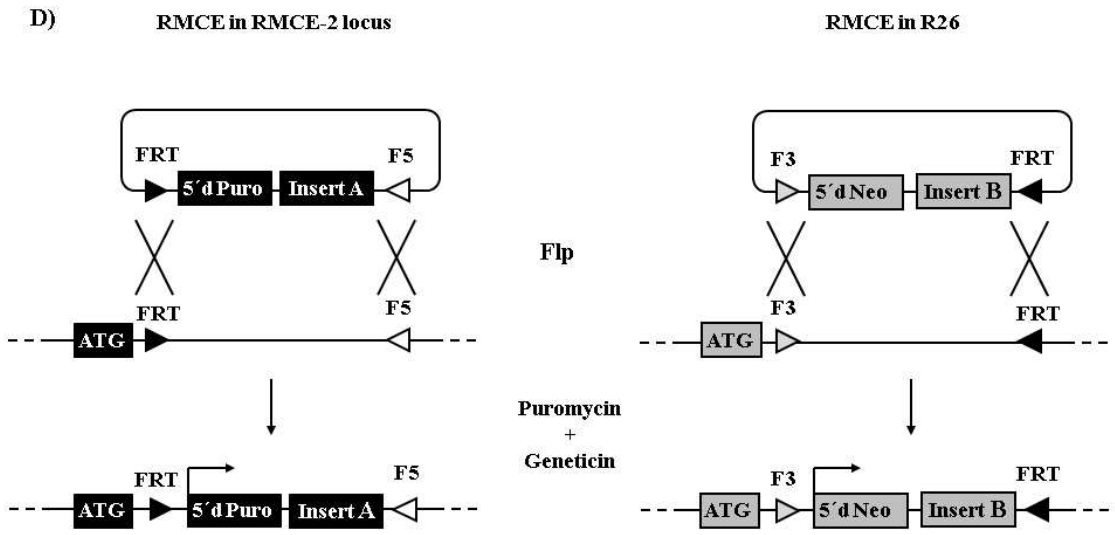

Fig. 7: Functionality of RMCE-2 system. A) The RMCE-2 exchange vector carries following features in 5´-3´direction: polyadenylation signal (pA), FRT site, puromycin resistance gene leaking start codon and promoter (5´dPuro), insert, F5 site. **B)** The genomic part of RMCE-2 is composed of following elements in 5´-3´direction: phospoglyceratkinase-promoter (PGK), start codon (ATG), FRT site, CAGGS promoter driven β-galactosidase gene (lacZ), F5 site. **C)** Cassette exchange is mediated through double reciprocal recombination of both pairs of FRT and F5 sites. Functionality of 5´dPuro is reconstituted through RMCE reaction, selection of positive clones can be carried out by puromycin treatment. **D)** RMCE-2 was designed to act independently from the R26 based system to allow the simultaneous use of both systems. Expression of both selection markers is exclusively given by correct integration of RMCE-2 cassette in RMCE-2 locus and correct exchange between R26 RMCE donor and acceptor cassette. Specificity between R26 RMCE and RMCE-2 is achieved by the choice of the utilized recognition sites and the architecture of marker systems exclusively activated by specific exchange.

To allow the combined application of RMCE-2 and R26 RMCE systems in one cell line, interactions between both systems had to be turned out by their architecture. Incompatibility between RMCE-2 and R26 RMCE systems is obtained through the choice and order of recombination sites and arrangement of selection systems.

The RMCE-2 system employs couples of FRT and F5 sites whilst the R26 RMCE system uses FRT and F3 pairs, making cassette exchange through double reciprocal recombination specific for each associated couple of acceptor and donor cassette. Furthermore, architecture of the marker systems affords antibiotic selection after specific exchange in both RMCE loci. Reconstitution of the selection marker in RMCE-2 depends

on the correct recombination of the FRT site, whereas it depends on recombination of the F3 site in the R26 system. Since FRT and F3 sites are part of the reading frame of the accordant resistance genes activation of those is exclusively given by exchange of R26 RMCE donor and acceptor cassette and RMCE-2 donor and acceptor cassette. RMCE-2 was designed to act independently from R26 RMCE. Using both systems in one ES cells line should afford the specific exchange in both systems. Cells bearing both RMCE loci exchanged correctly can be selected by concurrent treatment with both antibiotics, puromycin and geneticin (G418) (Fig. 7D).

To constitute the designed dRMCE system the genomic part of RMCE-2 was integrated into the murine ES cell line B6/RMCE, already bearing the R26 RMCE system, to yield a cell line comprising two loci prepared for RMCE. The locus of collagen, type I, alpha 1 (Col1a1) was chosen for integration of RMCE-2 as a promising candidate. This locus was previously targeted by Beard *et al*.. Transgenes inserted at the Col1a1 locus exhibited high transcriptional active in almost every tissue (180, 181).
The exact site of integration was located in an intergenic region about 0.5 kb downstream of the 3´UTR of the Col1a1 gene and about 7 kb upstream of the Sarcoglycan α gene. A targeting vector, pCol1a1T(RMCE_2Neo), was cloned for integration of the genomic part of the RMCE-2 system via homologous recombination (Fig. 8A). Beside the described elements of the RMCE-2 system pCol1a1T(RMCE_2Neo) carries a loxP flanked, PGK driven, Neo resistance gene to afford antibiotic selection after targeting. The targeted Col1a1(RMCE-2Neo) allele was confirmed by Southern blot (Fig. 8C). Signals were expected for Col1a1 wt allele and Col1a1(RMCE-2Neo) at 9.3 kb and 8.5 kb, respectively. Neo was subsequently removed by Cre-deletion after successful targeting, to make G418 available for selection after exchange in R26(RMCE) again. The resulting Col1a1(RMCE-2) locus was detected by Southern blot (Fig. 8D). Expected sizes for Col1a1 wt allele, Col1a1(RMCE-2Neo) and Col1a1(RMCE-2) were 8.3 kb, 10.4 kb and 9.5 kb, respectively. By insertion of RMCE-2 in Col1a1 of B6/RMCE the ES cell line B6/dRMCE was generated, carrying two independent RMCE alleles in R26(RMCE) and Col1a1(RMCE-2).

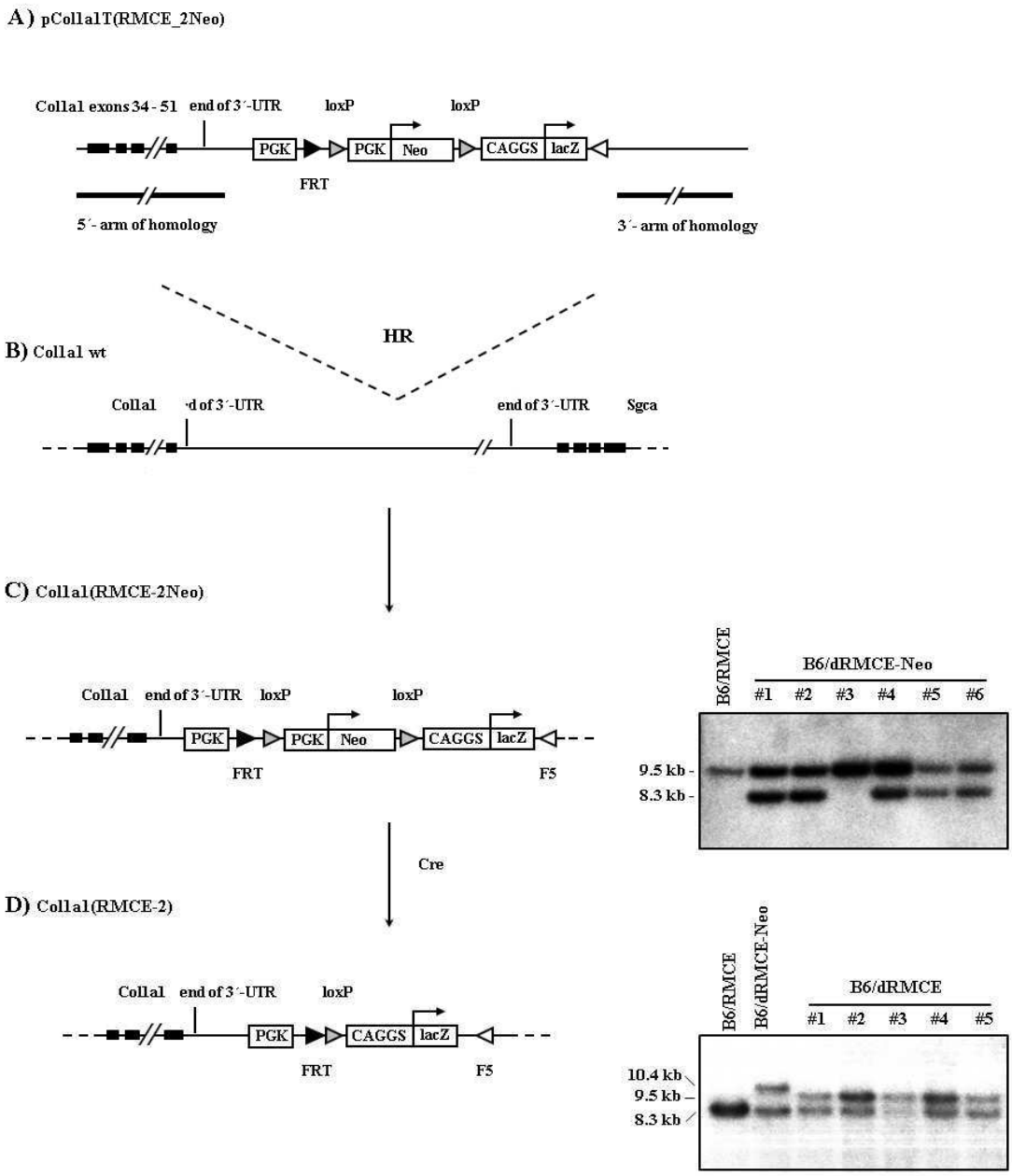

Fig. 8: Generation of ES cell line B6/dRMCE. A) The genomic part of RMCE-2 was integrated into the Col1a1 locus of B6/RMCE ES cells using the targeting vector pCol1a1T(RMCE_2Neo). A loxP flanked Neo resistance gene was used for selection after targeting. **B)** The site of integration is situated about 500 bp downstream of the 3´UTR of the Col1a1 gene. **C)** Targeted Col1a1(RMCE-2Neo) allele was detected by Southern Blot. Expected sizes for Col1a1 wt allele and Col1a1(RMCE-2Neo) were 9.3 kb and 8.5 kb, respectively. Neo was deleted by Cre after targeting. **E)** The resulting Col1a1(RMCE-2) locus was detected

by Southern blot. Expected sizes for Col1a1 wt allele, Col1a1(RMCE-2Neo) and Col1a1(RMCE-2) were 8.3 kb, 10.4 kb and 9.5 kb, respectively.

Exchange Vectors for both systems were cloned to perform simultaneous integration in R26(RMCE) and Col1a1(RMCE). Both vectors were designed as shRNA expression vectors. The vector pC-shIR5 was cloned as an exchange in Col1a1(RMCE-2) and for expression of shIGF1R2. For integration in R26(RMCE) and expression of shIGF1R2 the vector pR-shIGF1R2 was constructed. Transfection of both vectors in B6/dRMCE was performed concurrently to achieve integration of both shRNA expression cassettes. To elucidate whether exchange is specific for each RMCE-system cells were separately transfected with each singular exchange vectors. Selection was carried out with puromycin and, or G418, according to transfected exchange vectors.

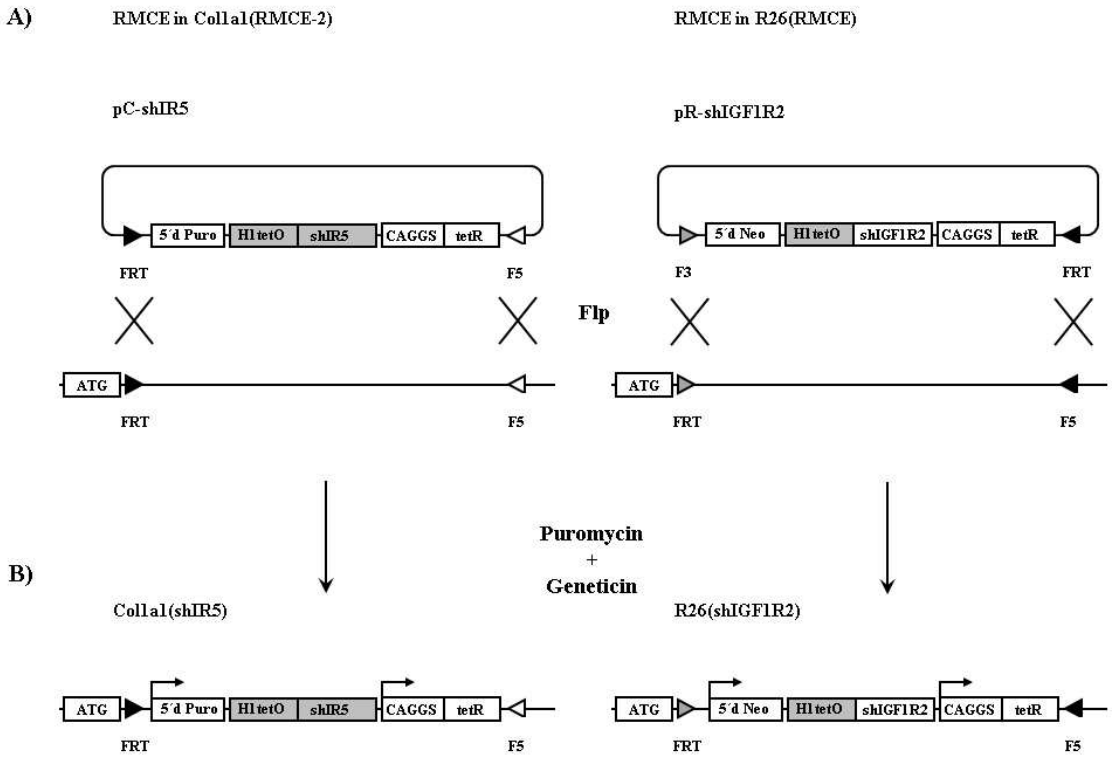

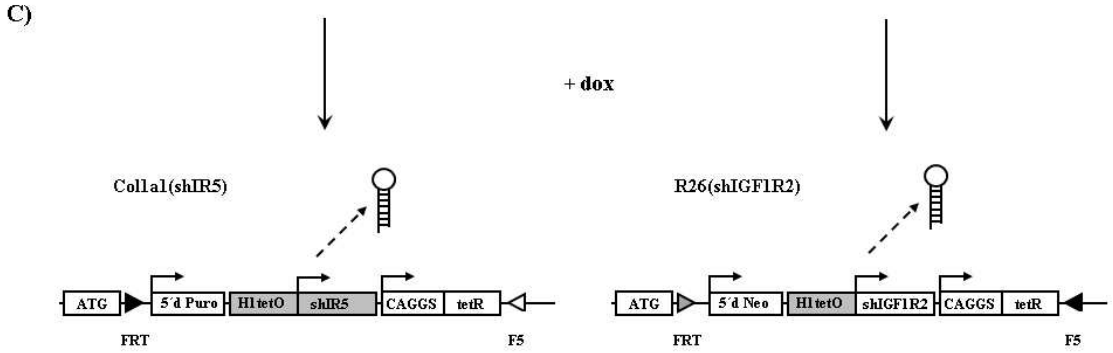

Fig. 9: Integration of inducible shIR5 and shIGF1R2 expression vectors applying dRMCE in B6/dRMCE cells. A) Col1a1 RMCE exchange vector pC-shIR5 and R26 RMCE exchange vector pR-shIGF1R2 for inducible RNAi were simultaneously transfected into B6/dRMCE do be integrated via dRMCE. **B)** Clones positive for Col1a1(shIR5) and R26(shIGF1R2) were selected using puromycin and G418 in respect to the selection markers of both RMCE-systems. **C)** Expression of shIR5 and shIGF1R2 by the H1tetO promoter can be induced by administration of doxycycline (dox).

Correct integration of each donor cassette into it´s dedicated RMCE loci was confirmed by Southern blot (Fig. 10). Two external probes were used for validation of each RMCE locus. Col5´and Col3´ probes were applied for validation of exchange in Col1a1(RMCE) and Rosa5´and Rosa3´ probes for exchange in R26(RMCE). Furthermore the internal probes iNeo and iPuro were used. Used restriction enzymes (RE) and expected fragment sizes for wild type (wt) alleles of R26 and Col1a1 as well as for RMCE alleles, R26(RMCE) and Col1a1(RMCE-2), before and after exchange given by each probe are listened in table 12.

allele / probe: RE	R26 (wt)	Col1a1 (wt)	R26 (RMCE)	Col1a1 (RMCE-2)	R26 (shIGF1R2)	Col1a1 (shIR5)
Rosa5´: HindIII	**4.4 kb**	**-**	**3.9 kb**	**-**	**6.2 kb**	**-**
Rosa3´: BamHI	**5.8 kb**	**-**	**9.5 kb**	**-**	**3.2 kb**	**-**
Col5´: MfeI	**-**	**10.7 kb**	**-**	**4.2 kb**	**-**	**5.0 kb**
Col3´: AvrII/BmtI	**-**	**8.3 kb**	**-**	**11.6 kb**	**-**	**6.0 kb**
iPuro: EcoNI	**-**	**-**	**8.9 kb**	**14.6 kb**	**6.7 kb**	**7.0 kb**
iNeo: BamHI	**-**	**-**	**-**	**-**	**5.5 kb**	**-**

Table 12: Expected fragment sizes in Southern blot analysis of dRMCE. Used restriction enzymes (RE) an expected fragment sizes resulting from each relevant allele are shown for corresponding probe. Wild type alleles, Col1a1(wt) and R26(wt), RMCE alleles before exchange R26(RMCE) and Col1a1(RMCE-2), as well as RMCE alleles after exchange Col1a1(shIR5) and R26(shIGF1R2) are listened.

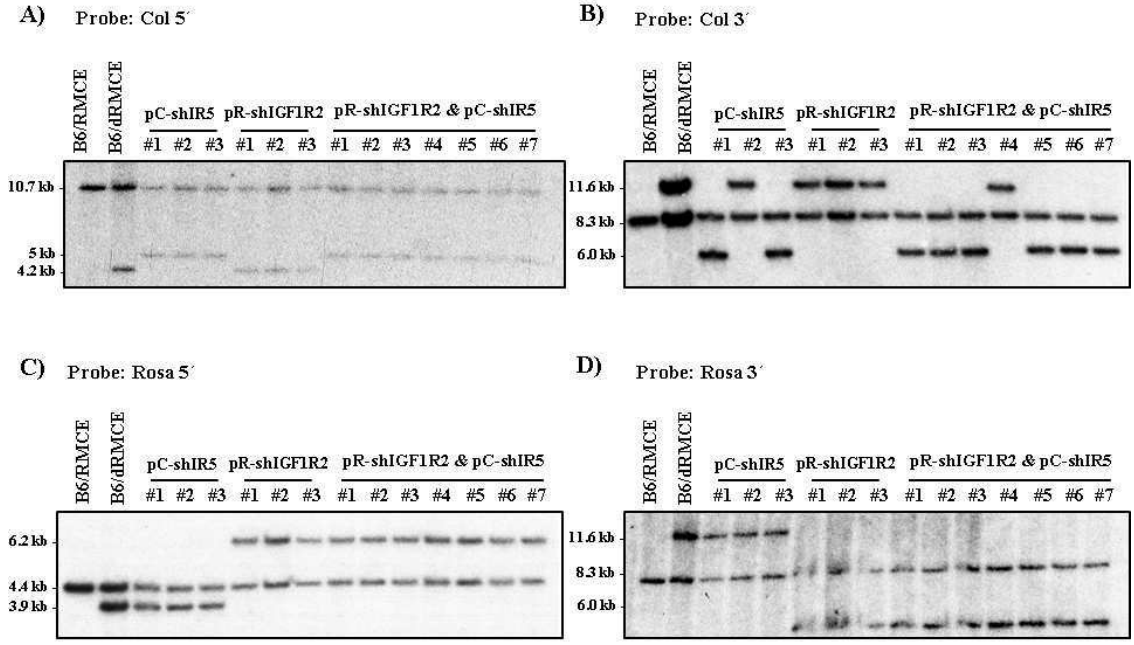

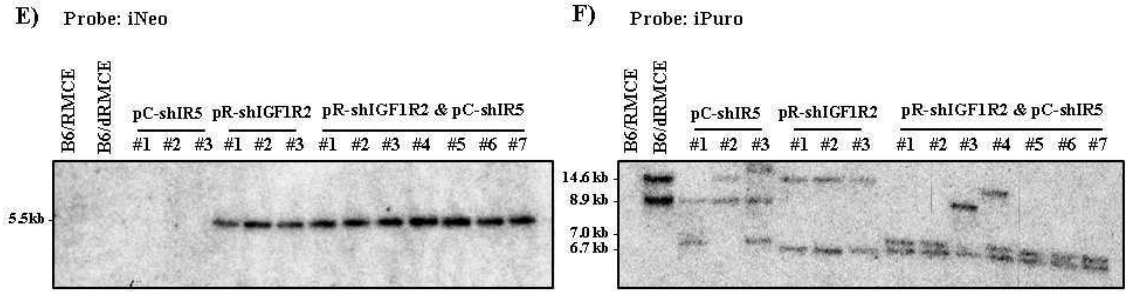

Fig. 10: Southern Blot analysis after dRMCE in B6/dRMCE. Correct exchange in R26(RMCE) and Col1a1(RMCE-2) is shown by using internal and external binding probes: **A)** Col5´, **B)** Col3´, **C)** Rosa5´, **D)** Rosa3´, **E)** iNeo and **F)** iPuro. Expected signals sizes for wt alleles and RMCE alleles before and after exchange are listened in table 12. Transfected exchange vectors are indicated above. pC-shIR5 and pR-shIGF1R2 were transfected together to achieve dRMCE, whilst both vectors were transfected solely for single integration into their distinct loci. Untransfected B6/RMCE and B6/dRMCE cells were used as control.

Among the 7 depicted clones, transfected with both exchange vectors, 5 displayed the expected pattern of both RMCE cassettes exchanged, showing signals of Col1a1(shIR5) and R26(shIGF1R2) as well as wt alleles of R26 and Col1a1.

All clones transfected with single R26 exchange vector, pR-shIGF1R2, had the expected signals of the exchanged R26(shIGF1R2) allele, not exchanged Col1a1(RMCE) allele and both wt alleles. Among clones transfected with single Col1a1 exchange vector, pC-shIR5, just clone #1 displayed signals of the exchanged RMCE-allele Col1a1(shIR5), unexchanged R26(RMCE) and both wt alleles.

Altogether 45 puromycin and G418 resistant clones yielded after divers accomplished transfections with both exchange vectors were analysed by Southern blot (data not shown). 36 of these had the expected pattern of both RMCE loci exchanged, demonstrating that dRMCE was successful in about 80 % of cells resistant to both antibiotics. 6 clones received from transfection solely with R26 exchange vector were verified (data not shown). Four of these were positive for single exchange in R26 in Southern blot. Negative clones gave wrong signals for R26 probes but not for the other applied probes, suggesting that recombinase mediated interactions of the R26 exchange

vector are restricted to its dedicated RMCE locus. Moreover, 10 clones obtained after transfection exclusively with the Col1a1 exchange vector were analysed (data not shown). Six of these were positive with all the probes. Two of the negative clones showed divergent signals for R26 probes, suggesting undesired interactions of the Col1a1 exchange vector with the R26 RMCE locus.

For further demonstration of RMCE integration the KDs, triggered by the inserted shRNAs cassettes were verified by qPCR analysis. Silencing of both target genes was verified in clones, harbouring either a single or both shRNA expression cassettes, after inducing RNAi by dox treatment (Fig. 11). Target gene expression in untreated (-dox) cells of each clone was set as 100 %. Doxycycline induced and uninduced B6/dRMCE cells served as control.

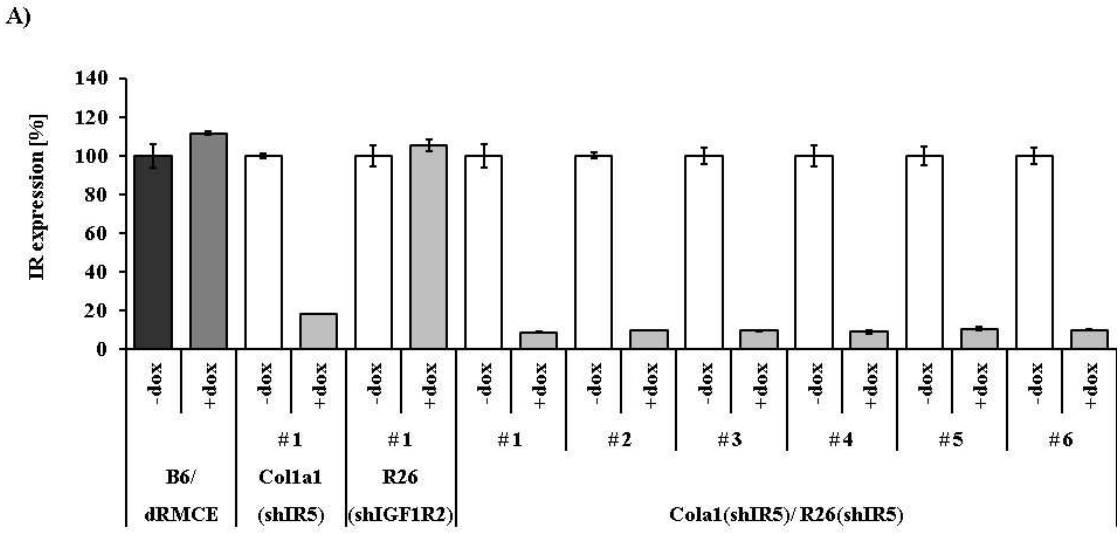

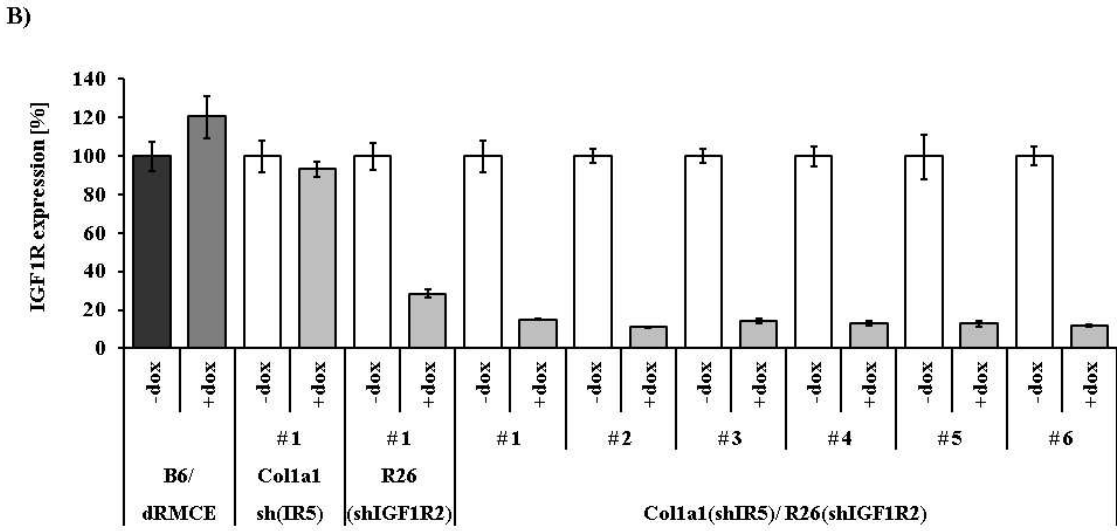

Fig. 11: KD in ES cells obtained from single and double RMCE in B6/dRMCE. Expression of **A)** IR and **B)** IGF1R was measured in clones bearing either Col1a1(shIR5) or R26(shIGF1R2) after single RMCE and in clones bearing both loci exchanged after dRMCE. Target gene expression was determined after inducing RNAi by dox administration (+dox, white bars). Accordant gene expression in untreated cells (-dox, grey bars) of each clone was set as 100%. Untransfected B6/dRMCE cells (black bars) served as negative control under induced and not induced conditions. Detection of target genes was performed in duplicate of each clone and are shown in percent of expression in induced B6/dRMCE cells (+dox, black bars). Values are mean ± SEM.

In accordance to the integrated shRNAs, clones bearing both exchanged RMCE loci, Col1a1(shIR5) and R26(shIGF1R2), displayed silencing of either target genes. IR expression was reduced to about 10 % and IGF1R expression to about 15 % of the original mRNA levels. Single transfected clones just exhibited target mRNA reduction accordant to the integrated shRNA expression unit. IR expressions were reduced to about 20 % in single transfected cells bearing Col1a1(shIR5), whilst IGF1R mRNA levels were unaffected. The opposite picture was observed in cells bearing R26(shIGF1R2). IGF1R mRNA levels were reduced to about 30 % whilst IR expression remained unchanged.

Taken together, a murine ES cell line was generated bearing two independent RMCE alleles, R26(RMCE) and Col1a1(RMCE). Functionality of dRMCE was demonstrated by simultaneous integration of two shRNA expression cassettes. Specific

exchange in both loci was confirmed by Southern blot and indirectly confirmed by KD of both target genes, demonstrated functionality of dRMCE in the given cell line. dRMCE showed to work with an efficiency of about 80%.

3.1.3 Evaluation of Col1a1 as a locus for transgenic expression (first strategy)

In parallel to the generation of B6/dRMCE Col1a1 was characterized avoiding the complexity of constituting the RMCE-2 allele to clarify whether the locus fulfills the central demands for RMCE applications in terms of transgene expression properties for shRNAs and mRNAs. An inducible shRNA expression construct (VaLo_shEgln1) was designed to be inserted at the positions intended for RMCE-2 integration (Fig. 12A). VaLo_shEgln1 bears the elements of the doxycycline inducible shRNA expression system: H1tetO promoter, shRNA and CAGGS promoter driven tetR gene and a PGK driven Neo gene for selection after targeting. Due to interest of an independent project, an shRNA against EGL nine homolog 1 (Egln1) was used for locus validation. Integration of VaLo_shEgln1 allowed evaluating the efficiency and functionality of the inducible shRNA expression system as well as the expression profile of transgenic mRNAs integrated in Col1a1. Col1a1(VaLo_shEgln1) positive clones were identified by Southern blot after targeting (Fig. 12B). Expected sizes for Col1a1 wt allele and Col1a1(VaLo_shEgln1) were 9.5 kb and 7.9 kb, respectively.

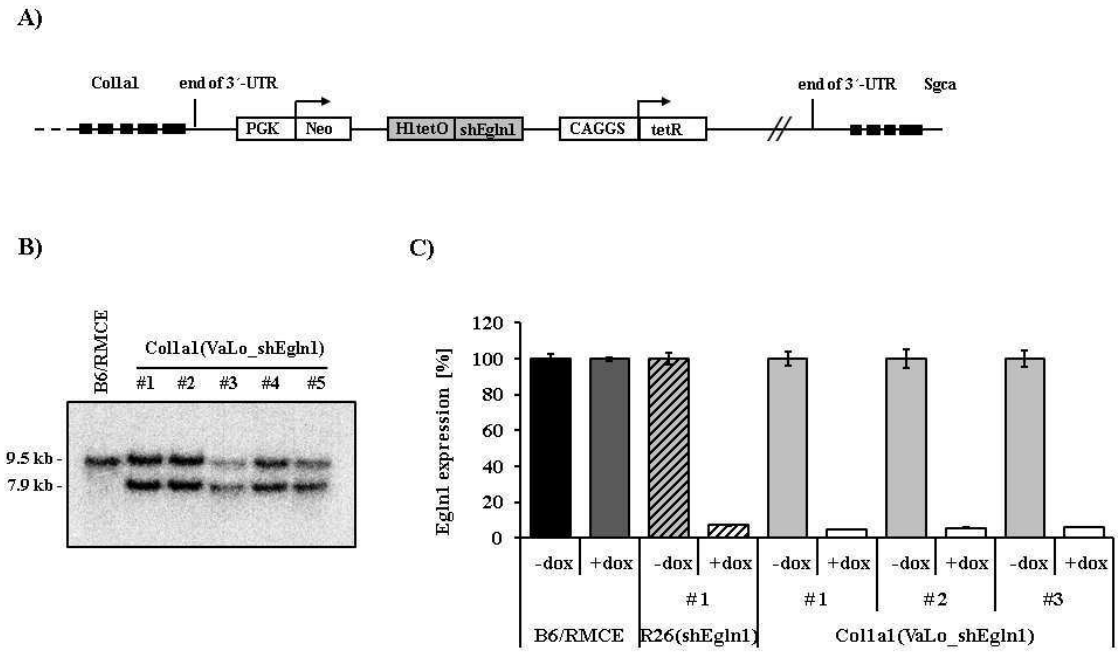

Fig. 12: VaLo_shEgln1 was used for characterization of Col1a1 as a locus for RMCE-2 application. VaLo_shEgln1 affords evaluation of Col1a1 as a locus for the application of the inducible RNAi system as well as for expression of transgenic mRNAs. **A)** The components of VaLo_shEgln1 were Neo driven by PGK promoter, pA, H1tetO promoter, shEgln1, and CAGGS driven tetR gene. VaLo_shEgln1 was integrated at the position designated for integration of RMCE-2 system downstream of Col1a1. **B)** Correct integration was verified by Southern blot. Expected sizes for Col1a1 wt allele and ol1a1(VaLo_shEgln1) were 9.5 kb and 7.9 kb, respectively. **C)** RNAi was induced in three ES cells bearing Col1a1(VaLo_shEgln1) (+dox, white bars) and compared to cells under not induced conditions (-dox, gray bars). Untreated (-dox, grey striped bar) and induced (+dox, white striped bars). R26(Egln1) cells served as a reference for KD efficiency. Not induced (-dox, dark grey) and induced wild type cells (+dox, black bars) served as negative control. Egln1 mRNA levels were detected in duplicated for each clone and are shown as percent of expression in induced wild type cells. Values are mean ± SEM.

First indications about the characteristics of Col1a1 were obtained from analyzing the shRNA mediated silencing of Egln1 in ES cells (Fig. 12C). Target mRNA reduction was measured under doxycyclin induced and not induced conditions in three clones bearing Col1a1(VaLo_shEgln1). Induced and not induced B6/RMCE cells served as negative control. Egln1 mRNA levels were reduced to about 5 % of their original concentration upon induction. R26(shEgln1) cells, expressing shEgln1 employing the

same inducible system, served as a reference for RNAi efficiency and displayed target gene reduction comparable to Col1a1(shEgln1) cells.

After obtaining promising results in ES cells heterozygote Col1a1(VaLo_shEgln1) mice were generated to examine RNAi efficiency and transgene expression from Col1a1 *in vivo*. Silencing of Egln1 was determined in male mice after inducing RNAi for 10 days by feeding chow containing 1g doxycyclin /kg. Not induced target mice as well as induced and not induced wt mice served as control. Remaining Egln1 levels were measured in total brain, heart, skeletal muscle, liver, kidney, spleen, epigonadal white adipose tissue (EWAT) and brown adipose tissue (BAT) by pPCR (Fig. 13A). R26(shEgln1) mice served as a reference for KD efficiency and functionality of the inducible system (Fig. 13B). Expression rates in induced wt mice were set as 100 % for each tissue. Egln1 expression in induced Col1a1(VaLo_shEgln1) +dox mice was reduced to levels ranging between 2 % remaining mRNA in heart, skeletal muscle and kidney as best results and about 16 % in spleen. Despite in liver and spleen observed RNAi efficiencies were comparable or even slightly higher compared to mRNA reduction observed in R26(shEgln1), resulting in a remaining Egln1 expression between 3% and 10%. Unfortunately untreated Col1a1(VaLo_shEgln1) -dox control mice exhibited significant reduction of Egln1 mRNA in several tissues without shRNA expression being induced by doxycyclin administration, reflecting an insufficient control of shRNA expression by the given RNAi system in Col1a1. Leakiness occurred strongest in kidney showing a KD to 13 %. Brain, heart, liver, spleen, EWAT and BAT display reductions of target gene transcription to between 30 % and 60 % in control target animals. Among the examined tissues tightly controlled RNAi was only observed in muscle. Tissue depended leakiness is a known disadvantage of the employed RNAi system. Integrated in R26 this effect commonly occurs in brain and kidney as confirmed by the shown data (Fig. 13B). Slight target mRNA reduction was observed for BAT of control animals, as well. In contrast to Col1a1(VaLo_shEgln1) samples, the remaining tissues, considered for R26, exhibited tight controlled RNAi.

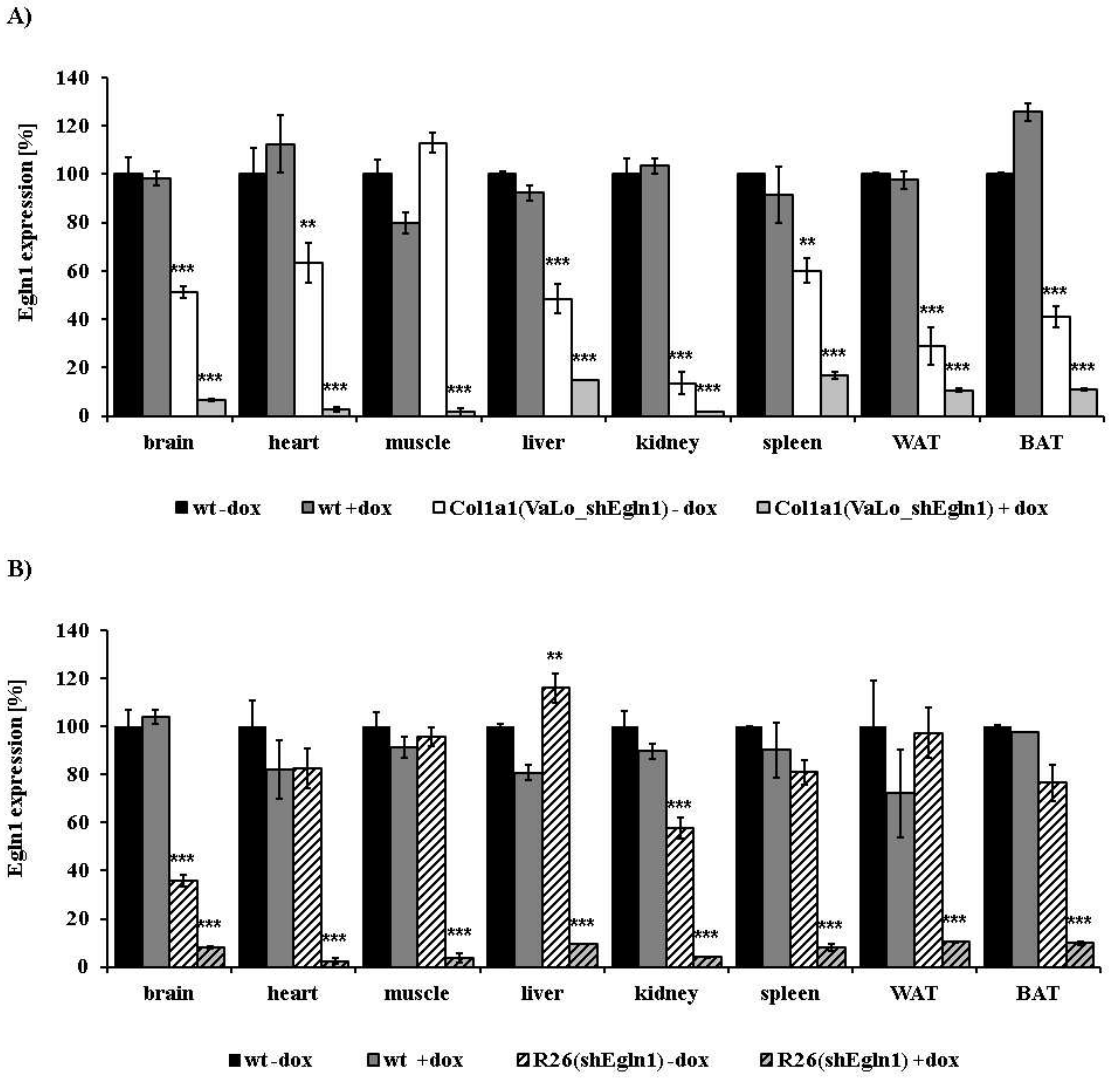

Fig. 13: Inducible RNAi in Col1a1(VaLo_shEgln1) mice. KD efficiency and inducibility of Col1a1(VaLo_shEgln1) were evaluated in brain, heart, skeletal muscle, liver, kidney spleen, epigonadal white adipose tissue (EWAT), brown adipose tissue (BAT). **A)** Egln1 expression is shown in untreated (-dox, light grey bars) and dox induced (+dox, white bars) Col1a1(VaLo_shEgln1) mice. Not induced (-dox, dark grey) and induced wild type mice (+dox, black bars) served as negative control. **B)** R26(shEgln1) mice, encoding shEgln1 in a VaLo_shEgln1 accordant construct integrated in R26, served as a reference for efficiency. Egln1 expression was detected in untreated R26(shEgln1) mice (-dox, light grey striped bars) and mice upon doxycyclin induction (+dox, white striped bars). Not induced (-dox, dark grey) and induced wild type mice (+dox, black bars) were used as negative control. Remaining Egln1 mRNA levels were estimated by qPCR and displayed as percentage of expression in doxycycline treated wild type mice (+dox, black bars). All values are mean ± SEM. For each group n=3. *, $P \leq 0.05$; **, $P \leq 0.01$; ***, $P \leq 0.001$ versus wt -dox.

Lastly, transgenic mRNA expression properties of Cola1a were verified by determining the transcription pattern of CAGGS driven tetR gene in Col1a1(ValLo_shEgln1) mice. Egln1 mRNA was detected in brain, skeletal muscle, liver, spleen, kidney and EWAT and BAT and was compared to the expression pattern given by R26 integrated teR gene transcribed by the same promoter (Fig.14). Results were adjusted by forming delta-Ct (dCt) obtained after subtraction of the cycle threshold (Ct) for the housekeeping gene heterochromatin protein 1 binding protein 3 (HP1BP3) from the CT of tetR mRNA. Col1a1(VaLo_shEgln1) mice exhibited significant lower tetR expression rates in brain, skeletal muscle, liver, kidney and EWAT, compared to R26 expressed tetR. dCT differed between 15 CTs in muscle and 7 CTs in kidney, approximately corresponding an 3,200 to 130 fold lower expression of Col1a1 encoded tetR gene, compared to R26 inserted gene. In contrast tetR expression from Col1a1(VaLo_shEgln1) was higher in BAT by 3 CTs and heart by 2 CTs, approximating an 4 to 250 times higher expression rate in these tissues, compared to R26 integrated tetR. Both loci revealed comparable tetR expression levels in spleen.

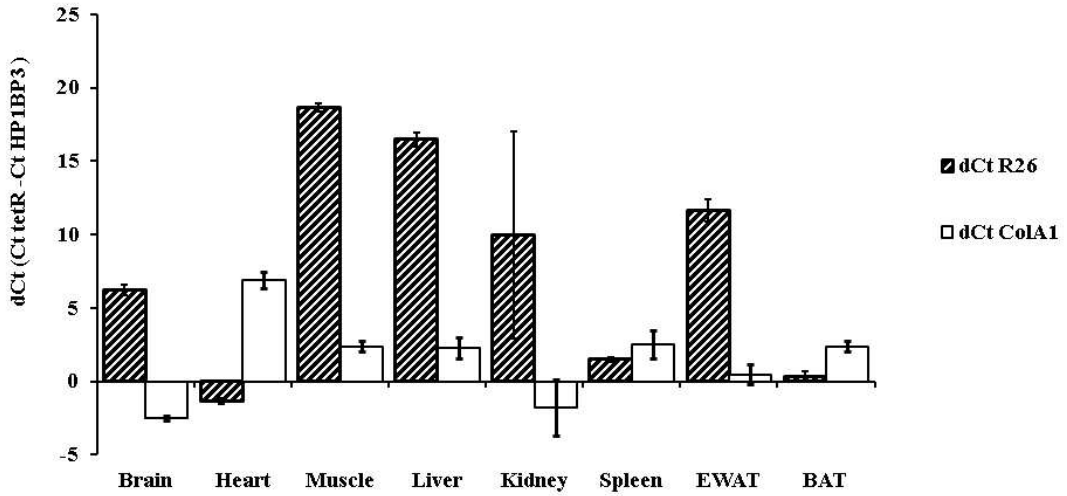

Fig. 14: Transgic mRNA expression in Col1a1(VaLo_shEgln1) mice. Expression of tetR was determined in brain, heart, skeletal muscle, liver, kidney spleen, epigonadal white adipose tissue (EWAT), brown adipose tissue (BAT) of Col1a1(VaLo_shEgln1) mice using qPCR. Expression rates of Col1a1 encoded tetR-gene (white bars) were compared to expression of tetR in R26(shEgln1) mice (white striped

bars), encoding tetR in a VaLo_shEgln1 accordant construct integrated in R26. Results were normalized by calculating dCT (CT tetR - CT HP1BP3). All values are mean ± SEM. For each group n=3.

In conclusion, VaLo_shEgln1 was employed to characterize Col1a1 as a locus for RMCE applications. Efficient RNAi was triggered by shRNAs expressed from Col1a1(VaLo_shEgln1). Indeed, the employed inducible RNAi system turned out to be not tightly controllable in Col1a1. Almost all examined tissues exhibited severe target gene reduction without shRNA expression being induced by dox administration. Furthermore expression pattern of tetR was analysed, as an example for transgene mRNAs integrated in Col1a1. Col1a1(VaLo_shEgln1) gave a considerable lower tetR expression in most considered tissues, compared to R26 integrated tetR. With regard to these results, Col1a1 was not considered as a locus for the integration of the genomic RMCE-2 part and the strategy of using two independent shRNA expression loci was not further evaluated.

3.1.4 Stable single copy integration of two shRNA expression units in R26 (second strategy)

The second strategy to obtain silencing of two target genes was the integration of two shRNA expression units combined in a single R26 RMCE exchange cassette. To determine whether the order of shRNA cassettes affects the activity of the promoters, two constructs were designed bearing the same shRNA units but in reverse successions (Fig. 15A). Tandem constructs were designed for the simultaneous expression of shIR5 and shIGF1R2. The vector pshIR5_shIGF1R2 carries H1tetO_shIR5 at the 5´ position and H1tetO_shIGF1R at the 3´position. In contrast, H1tetO_shIGF1R was followed by H1tetO_shIR5 in pshIGF1R2_shIR5. Both vectors were stably integrated via RMCE into R26 locus of B6/RMCE cells. Correct integration was controlled by Southern blot (Fig. 15B). Expected signal sizes were 4.3 kb for R26 wt allele, 3.8 kb for R26(RMCE) allele before exchange and 6.2 kb for R26(RMCE) allele after exchange.

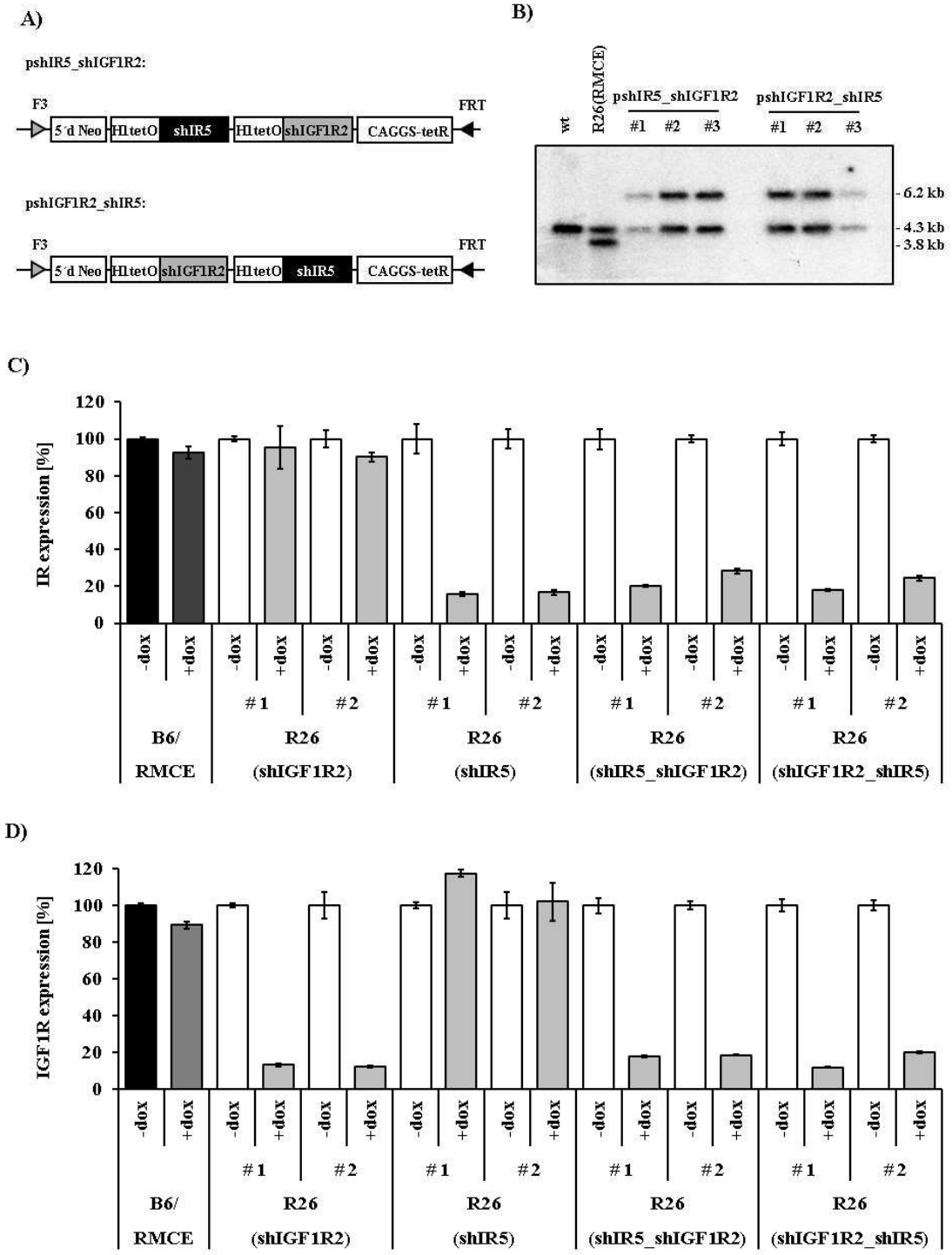
A)
pshIR5_shIGF1R2:
F3
5´d Neo
H1tetO
shIR5
H1tetO
shIGF1R2
CAGGS-tetR
FRT
pshIGF1R2_shIR5:
F3
5´d Neo
H1tetO
shIGF1R2
H1tetO
shIR5
CAGGS-tetR
FRT
B)
wt
R26(RMCE)
pshIR5_shIGF1R2
#1 #2 #3
pshIGF1R2_shIR5
#1 #2 #3
6.2 kb
4.3 kb
3.8 kb
C)
IR expression [%]
120
100
80
60
40
20
0
-dox
+dox
#1
#2
B6/ RMCE
R26 (shIGF1R2)
R26 (shIR5)
R26 (shIR5_shIGF1R2)
R26 (shIGF1R2_shIR5)
D)
IGF1R expression [%]
120
100
80
60
40
20
0
-dox
+dox
#1
#2
B6/ RMCE
R26 (shIGF1R2)
R26 (shIR5)
R26 (shIR5_shIGF1R2)
R26 (shIGF1R2_shIR5)

Fig. 15: Tandem shRNA expression constructs and achieved KD of target genes in ES cells. A) Two R26 exchange vectors comprising two H1tetO_shRNA units were design to achieve simultaneous silencing of IR and IGF1R **A)**. pshIR5_shIGF1R and pshIGF1R_shIR5 bear two independent shRNA expression units in reverse orders. Integration of exchange vectors was confirmed by Southern blot analysis. **B)** Expected sizes for R26 wt allele, R26(RMCE) allele before exchange and after exchanged were 4.3 kb, 3.8 kb and 6.2 kb, respectively. KD of IGF1R **C)** and of IR **D)** was estimated by qPCR in not induced (-dox, white bars) and induced (+dox, light grey bars) cells in duplicates of two clones per construct. Target gene reduction triggered by tandem constructs was compared to solely expressed shRNAs. Induced (+dox, dark gey bars) and not induced (-dox, black bars) B6/RMCE cells served as negative control. Remaining expression of target genes after induction is shown as percentage of not induced (-dox, light gey bars) cells of each accordant clones. All data are presented as mean ± SEM.

KD of both target genes was measured and compared to the efficiency given by solely expressed shRNA (Fig. 15C, D). Both tandem constructs reduced target gene expression at comparable magnitude. Remaining expression rates of IFG1R mRNA in R26(shIR5_shIGF1R2) and R26(shIGF1R2_shIR5) bearing clones were ranging between 12 % and 20 %. Concurrently IR mRNA levels were reduced to between 18 % and 28 % of the original concentration. Compared to the solely expressed shRNAs either double constructs triggered a distinct lowered but still strong reduction of both target mRNAs. IGF1 expression was reduced to 12% in R26(shIGF1R2) cells and IR expression to about 16 % in R26(shIR5) cells. To translate these results into an *in vivo* setting transgenic mice were generated from R26(shIGF1R2_shIR5) ES cells. RNAi was induced in 6 week old male mice by feeding chow containing 1g doxycyclin /kg. Tissue samples of pituitary, hypothalamus, total brain, heart, skeletal muscle, liver, kidney, spleen, pancreas, EWAT and BAT were dissected after 10 days of induction to estimate expression rates of IR and IGF1R by qPCR (Fig. 16).

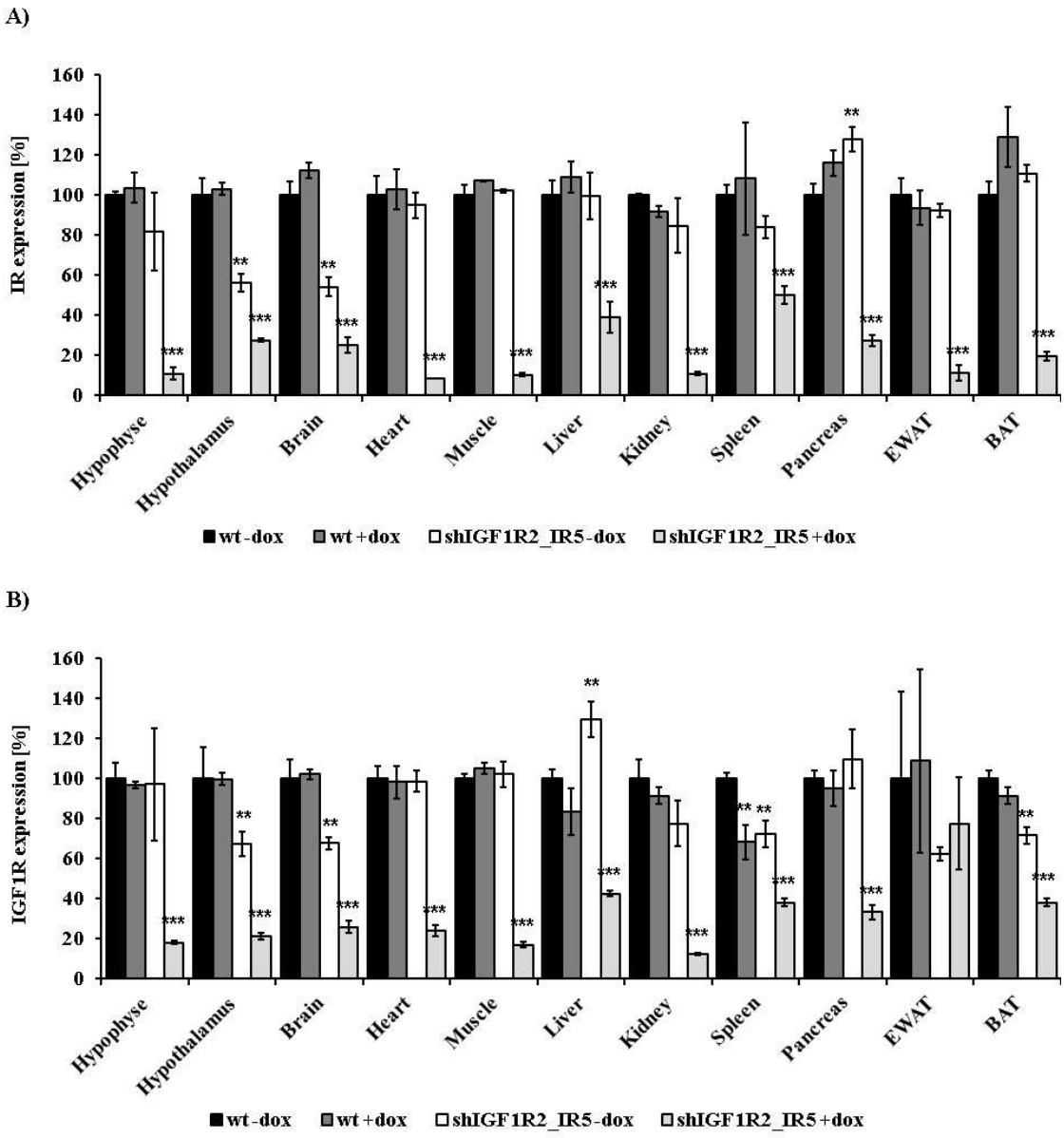

Fig. 16: KD of IR and IGF1R mediated by shIGF1R2_shIR5 *in vivo*. Silencing of IR **A)** and IGF1R **B)** was estimated in selected tissues collected from doxycyclin induced (shIGF1R_IR5 +dox, light grey bars) and not induced (shIGF1R_IR5 -dox, white bars) male target mice by qPCR. Induced (wt +dox, dark grey bars) and not induced (wt -dox, black bars) wilfd type males served as negative control. Remaining expression of target genes is displayed as percentage of not induced wt mice. For all groups n= 3, data are mean ± SEM. *, $P \leq 0.05$; **, $P \leq 0.01$; ***, $P \leq 0.001$ versus control.

A significant reduction of both target genes upon doxycyclin treatment was observed in all tissues examined from shIGF1R2_shIR5+dox mice. IR mRNA levels were reduced to about 10% remaining in pituitary, heart, skeletal muscle and EWAT, as strongest effects. Other tissues exhibited a reduction to between 20 % in BAT and 50 % in spleen. IGF1R expression was reduced to between 10 % and 30 % in the analysed tissues. Notably silencing of both target genes was considerably low in liver, otherwise providing high KD efficiencies. Results of measurements on EWAT samples displayed a high level of variation. Subsequently performed qPCR on EWAT samples of shIGF1R2_shIR5 +dox mice revealed a reduction of IGF1R expression to 40 % (Fig. 17A). However, accomplished reduction of both target genes was seen as sufficient to examine the coherency of IR and IGF1R function in terms of glucose metabolism.

3.2 Phenotypical analysis of insulin- and IGF1-receptor double knockdown mice

3.2.1 Confirmation of IR and IGF1R knockdown

The generated shIGF1R2_shIR5 mouse line enables the temporally inducible RNAi- mediated ablation of the insulin and the IGF1 receptor. This model offers a unique opportunity to study the potentially redundant roles of IR and IGF1R action in terms of energy homeostasis in adult mice, bypassing developmental defects arising from receptor ablation during embryonic development. To complete the experimental arrangement shIGF1R2 and shIR5 single KD mice were generated, serving as control groups in the following studies. Expression of shRNAs was induced in 6 week old male mice by administration of a doxycycline-containing diet, while control groups received normal chow. The following experiments were carried out within 4 weeks of induction, since ablation of both receptors was lethal after 4 weeks due to unspecified reasons.

Silencing of insulin and IGF1 receptors was analyzed after 4 weeks of dox treatment by qPCR (Fig. 17A-19A) and Western blot (Fig. 17B-19B) in pituitary, total brain, skeletal muscle, liver and brown adipose tissue (BAT). Due to the low expression levels of IGF1R in liver, KD was only demonstrated by qPCR and not confirmed by Western blot in this tissue (182, 183). Since shIGF1R_IR5 +dox and shIR5 +dox mice had completely lost their white fat after 4 weeks, epigonadal white adipose tissue (EWAT) samples were collected separately from 7 week old mice after 10 days of induction to demonstrate shRNA mediated gene silencing this tissue.

Upon doxycycline induction of shRNA transcription, both single KD mice display specific silencing of the correspending target gene with no impact on the expression of the second gene.

There was a similar decrease in IR expression of 15 % to 20% in the analyzed tissues of shIR5 +dox and shIGF1R2_shIR5 +dox mice. In contrast, double KD mice display a considerable lower silencing in IGF1R expression, 2-fold weaker in muscle, pancreas, EWAT and BAT, compared to shIGF1R single KD mice. This finding indicates a position effect within the tandem construct leading to lowered transcriptional activity of the H1tetO promoter at the first position. The circumstance that double KD mice display IGF1R silencing at a lower degree than the single KD control group must be considered in the interpretation of the following findings.

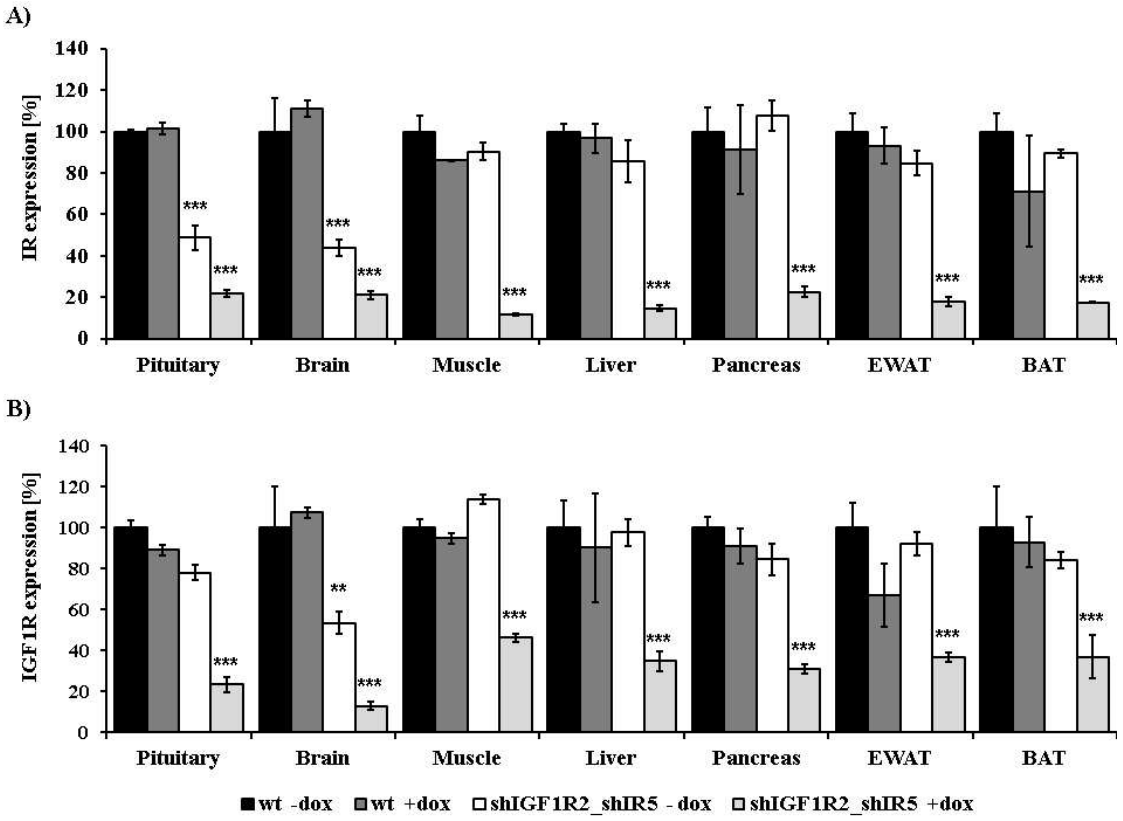
A)
IR expression [%]
140
120
100
80
60
40
20
0
***
Pituitary
Brain
Muscle
Liver
Pancreas
EWAT
BAT
B)
IGF1R expression [%]
**
wt -dox
wt +dox
shIGF1R2_shIR5 - dox
shIGF1R2_shIR5 +dox

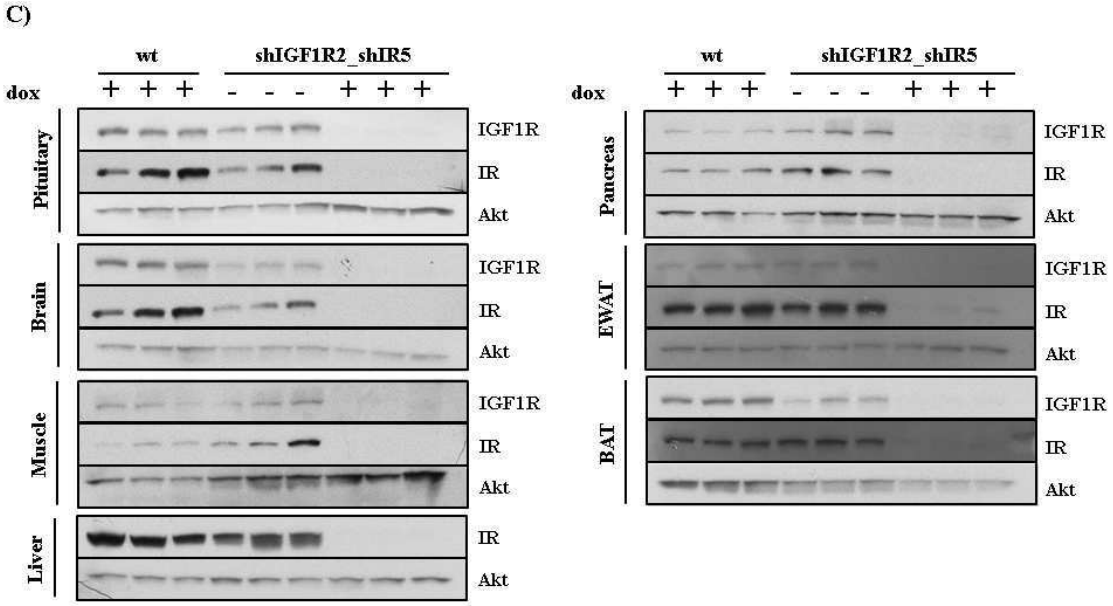
C)
wt
shIGF1R2_shIR5
dox
+ + + - - - + + +
Pituitary
Brain
Muscle
Liver
Pancreas
EWAT
BAT
IGF1R
IR
Akt

Fig. 17: KD of IR and IGF1R in shIGF1R2_shIR5 mice. Silencing of IR **A)** and IGF1R **B)** was estimated in selected tissues of dox induced (shIGF1R_IR5 +dox, light grey bars) and not induced (shIGF1R_IR5 -dox, white bars) male target mice by qPCR. Induced (wt +dox, dark grey bars) and not induced (wt -dox, black bars) wild type males served as negative control. Remaining expression of target genes is displayed s percentage of not induced wt mice. **C)** Western blot analysis of IR, IGF1R and Akt (loading control). For all groups n= 3. *, $P \leq 0.05$; **, $P \leq 0.01$; ***, $P \leq 0.001$ versus wt -dox control.

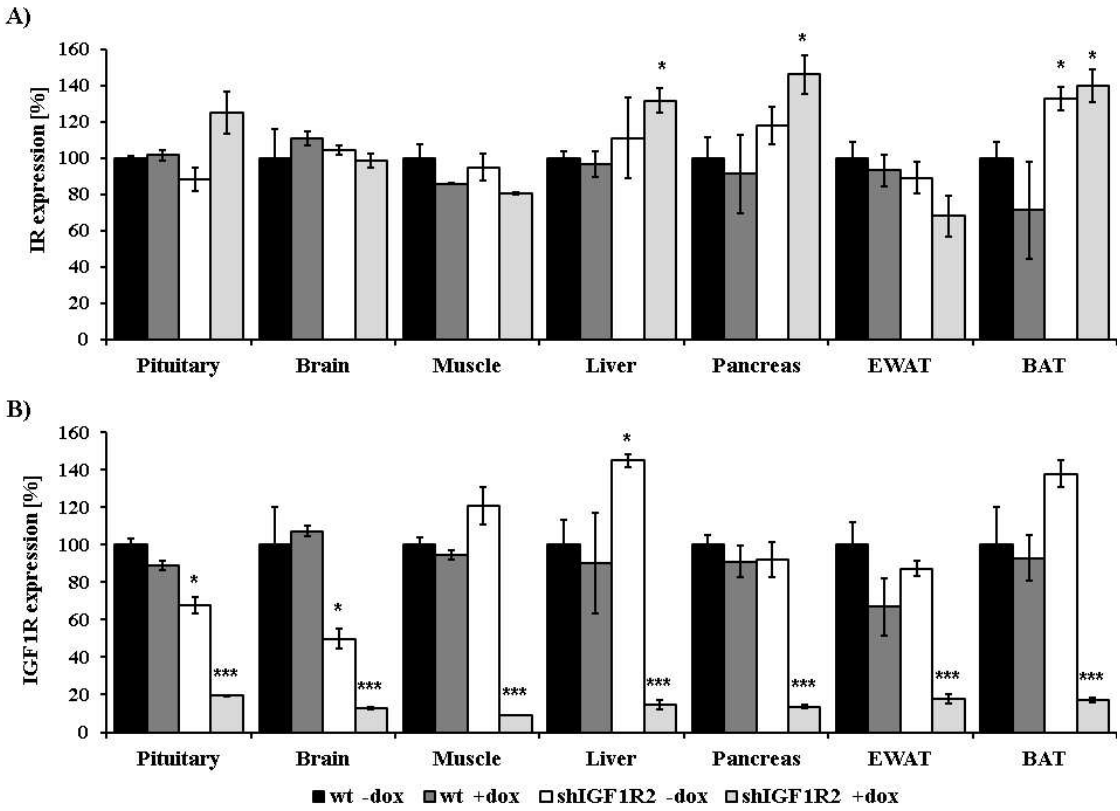

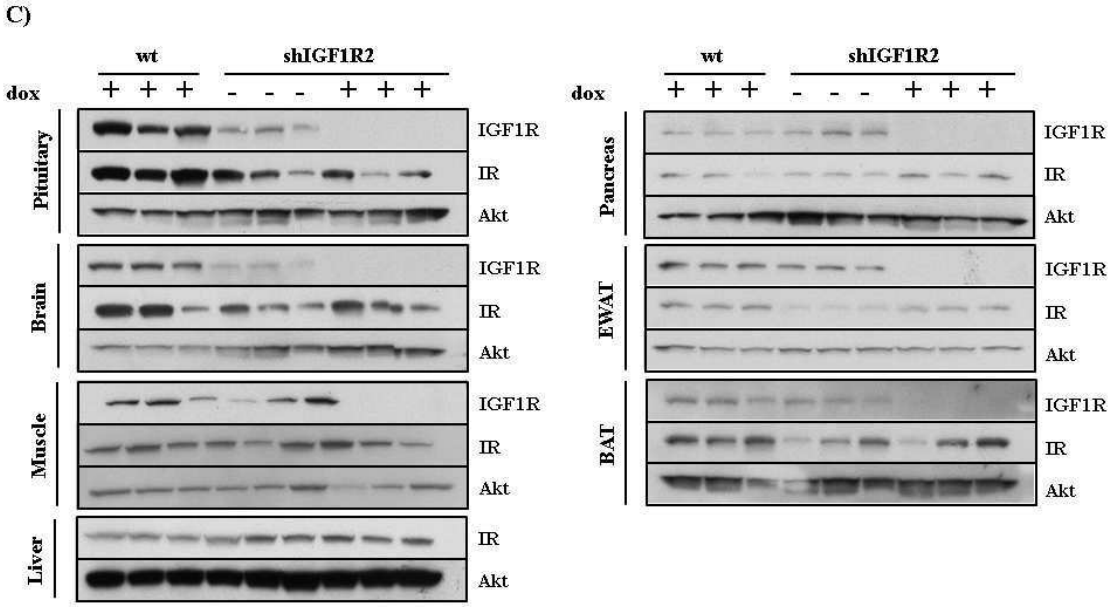

Fig. 18: KD of IGF1R in shIGF1R2 mice. Expression levels of IR **A)** and IGF1R **B)** were estimated in selected tissues of dox induced (shIGF1R_IR5 +dox, light grey bars) and not induced (shIGF1R_IR5 -dox, white bars) male target mice by qPCR. Induced (wt +dox, dark grey bars) and not induced (wt -dox, black bars) wild type males served as negative control. Remaining expression of target genes is displayed s percentage of not induced wt mice. **C)** Western blot analysis of IR, IGF1R and Akt (loading control). For all groups n= 3. *, $P \leq 0.05$; **, $P \leq 0.01$; ***, $P \leq 0.001$ versus wt -dox control.

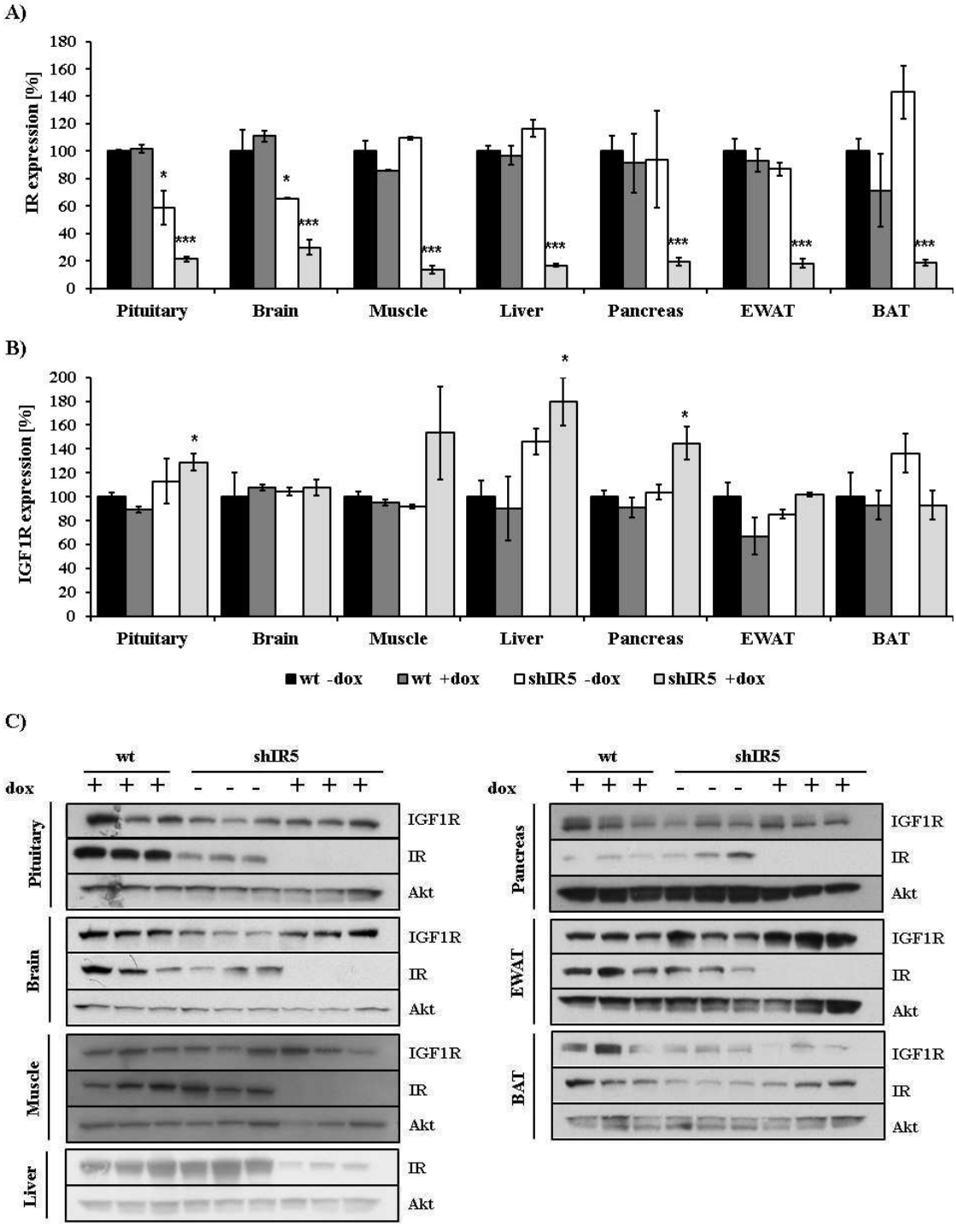

Fig. 19: KD of IR in shIR5 mice. Expression levels of IR **A)** and IGF1R **B)** were estimated in selected tissues of dox induced (shIGF1R_IR5 +dox, light grey bars) and not induced (shIGF1R_IR5 -dox, white

bars) male target mice by qPCR. Induced (wt +dox, dark grey bars) and not induced (wt -dox, black bars) wild type males served as negative control. Remaining expression of target genes is displayed s percentage of not induced wt mice. **C)** Western blot analysis of IR, IGF1R and Akt (loading control). For all groups n= 3. *, $P \leq 0.05$; **, $P \leq 0.01$; ***, $P \leq 0.001$ versus wt -dox control.

3.2.2 Serum levels of Insulin and IGF1 in double knockdown mice

The emergence of resistance to insulin and IGF1 in mice with silencing in both corresponding receptors was investigated by detection of circulation hormones, to demonstrate compensatory release (Fig. 20). Insulin levels were determined by Enzyme-linked Immunosorbent Assay (ELISA) in samples collected daily in the first week of induction and in a weekly interval for the 3 consecutive weeks. Furthermore, serum levels of IGF1 were analyzed after 4 weeks of dox treatment.

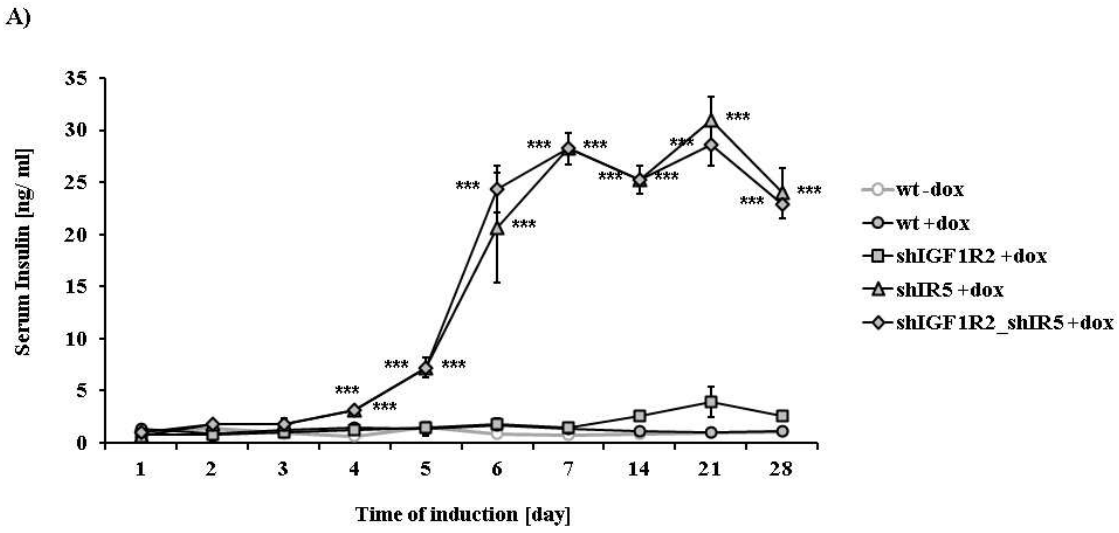

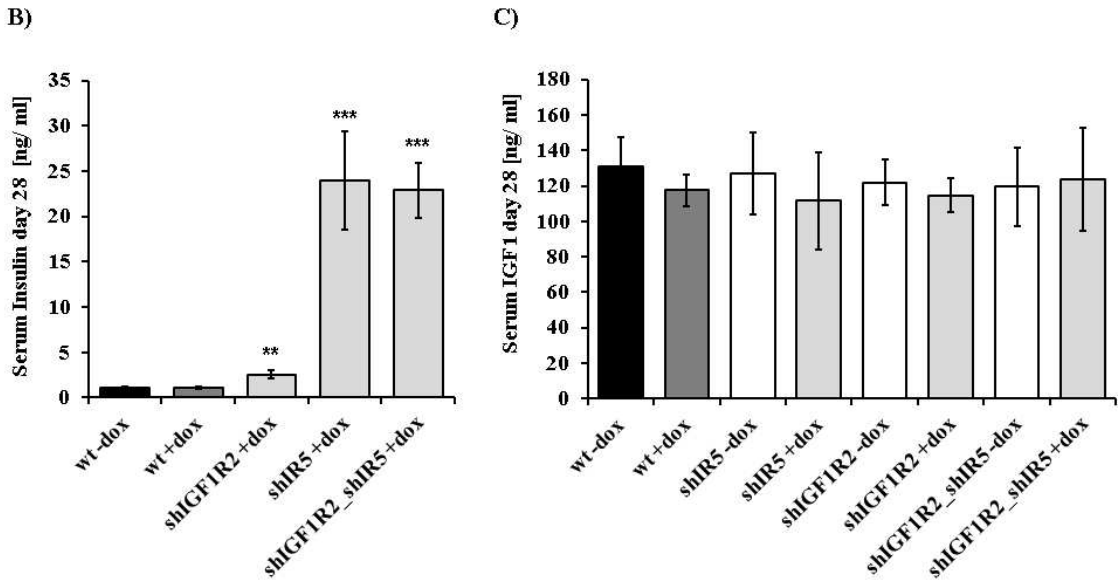

Fig. 20: Compensatory changes in serum levels of insulin, not of IGF1. A) Concentrations of circulating insulin were monitored from beginning of doxycyclin induction over a period of 4 weeks in shIGF1R_IR5 +dox (filled diamond), shIR5 +dox (filled triangle), shIGF1R +dox (filled rectangle), wt +dox (filled circle) and wt -dox (open circle) mice. Statistical significance was calculated using two-way ANOVA, followed by a Bonferroni post-test. *, $P \leq 0.05$; **, $P \leq 0.01$; ***, $P \leq 0.001$. **B)** Separate depiction of serum insulin levels of serum insulin levels in shIGF1R2 +dox, shIR5 +dox and shIGF1R2_shIR5 +dox mice in relation to wt -dox (black bar) and wt +dox (dark grey bar) controls at the end of experiment (day 28). Statistical significance was calculated using two-tailed t-test versus wt -dox. *, $P \leq 0.05$; **, $P \leq 0.01$; ***, $P \leq 0.001$. **C)** Serum concentrations of IGF1 were determined in dox treated (light grey bars) and untreated (white bars) mice of each group in week 4 after of dox induction. wt -dox (black bar) and wt +dox (dark grey bar) served as controls. For each group n= 5. All data are presented as mean ± SEM. Statistical significance was calculated using two-way ANOVA, followed by a Bonferroni post-test. *, $P \leq 0.05$; **, $P \leq 0.01$; ***, $P \leq 0.001$. For each group n= 5. All data are presented as mean ± SEM.

Serum insulin concentrations rose drastically beginning from day 3 of induction in induced shIGF1R2_IR5 +dox and shIR5 +dox mice, reflecting a compensatory increase of insulin secretion due to target tissue resistance. Serum concentration of both groups peaked at 28 ng/ml at day 7. Values fluctuated between 23 ng/ml and 30 ng/ml in the following 3 weeks. No clear differences in the kinetics of onset or magnitude of compensatory increase in insulin concentrations were observed between shIGF1R2_IR5 +dox and shIR5 +dox mice. A comparably subtle but significant, 3-fold, increase of serum insulin was observed in mice with silencing of the IGF1R, starting from week 2 of

induction. This elevation did not reach significance in ANOVA test performed on whole data representing temporal progress of insulin release (Fig. 20A). However, separate statistical analysis of insulin values at day 28 using two-tailed t-test revealed an increase, which was significant versus wt -dox controls (Fig. 20B). Control wt mice, induced and not induced, displayed no changes in insulin serum levels.

Serum concentrations of IGF1 were analyzed in samples taken in week 4 of dox treatment (Fig. 20C). No significant differences between induced KD mice and wt control groups were observed, demonstrating the absence of compensatory increased release of IGF1 due to whole body ablation of the IGF1R.

3.2.3 The effects of IR and IGF1R KD on energy homeostasis and somatic growth

Common physical parameters including body weight, fat content, body length and food intake were determined to investigate the effects of disturbed energy homeostasis and somatic growth.

Body weight of induced mice and control groups was monitored weekly from beginning of dox administration in the age of 6 weeks. The weight curve of induced mice is depicted in Fig. 21A. Not induced control groups as well as induced wt +dox mice are shown in Fig. 21B. Induced double KD mice (shIGF1R2_shIR5 +dox) continuously lost weight to a mean value of 11 g after 4 weeks. Moreover, also shIR5 +dox mice considerably lost body mass, however not to the same extent as double KD mice. Induced shIGF1R2 +dox mice however showed no alteration in body weight after start of induction. Here, body weight did not increase over 19 g, indicating an arrest of somatic growth due to ablation of the IGF1R. Among the control groups, induced and not induced wt mice, wt +dox and wt -dox, and shIR5 -dox mice continuously gained weight to a final body weight of about 22 g. Notably, not induced shIGF1R2_shIR5 -dox and shIGF1R2 - dox mice display lower body weight at any time, compared to wt mice and shIR5 -dox mice.

To further assess the effects of insulin and IGF1 receptor ablation on lipid metabolism, body fat content was dermined in week 5 of induction using nuclear

magnetic resonance (NMR). Fat content is displayed as percentage of whole body weight (Fig. 21C). Induced shIGF1R2_shIR5 +dox and shIR5 +dox mice exhibited a significant decrease in body fat percentage to about 5 %. In contrast, body fat in animals with silencing in IGF1R was significantly increased to about 18 % of whole body mass. Not induced shIGF1R2 -dox mice showed a slightly increased fat content, not reaching significance. Wild type mice and not induced control groups displayed fat percentage of about 10 %.

Since IGF1 action is a well-established anabolic signal, the effect of IGF1R silencing on somatic growth was verified by determination of body length after 4 weeks of doxycyclin treatment (Fig. 21C). Mean body length of shIGF1R2_IR5 +dox and shIGF1R2 +dox mice was significantly reduced to 85 and 86 mm. These data indicate that the cause for the observed reduction in body weight of IGF1R deficient mice is attributable to reduced somatic growth. Body length between control groups as well as induced shIR5 +dox mice was undistinguishable with about 90 mm.

Furthermore, average food intake was determined daily in 11-week-old mice after 4 weeks of induction (Fig. 21D). Food intake of shIGF1R2_IR5 +dox and shIGF1R2 +dox mice was drastically reduced to about 3.2 g per day. Not induced control groups as well as doxycyclin induced wt +dox and shIR5 +dox mice showed no alteration. Daily average food intake of these groups was about 4.1 g per day.

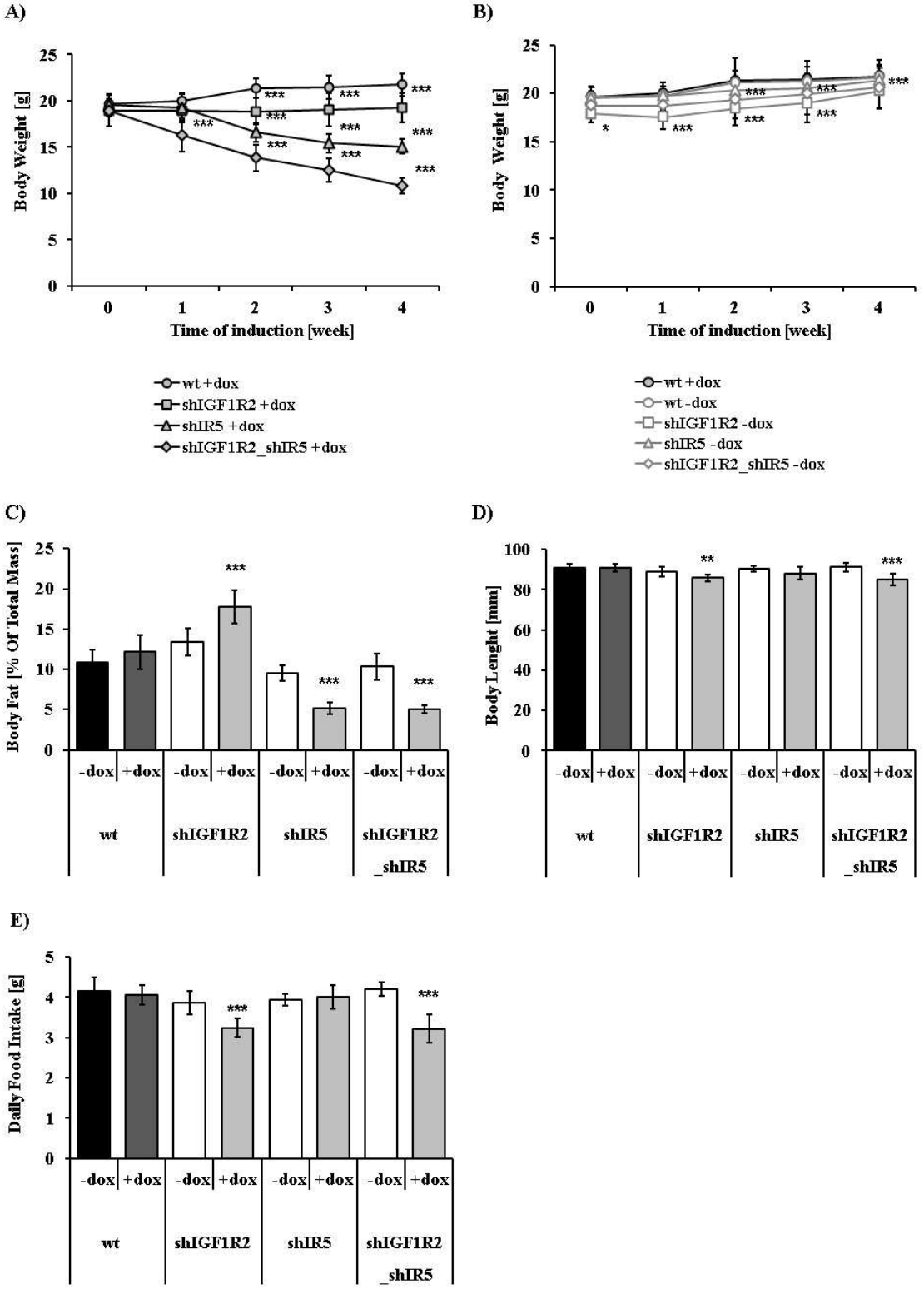
A)
Body Weight [g]
Time of induction [week]
wt +dox
shIGF1R2 +dox
shIR5 +dox
shIGF1R2_shIR5 +dox
B)
Body Weight [g]
Time of induction [week]
wt +dox
wt -dox
shIGF1R2 -dox
shIR5 -dox
shIGF1R2_shIR5 -dox
C)
Body Fat [% Of Total Mass]
-dox
+dox
wt
shIGF1R2
shIR5
shIGF1R2 _shIR5
D)
Body Lenght [mm]
E)
Daily Food Intake [g]

Fig. 21: Body weight, fat content, length and food intake. **A)** Body weight was monitored in a weekly interval from beginning of induction of induced wild type wt +dox (filled circle), shIGF1R +dox (filled rectangle), shIR5 +dox (filled triangle) and shIGF1R_IR5 +dox (filled diamond). **B)** wt +dox (filled circle) and not induced control groups wt -dox (open circle), shIGF1R -dox (open rectangle), shIR5 -dox (open triangle) and shIGF1R_IR5 -dox (open diamond) are depicted separately. For all groups n =10. **C)** Body fat content was detected in week 5 of induction in 11 week old induced (light gray bars) and not induced white bars) mice. For all groups n =10. **D)** Body length was determined in week 5 of induction in 11 week old induced (light gray bars) and not induced (white bars) mice. For all groups n =10. **E)** Average daily food intake of dox treated (light gray bars) and untreated (white bars) mice was measured in week 4. For all groups n =5. Wt -dox (black bars) and wt +dox mice served as controls in determination of body fat content, body length, and food consumption. All data are presented as mean ± SEM. The statistical significance was calculated using two-way ANOVA, followed by a Bonferroni post-test. *, $P \leq 0.05$; **, $P \leq 0.01$; ***, $P \leq 0.001$; *, $P \leq 0.05$; **, $P \leq 0.01$; ***, $P \leq 0.001$.

Taken together, shIGF1R2_shIR5 +dox mice exhibited a multitude of physical changes, primarily reflected by a drastical reduction in body weight. This observation goes along with effects that were observed in single and double KD mice. Loss of IR function results in a severely decreased body fat content. Ablation of the IGF1R reduced somatic growth, demonstrated by arrested weight gain and reduced body length. Furthermore, IGF1R deficient mice display reduced food intake.

3.2.4 The effect of IR and IGF1R silencing on glucose metabolism

To assess the impact of simultaneous KD of insulin- and IGF1-receptor on glucose metabolism, serum glucose concentrations were monitored for the duration of the experiment. The progression of blood glucose concentrations in dox induced mice of all groups is shown in Fig. 22A. Not induced control groups as well as induced wt mice are displayed separately in Fig. 22B.

Blood glucose concentrations started to rise in shIGF1R2_IR5 +dox and shIR5 +dox mice beginning from day 4 of induction, indicating the development of insulin resistance in target tissues. Notably, induced double KD mice, namely shIGF1R2_shIR5+dox, exhibited a distinctly faster increase of glucose levels during day 5 and 6 after induction, compared to shIR5 +dox mice. However, both lines reached

values of 450 mg/dl glucose at day 7 and fluctuated between 380 mg/dl and 550 mg/dl until the end of the analysis period. In contrast, induced shIGF1R +dox mice revealed no elevation but rather slightly lowered blood glucose values compared to wt control groups. This decrease did not reach significance in ANOVA test performed on whole data representing temporal progress of glucose levels in all groups (Fig. 22A). However, separate statistical analysis of glucose values in shIGF1R +dox mice at day 28 using two-tailed t-test revealed a decline, significant versus wt -dox controls at that point in time (Fig. 22B). Dox treated wt mice and not induced control groups showed no alterations over the time monitored.

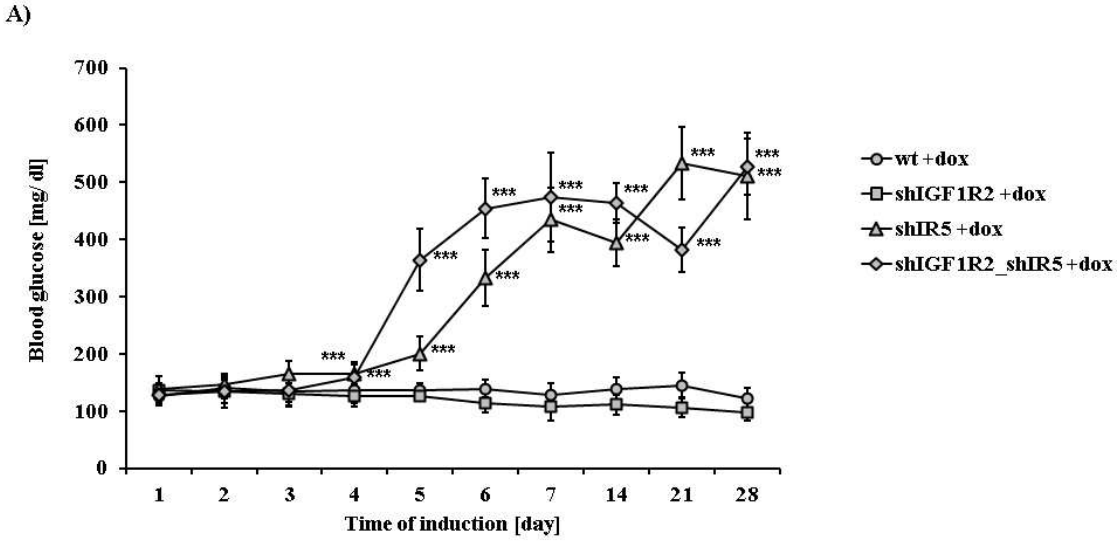

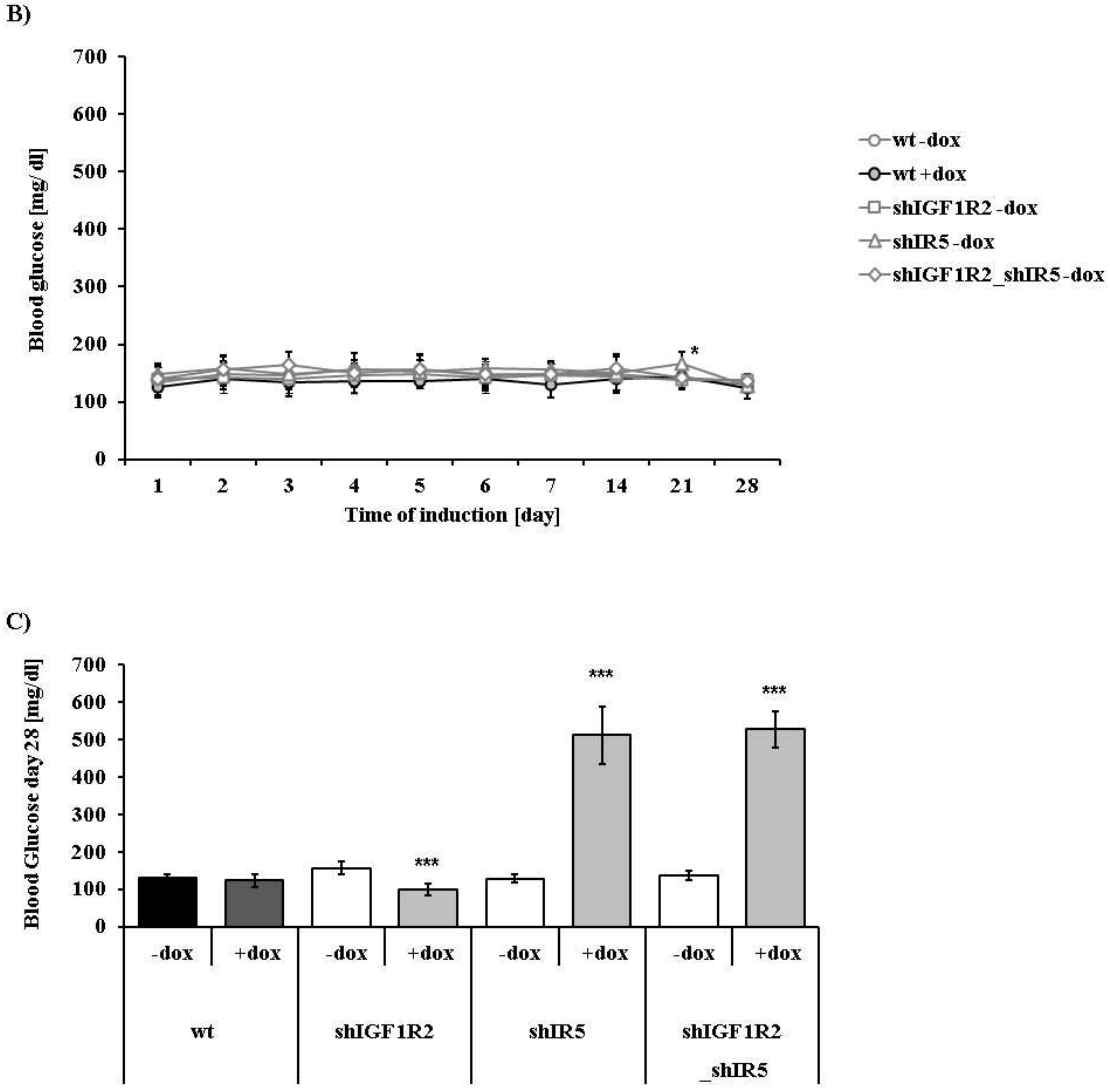

Fig. 22: Blood glucose levels in shIGF1R_IR5 mice. A) Blood glucose concentrations in male wild type wt +dox (filled circle), shIGF1R +dox (filled rectangle), shIR5 +dox (filled triangle) and shIGF1R_IR5 +dox (filled diamond) mice were detected for a period of 4 weeks, daily in the first week of induction and in a weekly interval for 3 more weeks. **B)** Blood glucose values of wt +dox (filled circle) and not induced controls wt -dox (open circle), shIGF1R -dox (open rectangle), shIR5 -dox (open triangle) and shIGF1R_IR5 -dox (open diamond) are displayed separately. The statistical significance was calculated using two-way ANOVA, followed by a Bonferroni post-test. *, $P \leq 0.05$; **, $P \leq 0.01$; ***, $P \leq 0.001$. **C) C)** Separate depiction of serum glucose levels of shIGF1R2 -dox (whithe bar) and shIGF1R2 +dox (light grey bar) mice in relation to wt -dox (black bar) and wt +dox (dark grey bar) controls at the end of experiment (day 28). Statistical significance was calculated using two-tailed t-test versus wt -dox. *, $P \leq 0.05$; **, $P \leq 0.01$; ***, $P \leq 0.001$. For each group n= 10. All data are presented as mean ± SEM.

To further elucidate to what extent double KD of IR and IGF1R affects insulin sensitivity of target tissues, insulin tolerance tests (ITT) and glucose tolerance tests (GTT) were performed.

ITT was performed in induced and not induced mice of all groups in week two after start of dox treatment (Fig. 23A, B). Induced shIR5 +dox and shIGF1R2_shIR5 +dox mice showed no response, i.e. decrease in blood glucose, upon administration of exogenous insulin. Reduction of blood glucose concentrations was significantly lowered in induced shIGF1R2 +dox mice after insulin stimulation compared to wt +dox mice. Response to insulin in not induced control groups, shIR5 -dox, shIGF1R2 -dox, shIGF1R2_shIR5 -dox, wt -dox and induced wt was indistinguishable (Fig. 23B).

In addition, GTT was performed in week 3 after beginning of induction (Fig. 23C, D). All KD mice exhibited reduced glucose clearance upon exogenous glucose administration (Fig. 23C). The highest degree of impairment was observed in shIGF1R2_shIR5 mice. Double KD of insulin and IGF1 receptor in shIGF1R2_IR5 +dox mice lead to a slightly higher rise in blood glucose concentrations upon exogenous administration, compared to shIR5 +dox mice. However, this difference did not reach statistical significance. Ablation of IGF1R in shIGF1R2 +dox mice significantly reduced peripheral glucose uptake, indeed at a less severe degree compared to shIR5 +dox mice. Glucose clearance was indistinguishable between not induced control groups (Fig. 23D).

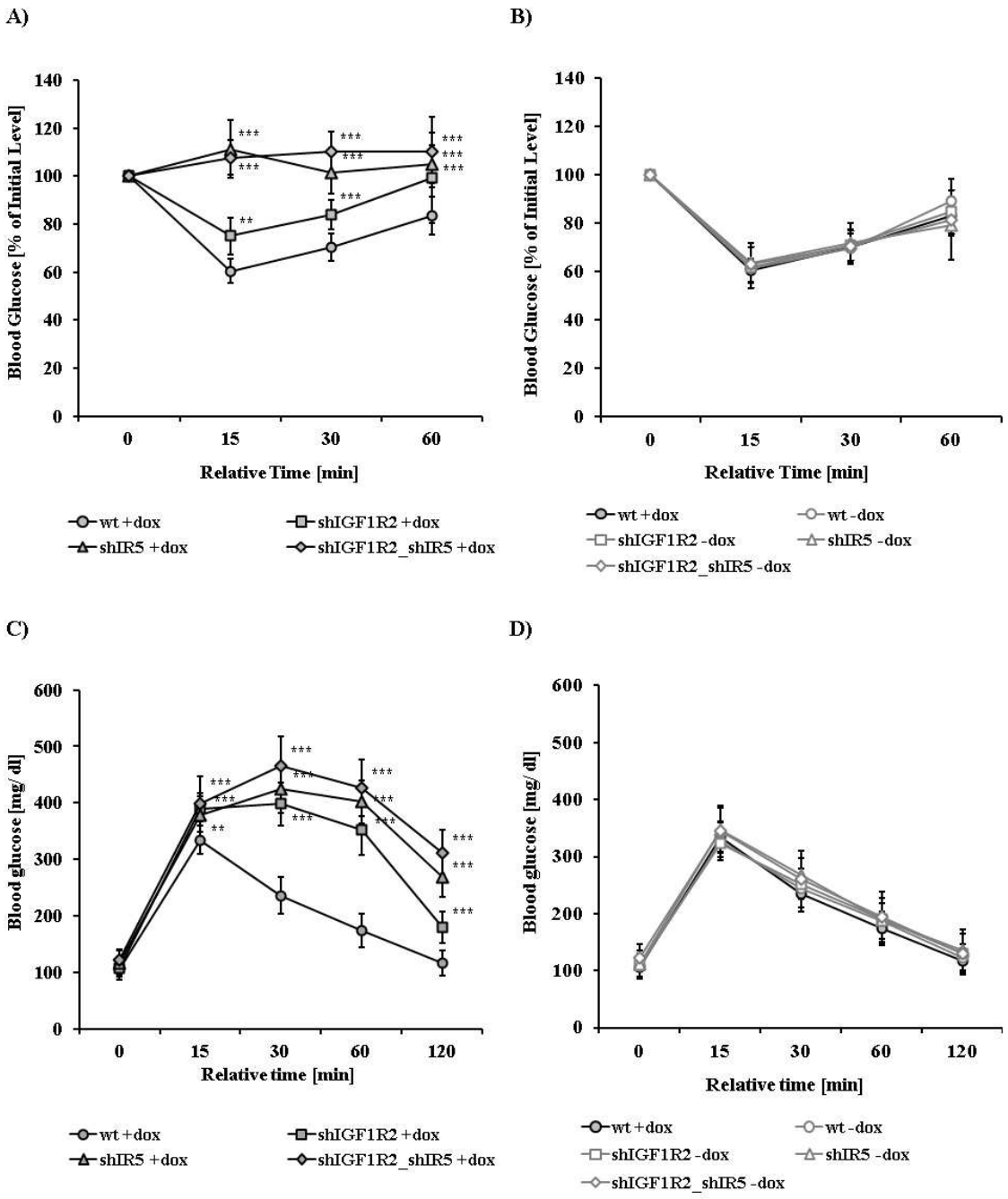

Fig. 23: Insulin and glucose tolerance in double KD mice. ITT was performed in week 2 after induction. **A)** Blood glucose levels of induced wild type wt +dox (filled circle), shIGF1R +dox (filled rectangle), shIR5 +dox (filled triangle) and shIGF1R_IR5 +dox (filled diamond) were determined 15, 30 and 60 min after injection of insulin. **B)** ITT results of control groups, wt +dox (filled circle) and not induced controls wt -dox (open circle), shIGF1R -dox (open rectangle), shIR5 -dox (open triangle) and shIGF1R_IR5 -dox (open diamond), are displayed separately. GTT was accomplished in week 3 after start of doxycyclin

induction. **C**) Blood glucose concentrations of induced wild type wt +dox (filled circle), shIGF1R +dox (filled rectangle), shIR5 +dox (filled triangle) and shIGF1R_IR5 +dox (filled diamond) were detected 15, 30, 60 and 120 min after injection of glucose. **D)** The GTT results of wt +dox (filled circle) and not induced wt -dox (open circle), shIGF1R -dox (open rectangle), shIR5 -dox (open triangle) and shIGF1R_IR5 -dox (open diamond) control groups are displayed separately. For each group n= 10. All data are presented as mean ± SEM. The statistical significance was calculated using two-way ANOVA, followed by a Bonferroni post-test. *, $P \leq 0.05$; **, $P \leq 0.01$; ***, $P \leq 0.001$.

In conclusion, mice with silencing in insulin and IGF1 receptor exhibited a stronger initial increase in serum glucose levels, compared to IR deficient mice, while the onset and magnitude of hyperglycemia were undistinguishable between both groups. Furthermore, double KD mice displayed a slightly reduced glucose clearance, compared to mice with silencing in IR, which however did not reach statistical significance.
In contrast, no changes in blood glucose levels were observed in IGF1R deficient mice. Interestingly, these mice displayed severely impaired glucose tolerance and reduced insulin sensitivity.

4 Discussion

4.1 Generation of murine ES cell line bearing two RMCE alleles (first strategy)

The technical challenge of this thesis was the development of a system that allows the simultaneous shRNA-mediated knock down (KD) of two independent target genes in transgenic mice. The ablation of two target genes allows addressing a wider field of research issues by the RNAi technology, e.g. by silencing of redundant functions or compensatory pathways. Specifically, this study aimed to generate a tool to simultaneously and inducibly silence the insulin receptor and IGF1 receptor in a temporally controlled manner to analyze the role of IGF1R in compensating functions of IR in control of glucose metabolism and the development of type 2 diabetes mellitus (T2DM). Two distinct strategies were pursued to enable the integration of two shRNA expression cassettes, allowing the tet-repressor mediated temporal control of RNAi, to achieve the KD of two target genes.

The first strategy based on the generation of a cell line harbouring two alleles prepared for cassette exchange, allowing the simultaneous integration of two independent shRNA expression cassettes at the two genomic loci. This dRMCE technology provides a platform for a wide range of applications. Beside the simultaneous expression of two shRNAs, spare combinations of shRNA and mRNA expression units can be integrated in a simple and fast way using dRMCE. The most significant advantage of dRMCE is given by the employment of two segregating RMCE alleles. Proper assembly of experiments comprising two modified factors require the analysis of single modified mice lines as control groups. The dRMCE approach enables to achieve all three mouse lines just by generation and breeding of dRMCE-mice, carrying each shRNA expression unit in independently inherited loci. Reducing pre-experimental work in transgenic mouse generation to one line makes complex experiments using double modified mice much

more work-, time- and especially cost-efficient. These benefits make dRMCE an interesting technique for several applications.

An established RMCE system mediating integration in Rosa26 (125) served as a technical basis for the constitution of the dRMCE cell line. A second Flp-based RMCE-system, designated as RMCE-2, was designed to act independently from the one in Rosa26 to allow simultaneous and specific exchange in both RMCE loci. The specificity of cassette exchange in both systems was given by the use of 3 pairs of heterospecific FRT versions (168). RMCE-2 employed couples of FRT and F5 sites whilst the R26 RMCE system makes use of FRT and F3 pairs, limiting cassette exchange through double reciprocal recombination to each associated couple of acceptor and donor cassette. Moreover, the architecture of the marker systems afforded antibiotic selection after specific exchange in both RMCE loci. Reconstitution of a puromycin resistance gene in RMCE-2 depends on the correct recombination of the FRT site, whereas activation of a neomycin resistance gene depends on recombination of the F3 site in the R26 system. Since FRT and F3 sites were part of the reading frame of the accordant resistance genes activation of those is exclusively given by exchange of R26 RMCE donor and acceptor cassette and RMCE-2 donor and acceptor cassette.

A second more critical task was the identification of a genomic locus for integration of the RMCE-2 acceptor cassette, providing ubiquitous and high expression of transgenic shRNAs and mRNAs as well as tight control of the employed inducible RNAi system. Further, structural demands had to be fulfilled by a candidate locus. Integration of the RMCE-2 cassette should be preferably neutral in sense of minimizing the risks of interference with endogenous functions to avoid a possible phenotype, e.g. through disruption of ORFs, promoter elements or regulatory elements, as well as trans effects of integrated transgenic promotors. For this reason a site of integration in an intergenic region downstream of a well defined 3´ UTR was favoured. Additionally, the chromosomal position of the site of integration has to ensure independent inheritance of RMCE-2 allele and R26(RMCE) allele. The locus of Cola1 was chosen for integration of the genomic part of RMCE-2 as a promising candidate. Col1a1 was previously characterized by Beard *et al*. (181) who demonstrated strong and ubiquitous expression

of integrated cDNAs, independent from the expression pattern of the Col1a1 gene. These preceded studies strongly suggested properties of the Col1a1 locus fulfilling the demands for dRMCE applications. Beard *et al.* (181) targeted an intergenic region about 0.5 kb downstream of the 3´UTR of the Col1a1 gene with the neighboring gene Sarcoglycan α (Sgca) in reverse orientation and in a distance of 7 kb. This positioning 3´of both ORFs, with no further known transcripts between, was seen as a good option for integration of the RMCE-2 acceptor cassette avoiding unwanted effects on endogenous gene activity. At last, Col1a1 is located on Chromosome 11, assuring independent inheritance from the R26 locus on Chromosome 6.

The genomic part of RMCE-2 was integrated in Col1a1 of a ES cell line bearing R26(RMCE), yielding a cell line with two loci prepared for cassette exchange. Functionality of dRMCE was successfully demonstrated by the simultaneous and independent integration of two RMCE donor cassettes for shRNA expression in R26(RMCE) and Col1a1(RMCE-2). Specificity of the dRMCE reaction for both distinct loci was demonstrated by Southern blot analysis. 80 % of cells resistant to both antibiotics turned out to be positive for both exchanged alleles in Southern blot analysis. This rate of yield was arithmetically the optimum to be expected since R26(RMCE), as the basic system of dRMCE, provides about 90 % positive clones, when used in single RMCE (125). As a test for specificity of each exchange reaction in each independent system, cells bearing both RMCE alleles were transfected with single exchange vectors, either for integration in R26(RMCE) or Col1a1(RMCE-2). Several Cells transfected with Col1a1 exchange vector showed changed signal pattern of R26 specific probes, suggesting interactions between Col1a1 exchange vector and R26(RMCE) locus.

Single site recombination of the FRT sites, used in both RMCE systems, might facilitate the integration of Col1a1 exchange vector in R26(RMCE). Such a recombination event separates the truncated Puro gene from the pA, intended to block transcription after incorrect integration, and allows it ´s expression through transcriptional activities at the site of integration. Certainly the number of analysed clones was much too small for a reasonable evaluation of these effects, but point at a possibly reduced specificity of RMCE reaction in presence of the second RMCE locus.

Anyhow, specific integrations obviously seem to superpose unspecific interactions events between both RMCE systems and avoid the outcome of false integrations, as demonstrated by the high succession rate of dRMCE.

As a further demonstration of dRMCE integration target gene silencing, triggered by the both integrated shRNA expression cassettes was estimated in ES cells. Remaining levels of both target genes mRNAs were reduced to comparable levels by vectors integrated via dRMCE when compared to the same vector solely integrated. This result demonstrates the functionality of dRMCE integrated shRNA expression vectors and further demonstrates the specific integration of R26 and Col1a1 exchange vectors into the accordant RMCE locus, since KD of target genes occurs only in clones expected to express corresponding shRNA.

In parallel to the generation of the dRMCE system a simple RNAi construct was integrated into the Col1a1 locus to analyse it´s transgenic expression properties, avoiding the complexity of constituting RMCE-2. The used construct allowed evaluating the functionality of the employed inducible RNAi system, the degree of shRNA triggered target gene silencing and expression of transgenic mRNA. Transgenic mice were generated after obtaining promising *in vivo* results, showing KD levels comparable to those yielded by R26. Remaining mRNA levels of the target gene as well expression levels of the tetR mRNA were determined in several tissues. Unfortunately expectations for Col1a1 were nut fulfilled. Expression levels of tetR mRNA showed to be considerable lower, 130 to 3,200 times, in most considered tissues, than those given by R26 integrated tetR genes. Indeed, silencing effects achieved by Col1a1 expressed shRNA *in vivo* were comparable or even slightly higher than those of the same shRNA expressed from R26, but regrettably, control mice showed significant reductions of target gene mRNA in several tissues without shRNA expression being induced by doxycycline treatment. Uninduced KD occurs strongest in kidney showing a KD to 13 % of remaining target gene expression. Brain, heart, liver, spleen, WAT and BAT are ranging between a reduction to about 60 % to 30 %. This unwanted KD results from a insufficient regulation of the H1tetO -tetR system leading to shRNA expression without induction. Among the analyzed tissues only muscle shows tight controlled shRNA expression, only after Dox

administration. This tissue depended leakiness is a known disadvantage of the used shRNA expression system. Integrated in R26(RMCE) this effect most commonly occurs in brain and kidney and at lower degree in other tissues.

Most likely the high degree of leakiness can be attributed to the low tetR expression found in most tissues. Further factors might be tissue specific CpG methylation patterns or chromatin condensation status at the site of integration, impairing the binding of tetR or its ability to block Polymerase III depend transcription. Further investigation on methylation status, shRNA expression levels, use of insulator sequences, such as the chicken hypersensitive site-4 (cHS4) (202) etc. might help to understand and to avoid tissue depend leakiness of the H1tetO system. Anyhow, testing more loci for their expression properties seems to be a more promising option to obtain a dRMCE system deployable for all estimated areas of use. In general loci of strong and ubiquitous expressed house keeping genes are used for transgene expression issues. While interrupting endogenous gene functions were to be preserved in this work, several sites inside the ORFs of house keeping genes has been tested as versatile integration loci for expression of transgenic cDNAs or shRNAs. Disregarding the heterozygote interruption of endogenous gene function, testing these loci as sites for RMCE-2 seems to be a promising option. Examples are the hypoxanthine phosphoribosyltransferase 1 (Hprt1) loci, used for constitutive shRNA expression, or the beta actin locus, used for cDNA expression (155, 203, 204).

During the accomplishment of this project Turan *et al*. (205) demonstrated the functionality of a dRMCE system following the same principle applied in this work.

In contrast to the application presented in this thesis, genomic parts were not integrated at defined loci for transgenic gene expression. In conclusion, the functionality of the designed dRMCE was successfully demonstrated and reached the optimum integration rate to be expected. Albeit Col1a1 did not fully fit expectations and can not be used for inducible RNAi applications, the locus can be used for insertion of constitutivly active RNAi constructs, since achieved KD of Col1a1 expressed shRNA was high in all investigated tissues. Further mRNA expression in Col1a1 was lower, compared to R26, but might be sufficient for applications of transgenic mRNA expression. The constructed

RMCE-2 system can be used for further work on dRMCE technique, since the benefits of dRMCE, as described above, justify further investigation on dRMCE and especially screening of alternative loci as a site for the integration of the genomic part of RMCE-2.

4.2 Stable single copy integration of two shRNA expression units in R26 (second strategy)

The second strategy to obtain silencing of two independent target genes based on the combination of two dox inducible shRNA expression units in a single exchange vector for the integration into the R26(RMCE) allele. The combination of multiple shRNA expression units in one vector has been demonstrated before (206-208), but so far the adaptability of RMCE technology and the suitability of R26 locus for single copy integrations of tandem constructs have not been demonstrated. The tandem approach was very straight forward, compared to the dRMCE approach, since it employs the established R26 system and requires no further genomic modification. In contrast to the described double RMCE system this approach requires the independent generation of single KD control lines necessary, extending pre-experimental costs.

Two tandem constructs, harbouring the expression units for shRNAs directed against IR and IGF1R in contrariwise orders, were analysed for their silencing efficiency in ES cells. Both constructs displayed reduction of both target gene's expression at a degree comparable to solely expressed shRNAs and revealed no position dependence in promoter activity in ES cells. Heterozygote mice bearing a shIGF1R2_shIR5 tandem construct displayed silencing of both receptors. Both promotors of the tandem construct displayed the same tissue dependent leakiness of the inducible H1tetO -tetR system in total brain as single RNAi cassettes does. Although no effects of the promoter's positions were observed in ES cells, measurements of target gene expression in mice revealed a lowered silencing efficiency of the shRNA encoded at the first position in most analysed tissues. Double KD mice displayed a twofold weaker silencing in IGFF1R expression in several tissues compared to shIGF1R single KD mice. IGF1R mRNA was reduced to just

about 40% in muscle, pancreas, EWAT and BAT of double KD mice. Weather the downstream neighbouring promotor negatively influenced transcriptional activity or both shRNA compete within the RNAi pathway was not further investigated in this thesis.

However, the generated mice line provided silencing in IR and IGF1R, allowing to investigate the effects of concurrent diminished expression of both receptors. The circumstance that double KD mice displayed IGF1R silencing at a lower degree than the single KD control group must be considered in the interpretation of the following findings.

4.3 Phenotypical analysis of insulin- and IGF1-receptor double knockdown mice

The genetic techniques successfully developed in this thesis made it possible to generate a mouse model that allows the concurrent RNAi-mediated ablation of the insulin and the IGF1 receptor. Temporally controlled double KD provides an excellent option to investigate the impact of whole body loss-of-function of both receptors, since conventional homozygous knock outs of either of these receptors results in embryonic and perinatal lethality (87, 209).

The insulin receptor (IR) plays a central role in nutrient metabolism by regulating glucose and lipid homeostasis and inhibition of its signalling cascade leads to the development T2DM (209 -213). Inactivation of IR function in mice provides a basic diabetic model of insulin resistance through disruption of intracellular downstream signalling (for review see (214). The IGF1 receptor (IGF1R) is structurally closely related to the IR (33, 58, 60) The high degree of Homology facilitates low affinity binding of IGF1 and insulin to the IR and IGF1R, respectively (74, 80, 100-102). Nevertheless, although both receptors share the same major intracellular signalling pathways (33, 58-60), the biological effects of IGF1 signalling differ considerably from those of insulin. To date, IGF1 is mostly seen as an anabolic hormone and as a potent inhibitor of apoptosis (62-64, 87, 100). However, experimental evidence derived from

clinical trials as well as *in vitro* and *in vivo* studies assign an important role to the IGF1 system in maintaining glucose homeostasis and in the development of T2DM. Low levels of circulating IGF1 were observed in type 2 diabetic patients and clinical trails revealed insulin-like effects of administered exogenous IGF1, reducing serum glucose levels at a magnitude of 4-7% of the effect of insulin itself (66, 68, 111-114). In line with these observations, administration or overexpression of IGFBPs, thereby modulating IGF1´s bioavailability, were demonstrated to impair glucose homeostasis (110, 115-118). These described insulin like effects of IGF1 are mainly attributed to peripheral glucose uptake in skeletal muscle, while the role of hepatocytes and adipocytes in this context is controversially discussed (70, 111, 120-124). Furthermore, IGF1 signalling has shown to influence insulin action itself, since function of the IGF1R turned out to be crucial for adequate glucose induced insulin release by the pancreatic β-cells (215 -217).

The simultaneous ablation of IR and IGF1R allows to examine whether both receptors display redundant functions in regard to glucose and energy homeostasis and to assess the role of the IGF1 receptor in the emergence of T2DM. Accordingly, the generated double KD line was analyzed in terms of metabolic parameters. As a central focus of interest, the development of insulin resistance in shIGF1R2_shIR5 mice was investigated by monitoring serum levels of insulin and glucose. Performance of insulin tolerance tests (ITT) and glucose tolerance tests (GTT) afforded to further elucidate in which magnitude double KD of IR and IGF1R effects insulin sensitivity of target tissues. The impact of receptor ablation on overall energy homeostasis and somatic growth was assessed by monitoring physical parameters, including body weight, body fat content, body length and food consumption.

Mice that lack the insulin receptor exhibited a pronounced diabetic phenotype, reflected by elevated blood glucose levels, compensatory insulin release as well as severe impaired glucose tolerance and insulin sensitivity. Moreover, reduced body fat content and the complete lack of epigonadal white fat pads, indicated reduced uptake of circulating lipids and increased hydrolysis of triglycerides due to abrogated insulin action. However, further analyses have to be performed to characterize the changes in energy metabolism e.g. by analysis of serum lipid species and the expression of genes

involved in lipid and glucose metabolism. Disturbed energy homeostasis was also reflected by a severe loss of whole body weight. These findings of IR KD mice are in line with the results of previous studies employing shIR5 mice (218).

Parameters of insulin and glucose metabolism display a mixed picture in the second control group with KD of the IGF1R. These animals displayed severe resistance to exogenous glucose, with only a minor reduction in insulin sensitivity, a slight increase in basal serum insulin levels and no elevation in basal blood glucose levels but rather a slight decline. These current findings are largely in line with observations of studies demonstrating impaired glucose stimulated insulin secretion after β-cell specific ablation of the IGF1R (215 -216). Mice exhibited reduced glucose stimulated insulin release, with unaltered β-cell mass, causing impaired glucose clearance in both studies. These findings were accompanied by a mild increase in basal insulin levels, at a comparable degree to our observations, maintaining basal serum glucose concentrations at a normal level. No peripheral insulin resistance was found in both studies. Furthermore, *in vitro* studies in the MIN-6 β-cell line revealed dysregulation of ATP level controlling mechanisms, contributing to glucose stimulated insulin release, after silencing of the IGF1R (217).
Although no increase of basal glucose levels was observed in IGF1R KD mice, impaired glucose clearance after insulin challenge indicated the development of peripheral insulin resistance due to IGF1R ablation. However, these effects seem to be relatively mild since elevated basal insulin levels were sufficient to maintain glucose homeostasis reflected by decreased basal blood glucose levels under physiological conditions compared to controls. In contrast to our observations, a severe diabetic phenotype was described for mice expressing a dominant negative IGF1R mutant in skeletal muscle, leading to functional inactivation of IGF1R and IR (70). These mice displayed hyperglycemia as well as a high degree of glucose and insulin resistance. The findings of this study were attributed to missing IGF1R function because IR ablation in muscle caused no distinct diabetic phenotype (27). Neither occurrence of serious insulin resistance nor development of hyperglycemia was confirmed in the present study, despite a considerable KD of IGF1R in muscle. In contrast to reduced body fat percentage in IR KD mice, ablation of

IGF1R caused a significant elevation in body fat content, accompanied by a body weight decline. Increased number and size of adipocytes were described after tissue specific ablation of IGF1R in white adipose tissue and was assumed to be a consequence of increased insulin-stimulated glucose uptake and subsequent lipogenesis (219). Furthermore, increased body fat content and decreased whole body weight were described after brain specific ablation of IGF1R as a secondary effect due to neural developmental defects disturbing the somatic axis and leading to reduced GH release (220) Indeed, GH-deficient mouse models display similar phenotype regarding fat content and body weight (221 -223). Certainly, lowered GH levels should cause a reduced IGF1 release, that was not observed in the present study but was detected after brain specific IGF1R KO (220). Indeed, Klöting *et al*. (219) demonstrated increased IGF1 release from adipocytes after ablation of IGF1R in adipose tissue that might in part compensate missing GH stimulation.

However, in the current study the phenotypic changes observed in shIGF1R mice might result from both described effects on adipose tissue, since IGF1R silencing was ubiquitous in the applied model and GH levels were not determined. In conclusion, the findings of this and preceded studies demonstrate no diabetes-like phenotype in terms of lipid metabolism after ablation of IGF1R. However, detailed analyses of serum lipid species and specifically the expression of enzymes involved in lipid biosynthesis or breakdown in adipose tissue and liver are necessary to draw any further conclusions. Monitoring body weight over the course of the experiment revealed that mice with silencing in IGF1R did not gain weight after start of dox treatment. This stagnation can be attributed to disruption of somatic growth and changed food consumption behaviour, found in shIGF1R2 KD mice. Accordingly, a reduction of food intake was observed in rats after central administration of an IGF1R antagonist. (224). Furthermore, reduced food consumption can be a consequence of altered leptin release from adipocytes and subsequent changes in hypothalamic neuropeptide expression (225-230). Circulating serum leptin levels strongly correlate with adipocyte size and number (231-233), which were both elevated in mice with brain-specific but not adipocyte-specific IGF1R deletion (219, 220). Although no changed food intake behaviour was revealed by both studies, the

inhibitory effects of leptin on calorie intake by acting on the central nervous system is well established (234-238). This assumption cannot be confirmed by the findings of this study because neither morphology of adipose tissue was analysed nor serum leptin levels were determined. Since food intake was monitored for just one week, we can not rule out the possibility that this effect was just temporary. The fact that body weight of mice with silencing in IGF1R just stagnated without severe reduction and displayed increased body fat content might indicate a temporary restricted change in food intake behaviour. If so, reduced weight gain would largely depend on disruption of somatic growth in mice with silencing in IGF1R, clearly demonstrated by reduced body length. Furthermore, reduced weight gain in not induced shIGF1R2 and shIGF1R2_shIR5 mice points to a disruption of the somatic axis due to constitutive shRNA expression in the brain even in the absence of dox. Growth retardation is a well-established phenotype of IGF1R loss-of-function mutants and was demonstrated in mice with conventional heterozygous deletion as well as after tissue specific ablation in brain and muscle (87, 220, 239, 240). Reduced body weight was either attributed directly to systemic disruption of IGF1 signaling or to neural developmental defects leading to reduced GH release in these studies (87, 219, 239).

For the interpretation of the findings in double KD mice it must be considered that these displayed just approximately half of the silencing efficiency that was displayed by control group with single KD of IGF1R. Double KD mice, lacking IR and IGF1R, exhibited metabolic changes comparable to mice with single silencing in IR, displaying elevated blood glucose levels, compensatory insulin release, impaired glucose and insulin resistance as well as severe reduction of whole body weight and fat content.

Neither onset kinetics nor degree of compensatory insulin release differed between mice lacking both receptors or just the IR, indicating either that insulin resistance is developed to the same extend, or compensatory mechanisms were activated at their maximum, in both mice lines. As demonstrated previously, IGF1R ablation caused impaired glucose-induced insulin release (215-217), but did not altered compensatory release in the present study, pointing to a dominant effect of β-cell mass expanison and enhanced function in response to target tissue resistance to insulin (241-244).

Assessment of blood glucose levels in double KD mice revealed an earlier onset of hyperglycemia when compared to mice with single silencing in IR. This accelerated response might reflect a potential role of the IGF1R in insulin signaling. This finding is in line with the observed mild insulin resistance in mice with IGF1R ablation after insulin challenge. Possibly, hybrids of IR and IGF1R or even IGF1R homodimers maintain insulin signalling in the presence of severe hyperinsulinemia. Especially in the initial phase of compensatory insulin secretion, IR KD mice may still be able to dispose of the excess glucose via IGF1R signal transduction. However, this capability will be blunted in double KD mice, possibly explaining the sharper initial rise of blood glucose levels. However, function of IGF1R in this context does not seem to be critical enough to affect the overall magnitude of hyperglycemia in the further course of the experiment. The change in kinetics of glucose increment was the only significant finding indicating a worsening of a diabetic parameter between double KD and single IR KD mice. Furthermore, despite the observed gain of fat mass after IGF1R ablation (219-220), double KD mice lacking both receptors display a phenotype compliant with IR single KD in terms of reduced body fat content and the lack of epigonadal white fat pads, reflecting increased lipolysis and reduced uptake of lipids as a consequence of impaired insulin action on adipocytes. However, these findings in double KD mice cannot be clearly assigned to a dominant effect of IR ablation, since IGF1R reduction in adipose tissue of single KD mice is much more efficient compared to double KD mice. Further investigation on the expression of genes involved in lipogenesis and lipolysis might help to understand the interaction between IR and IGF1R ablation regarding lipid metabolism in adipocytes.

Beside the metabolic changes, a multitude of physical parameters was altered in double KD mice, particularly a drastical reduction of body weight. Weight loss is a common diabetic symptom and was observed in IR single KD and, to a higher degree, in double KD mice. Increased weight loss of dKD mice can not be clearly attributed to a more severe affected energy metabolism, since double KD and IGF1R single KD mice displayed significantly reduction in food intake and somatic growth which might be seen

as the central factors in this context. Reduced food intake due to IGF1R ablation was described before (224) and might be a consequence of elevated fat mass leading to increased leptin release from adipocytes (219, 202). The possibility that changed food intake behavior was only transient must be considered, questioning the relevance of reduced food consumption for body weight reduction in mice with IGF1R KD. Growth retardation as a consequence of disturbing the somatic axis was an expected result of IGF1R KD (87, 220, 239), as described above, and was reflected by reduced body length of double KD mice to the same degree as in IGF1R single KD mice. Reduced food intake and somatic growth seem to be the most apparent factors by which IGF1R ablation contributes induces the drastic weight loss of double KD mice. However, contribution of metabolic effects to this phenotype cannot be ruled out.

The simultaneous ablation of both receptors was lethal after 4 weeks. This increased mortality probably is a combinatory effect of disturbed glucose and lipid metabolism, reduced food intake behaviour and interrupted somatic growth. Due to the increased lethality all experiments were carried out in semi adult mice, up to 10 weeks of age. A potentially more important role of the IGF1R in aged mice was described by Bokov *et al*. (239) who observed progressive insulin resistance in heterozygous IGF1R KO mice of advanced age. The role of simultaneous silencing of IR and IGF1R in aged mice was not investigated and provides an interesting topic for follow-up studies.

Taken together, simultaneous whole body silencing of the insulin and the IGF1 receptor did not cause an enhanced middle-term diabetic phenotype in semi adult mice, displaying disturbance of glucose and lipid metabolism to the same extend as control mice with single ablation of the IR. Compensatory insulin release was undistinguishable between mice after silencing of IR or both IGF1R and IR receptor. Although mice with silencing of both receptors exhibited a more pronounced decline in body weight than IR KD mice, this decrease was rather a consequence of the combined effects of diabetic weight loss, reduced food intake and disturbed somatic growth, than due to a more pronounced impairment of metabolism. The only evidence for a worsening of metabolic parameters were the kinetics of developing hyperglycemia after silencing of both

receptors. This finding confirms the previously described ability of IGF1R receptors or IGF1R/IR hybrids to adopt functions of the IR and thereby contributing to insulin action, which was also demonstrated by a lowered response of peripheral tissues upon insulin challenge found in IGF1R single KD control mice. However, this phenotype appears relatively mild and was not observed under basal conditions, since neither the magnitude of hyperglycaemia, nor peripheral glucose disposal were altered between double KD mice and IR KD mice after the initial phase of induction. These findings suggest that IGF1R might display a compensatory function in marginal or pre-diabetic insulin resistance but is not a determining factor in severe loss of IR function in semi adult mice.

5 Summary

Diabetes mellitus type 2 (T2DM) is a serious and frequent disease, characterized by deregulation of glucose metabolism as a consequence of dysfunction of the insulin signaling system. The relevance of the IGF1 receptor (IGF1R) in compensating functions of the structurally closely related insulin receptor (IR) was subject to several studies but has not been clarified so far. To investigate a possible redundant function of both receptors two strategies were pursued to obtain the simultaneous RNAi-mediated knockdown (KD) of both receptors in transgenic mice. The first strategy based on the generation of a ES cell line bearing two alleles prepared for recombinase mediated cassette exchange (RMCE) in the loci of Rosa 26 (R26) and Collagen, type I, α1 (Col1a1) facilitating the integration of two shRNA expression cassettes. The Functionality of double RMCE was demonstrated, although expression properties of the Collagen locus did not meet our requirements. As a second strategy two shRNA expression units allowing tet-repressor (tetR)-mediated temporal control of RNAi, were combined in a tandem construct, integrated into the Rosa26 locus of ES cells using RMCE technologie. Transgenic mice harbouring this tandem construct displayed temporal controllable RNAi, reducing IR expression to 15-25% and IGF1R expression to 20-45%. Simultaneous whole body silencing of both receptors did not cause an enhanced middle-term diabetic phenotype in semi adult mice, displaying disturbance of glucose and lipid metabolism to the same degree as mice with single ablation of the IR. A faster initial increase of blood glucose was observed in double KD mice, possibly a consequence of a rudimental ability of the IGF1R or IGF1R/IR hybrids to adopt functions of the IR, also demonstrated by a lowered response of IGF1R single KD mice on insulin challenge. Certainly this effect seems not to be distinct enough to appear after complete silencing of IR, since neither the magnitude of hyperglycaemia, nor peripheral glucose disposal were distinguishable between double KD mice and IR KD mice after the initial phase. These findings indicate that IGF1R might in part compensate loss of IR function in marginal or pre-diabetic insulin resistance but is not crucial in severe loss of IR function in semi adult mice.

6 Zusammenfassung

Diabetes mellitus Typ 2 (T2DM) ist eine ernste und häufig auftretende Erkrankung, charakterisiert durch Defekte des Insulin Systems, die eine gestörte Glucosehomöostase zur Folge haben. Die Bedeutung einer möglichen Kompensation der Funktion des Insulinrezeptors (IR) durch den strukturell eng verwandten IGF1-Rezeptor (IGF1R) wurde in vielen Studien untersucht, aber bisher nicht eindeutig geklärt. Um eine potenzielle redundante Funktion der Rezeptoren untersuchen zu können, wurden zwei neuartige technologische Strategien verfolgt, durch die eine zeitgleiche RNAi vermittelte Hemmung der Expression beider Rezeptoren in transgenen Mäusen ermöglicht werden sollte. Im Rahmen der ersten Strategie wurde eine ES Zelllinie generiert, in der zwei genomische loci, Rosa26 und Collagen, type I, alpha 1 (Col1a1), mit RMCE-Kassetten präpariert wurden, um so die gleichzeitige Integration zweier shRNA-Expressionskassetten zu ermöglichen. Die Funktionalität dieses doppelten RMCEs konnte erfolgreich demonstriert werden. Jedoch zeigte sich, dass die Expressionseigenschaften des Col1a1 Locus nicht alle notwendigen Bedingungen erfüllen. In einer zweiten Strategie wurden zwei shRNA-Expressionseinheiten, die eine tet-repressor (tetR) vermittelte zeitliche Kontrolle der RNAi erlaubten, in einem Tandemkonstrukt kombiniert. Dieses wurde mittel RMCE in den Rosa26 locus muriner ES Zellen integriert. Das Tandemkonstrukt erlaubte in transgenen Mäusen eine zeitliche Kontrolle des RNAi Effektes und die Reduktion der IR-Expression auf 15-25% sowie der IGF1R-Expression auf 20-45%. Die gleichzeitige ubiquitär unterdrückte Expression von IR und IGF1R bewirkte keinen verstärkten diabetischen Phänotyp in semiadulten Mäusen. Diese zeigten keinen Unterschied in der Beeinträchtigung des Glucose- und Lipidmetabolismus im Vergleich zu Mäusen, in denen nur die Expression des IR gehemmt wurde. Ein initial stärkerer Anstieg der Blutglucosewerte in Mäusen, in denen beide Rezeptoren herunterreguliert wurden, deutete auf eine mögliche Fähigkeit des IGF1R oder von IR/IGF1R-Hybriden hin, Funktionen des IR zu erfüllen. Einen weiteren Anhaltspunkt für eine redundante Funktion gab die abgeschwächte Reaktion IGF1R defizienter Mäuse auf die Stimulation mit Insulin. Allerdings scheint dieser Effekt nicht

ausgeprägt genug zu sein, um sich bei einem vollständigen Verlust des IR zu manifestieren, da im weiteren Verlauf des Experimentes keine Unterschiede in der Ausprägung der Hyperglycämie oder der peripheren Glucoseaufnahme festgestellt werden konnten. Diese Ergebnisse deuten darauf hin, dass der IGF1R teilweise den Verlust der IR-Funktion in schwach ausgeprägter oder prädiabetischer Insulinresistenz ausgleichen kann. Dieser Effekt scheint allerdings keine Bedeutung bei einem stark ausgeprägten Funktionsverlust des IR in semiadulten Mäusen zu haben.

7 References

1. Word Health Organization; Diabetes; Fact sheet N°312; Geneva: World Health Organization, August 2011.
2. Pilkis, S.J., and Granner, D.K. 1992. Molecular physiology of the regulation of hepatic gluconeogenesis and glycolysis. Annu Rev Physiol 54:885-909.
3. World Health Organization. Prevention of diabetes mellitus. Technical Report Series no. 844. Geneva: World Health Organization, 1994.
4. Kahn, B. B., and Flier, J. S. 2000. Obesity and insulin resistance. J. Clin. Investig. 106: 473–481.
5. Saltiel, A. R. 2001. New perspectives into the molecular pathogenesis and treatment of Type 2 diabetes. Cell, 104:517-529.
6. Weir, G.C., and Bonner-Weir, S. 2004. Five stages of evolving β-cell dysfunction during progression to diabetes. Diabetes 53(3)16-21.
7. Goldstein B.J. 2002. Insulin resistance as the core defect in type 2 diabetes mellitus. Am J Cardiol 90:3-10.
8. Sanders, L.J. 2002. From Thebes to Toronto and the 21st Century: An Incredible Journey. Diabetes Spectrum 15:56-60.
9. King, K.M., and Rubin, G. 2003. A history of diabetes: from antiquity to discovering insulin. Br J Nurs 12:1091-1095.
10. Guder W. G. 2005. Das Laborbuch für Klinik und Praxis, Urban&FischerVerlag, S. 255- 260, ISBN 3-437-23340-8.
11. Gyr N. E. 2003. Internistische Notfälle: sicher durch die Akutsituation und die nachfolgenden 48 Stunden, Thieme Verlag, S.490, ISBN 3-13-510607-1.
12. American Diabetes Association. 2011. Standards of medical care in diabetes. Diabetes Care. 34:11-61.
13. Bray, G.A. 2004. Medical consequences of obesity. J Clin Endocrinol Metab 89:2583-2589.
14. Risérus, U., Willett, W.C., and Hu, F.B. 2009. Dietary fats and prevention of type 2 diabetes. Progress in Lipid Research 48:44-51.
15. Ripsin, C.M., Kang, H., and Urban R.J. 2009. Management of blood glucose in type 2 diabetes mellitus. Am Fam Physician 79:29-36.
16. Boden, G., and Carnell, L.H. 2008. Obesity and Free Fatty Acids (FFA) E ndocrinol Metab Clin North Am. 37(3):635–645.
17. Kashyap, S.R, and Defronzo R.A. 2007. The insulin resistance syndrome: physiological considerations. Diabetes and Vascular Disease. 4(1):13-9.
18. Jiao, P., Ma, J., Feng, B., Zhang, H., Diehl, J.A. Chin, Y.E., Yan, W., and Xul, H. 2010. FFA-Induced Adipocyte Inflammation and Insulin Resistance: Involvement of ER Stress and IKKβ Pathways. Obesity 19(3):483-91.
19. Floyd, J.C., Fajans, S.S., Conn, J.W., Knopf, R.F., and Rull J. 1966. Stimulation of insulin secretion by amino acids. J Clin Invest. 45(9):1487-1502.

20. Malaisse, W.J. and Malaisse-Lagae, F. 1968. Stimulation of insulin secretion by non-carbohydrate metabolites. Journal of Laboratory and Clinical Medicine 72:438-448.
21. Pelkonen, R., Miettinen, A., Taskinen, M. and Nikkila, A. 1968. Effect of acute elevation of plasma triglyceride and FFA levels on glucose utilization and plasma insulin. Diabetes 17:76-82.
22. Crespin, S., Greenough, W. and Steinberg, D. 1969. Stimulation of insulin secretion by infusion of free fatty acids. Journal of Clinical Investigation 48:1934-1943.
23. MacDonald, M. and Fahein, L. 1988. Glyceraldehyde phosphate and methyl esters of succinic acid. Two "new" potent insulin secretagogues. Diabetes 37:997-999.
24. Cushman, S.W., and Wardzala, L.J. 1980. Potential mechanism of insulin action on glucose transport in the isolated rat adipose cell. Apparent translocation of intracellular transport systems to the plasma membrane. J. Biol. Chem. 255:4758-4762.
25. Cushman, S.W., Wardzala, L.J., Simpson, I.A., Karnieli, E., Hissin, P.J., Wheeler, T.J., Hinkle, P.C., and Salans, L.B. 1984. Insulin-induced translocation of intracellular glucose transporters in the isolated rat adipose cell. Fed Proc 43:2251-2255.
26. Birnbaum, M.J. 1992. The insulin-sensitive glucose transporter. Int. Rev. Cytol. 137:239-297.
27. Saltiel, A.R., and Kahn, C.R. 2001. Insulin signalling and the regulation of glucose and lipid metabolism. Nature 414:799-806.
28. Zhao, A.Z., Huan, J.N., Gupta, S., Pal, R., and Sahu, A. 2002. A phosphatidylinositol 3-kinase phosphodiesterase 3B-cyclic AMP pathway in hypothalamic action of leptin on feeding. Nat. Neurosci.5(8):727-8.
29. Air, E. L., Benoit, S. C., Cleggs, D. J., Seeley, R. J., and Woods S. C. 2002. Insulin and leptin combine additively to reduce food intake and body weight in rats. Enocrinology 6:2449-52.
30. Taniguchi, C.M., Emanuelli, G., and B., Kahn, C.R. 2006. Critical nodes in signalling pathways: insights into insulin action. Nature Reviews Molecular Cellular Biology 7 85–96.
31. Steiner, D.F., Cunningham, D., Spigelman, L., and Aten, B. 1967. Insulin biosynthesis: evidence for a precursor. Science 157:697-700.
32. Dean, P.M. 1973. Ultrastructural morphometry of the pancreatic β-cell. Diabetologia 9:115-119.
33. Orci, L., Malaisse-Lagae, F., Ravazzola, M., Amherdt, M. and Renold, A.E. 1973. Exocytosis-endocytosis coupling in the pancreatic beta cell. Science 181:561-562.
34. Olofsson, C.S., Göpel, S.O., Barg, S., Galvanovskis, J., Ma, X., Salehi, A., Rorsman, P., Eliasson, L. 2002. Fast insulin secretion reflects exocytosis of docked granules in mouse pancreatic B-cells. Pflugers Arch 444:43-51.
35. Cerasi, E. 1975. Mechanisms of glucose stimulated insulin secretion in health and in diabetes: some re-evaluations and proposals. Diabetologia 11:1-13.

36. Unger, R.H., 1991 Diabetic hyperglycemia: link to impaired glucose transport in pancreatic ß cells. Science 251, 1200-1205.
37. Thorens, B., 1992. Molecular and cellular physiology of GLUT2, a high-Km facilitated diffusion glucose transporter. Int. Rev. Cytol. 137A, 209-238.
38. Henquin, J. C. 2000 Triggering and amplifying pathways of regulation of insulin secretion by glucose. Diabetes 49:1751–1760.
39. Thorens, B. 1995. Glucagon-like peptide-1 and control of insulin secretion. Diabète & métabolisme 21(5):311–8.
40. Holst, J. J. 1994. Glucagonlike peptide 1: a newly discovered gastrointestinal hormone. Gastroenterology 107:1848-1855.
41. Aronoff, S. L., Berkowitz K., Shreiner B., and Want L. 2004. Glucose Metabolism and Regulation: Beyond Insulin and Glucagon. Diabetes Spectrum 17 (3):183-190.
42. Brüning, J.C., Michael, M.D., Winnay, J.N., Hayashi, T., Hörsch, D., Accili, D., Goodyear, L.J., and Kahn C.R. 1998. A muscle-specific insulin receptor knockout exhibits features of the metabolic syndrome of NIDDM without altering glucose tolerance. Mol Cell 2(5):559-69.
43. Kulkarni, R. N., Brüning, J. C., Winnay, J. N., Postic, C., Magnuson, M. A., and Kahn C. R. 1999. Tissue-specific knockout of the insulin receptor in pancreatic beta cells creates an insulin secretory defect similar to that in type 2 diabetes. Cell 5(3):329-39.
44. Brüning, J.C., Gautam, D., Burks, D. J., Gillette, J., Schubert, M., Orban, P.C., Klein, R., Krone, W., Müller-Wieland, D.M., and Kahn C.R. 2000. Role of Brain Insulin Receptor in Control of Body Weight and Reproduction. Science 289(5487):2122-2125.
45. Michael, M.D., Kulkarni, R.N., Postic, C., Previs, S.F., Shulman, G.I., Magnuson, M.A., and Kahn C.R. 2000. Loss of insulin signaling in hepatocytes leads to severe insulin resistance and progressive hepatic dysfunction. Mol Cell 6(1):87-97.
46. Blüher, M., Michael, M.D., Peroni, O.D., Ueki, K., Carter, N., Kahn, B.B., and Kahn, C. R. 2002. Adipose tissue selective insulin receptor knockout protects against obesity and obesity-related glucose intolerance. Dev Cell. 3(1):25-38.
47. Baumgartl, J., Baudler, S., Scherner, M., Babaev, V., Makowski, L., Suttles, J., McDuffie, M., Tobe, K., Kadowaki, T., Fazio, S., Kahn, C.R., Hotamisligil, G.S., Krone, W., Linton, M., and Brüning J.C. 2006. Myeloid lineage cell-restricted insulin resistance protects apolipoproteinE-deficient mice against atherosclerosis. Cell Metab 3(4):247-56.
48. Ullrich, A., Gray, A., Tam, A.W., Yang-Feng, T., Tsubokawa, M., Collins, C., Henzel, W., Le Bon, T., Kathuria, S., and Chen, E. 1986. Insulin-like growth factor I receptor primary structure: comparison with insulin receptor suggests structural determinants that define functional specificity. Embo J. 5:2503-2512.
49. Shier, P., and Watt, V.M. 1989. Primary structure of a putative receptor for a ligand of the insulin family. J Biol Chem 264:14605-14608.

50. Van Obberghen, E., Ksauga, M., Le Cam, A., Hedo, J.A., Itin, A., and Harrison, L.C. 1981. Biosynthetic labeling of insulin receptor: studies of subunits in cultured human IM-9 lymphocytes. Proc Natl Acad Sci U S A 78:1052-1056.
51. Kasuga, M., Fujita-Yamaguchi, Y., Blithe, D.L., and Kahn, C.R. 1983. Tyrosine-specific protein kinase activity is associated with the purified insulin receptor. Proc Natl Acad Sci USA 80:2137-2141.
52. Kahn, C.R., and White, M.F. 1988. The insulin receptor and the molecular mechanism of insulin action. J Clin Invest 82:1151–1156.
53. Eck, M.J., Dhe-Paganon, S., Trub, T., Nolte, R.T., and Shoelson, S.E. 1996. Structure of the IRS-1 PTB domain bound to the juxtamembrane region of the insulin receptor. Cell 85:695-705.
54. Miralpeix, M., Sun, X.J., Backer, J.M., Myers, M.G., Jr., Araki, E., and White, M.F. 1992. Insulin stimulates tyrosine phosphorylation of multiple high molecular weight substrates in Fao hepatoma cells. Biochemistry 31:9031-9039.
55. Ward, C., Lawrence, M., Streltsov, V., Garrett, T., McKern, N., and Lou, M.Z. 2008. Structural insights into ligand-induced activation of the insulin receptor. Acta Physiol. (Oxf.) 192(1): 3-9.
56. Boura-Halfon, S., and Zick, Y. 2009. Phosphorylation of IRS proteins, insulin action, and insulin resistance. Am J Physiol Endocrinol Metab 296:581-591.
57. Holgado-Madruga, M., Emlet, D.R., Moscatello, D.K., Godwin, A.K., and Wong, A.J. 1996. A Grb2-associated docking protein in EGF- and insulin-receptor signalling. Nature 379:560-564.
58. Virkamäki, A., Ueki, K., and Kahn, C.R. 1999. Protein-protein interactions in insulin signaling and the molecular mechanisms of insulin resistance. J Clin Invest 103:931-943.
59. Pessin, J.E., and Saltiel, A.R. 2000. Signaling pathways in insulin action: molecular targets of insulin resistance. J Clin Invest 106:165–169.
60. Hadari, Y. R., Tzahar, E., Nadiv, O., Rothenberg, P., Roberts, C. T., LeRoith, D., Yarden, Y. and Zick, Y. 1992. Insulin and insulinomimetic agents induce activation of phosphatidylinositol 3'-kinase upon its association with pp185 (IRS-1) in intact rat livers. J. Biol. Chem. 267(25):17483.
61. Terauchi, Y., Tsuji, Y., Satoh, S., Minoura, H., Murakami, K., Okuno, A., Inukai, K., Asano, T., Kaburagi, Y., Ueki, K., Nakajima, H., Hanafusa, T., Matsuzawa, Y., Sekihara, H., Yin, Y., Barrett, J.C., Oda, H., Ishikawa, T., Akanuma, Y., Komuro, I., Suzuki, M., Yamamura, K., Kodama, T., Suzuki, H., Yamamura, K., Kodama, T., Suzuki, H., Koyasu, S., Aizawa, S., Tobe, K., Fukui, Y., Yazaki, Y., and Kadowaki T. 1999. Increased insulin sensitivity and hypoglycaemia in mice lacking the p83α subunit of phosphoinositol-3 kinase. Nat Genet 21:230- 235.
62. Fruman, D.A., Mauvais-Jarvis, F., Pollard, D.A., Brazil, D., Bronson, R.T., Kahn, C.R., and Cantley L.C. 2000. Hypoglycemia, liver necrosis and perinatal death in mice lacking all isoforms of phosphoinositide 3-kinase p85. Nat Genet 26:379-82.
63. Alessi, D.R., James, S.R., Downes, C.P., Holmes, A.B., Gaffney, P.R., Reese, C.B., and Cohen, P. 1997. Characterization of a 3-phosphoinositide-dependent

protein kinase which phosphorylates and activates protein kinase Balpha. Current Biology 7 261–269.

64. Stephens, L., Anderson, K., Stokoe, D., Erdjument-Bromage, H., Painter, G.F., Holmes, A.B., Gaffney, P.R., Reese, C.B., McCormick, F., Tempst, P. , Coadwell, W.J., and Hawkins, P.T. 1998. Protein kinase B kinases that mediate phosphatidylinositol 3,4,5-trispho-sphate-dependent activation of protein kinase B. Science 279:710–714.
65. Hresko, R.C., and Mueckler, M. 2005. mTOR.RICTOR is the Ser473 kinase for Akt/protein kinase B in 3T3-L1 adipocytes. Journal of Biological Chemistry 280:40406–40416.
66. Sarbassov, D.D., Guertin, D.A., Ali, S.M., and Sabatini, D.M. 2005. Phosphorylation and regulation of Akt/PKB by the rictor-mTOR complex. Science 307:1098–1101.
67. Proud, C.G. 2006. Regulation of protein synthesis by insulin. Biochem Soc Trans. 34:213-6.
68. Leney, S.E., and Tavare, J. M. 2009. The molecular basis of insulin-stimulated glucose uptake: signaling, trafficking and potential drug targets. J. Endocrinol. 203:1–18.
69. Boulton, T.G., Nye, S.H., Robbins, D.J., Ip, N.Y., Radziejewska, E., Morgenbesser, S.D., De Pinho, R.A., Panayotatos, N., Cobb, M.H., and Yancopoulos, G.D. 1991. ERKs: a family of protein-serine/threonine kinases that are activated and tyrosine phosphorylated in response to insulin and NGF. Cell 65:663–675.
70. Cheatham, B., and Kahn, C.R. 1995. Insulin action and the insulin signaling network. Endocr Rev 16(2):117-42.
71. Salmon, W.D., and Daughaday, W.H. 1957. A hormonally controlled serum factor which stimulates sulfate incorporation by cartilage in vitro. J Lab Clin Med. 48:825-836.
72. Baker, J., Liu, J.P., Robertson, E.J. and Efstratiadis, A. 1993. Role of insulin-like growth factors in embryonic and postnatal growth. Cell 75:73-82.
73. Ranke, M.B. 1987. A note on adults with growth hormone deficiency. Acta Paediatrica Scandinavica Supplementum 331:80-82.
74. Daughaday, W.D., Hall, K., Raben, M.S., Salmon, W.D., Jr., Van den Brande, J. L., and Van Wyk, J.J. 1972. Somatomedin: proposed designation for sulphation factor. Nature 235:107.
75. Blundell, T.L., Bedarkar, S., and Humbel, R.E. 1983. Tertiary structures. rcceptor binding, and antigenicity of insulin like growth factors. Federatiori Proceedings 42:2592-2597.
76. Pandini, G., Frasca, F., Mineo, R., Sciacca, L., Vigneri, R., and Belfiore, A. 2002. Insulin/insulin-like growth factor I hybrid receptors have different biological characteristics depending on the insulin receptor isoform involved. J Biol Chem 277: 39684–39695.

77. Adams, T.I., Epa, V.C., Garrett, T.P., and Ward, C.W. 2000. Structure and function of the type 1 insulin-like growth factor receptor. Cell Mol Life Sci 57:1050–1093.
78. Liu, Y.F., Paz, K., Herschkovitz, A., Alt, A., Tennenbaum, T., Sampson, S.R., Ohba, M., Kuroki, T., Le Roith, D., and Zick, Y. 2001. Insulin stimulates PKCzeta -mediated phosphorylation of insulin receptor substrate-1 (IRS-1). A self-attenuated mechanism to negatively regulate the function of IRS proteins. J Biol Chem; 276(17):14459-65.
79. Sell, C., Dumenil, G., Deveaud, C., Miura, M., Coppola, D., De Angelis, T., Rubin, R., Efstratiaids, A., and Baserga, R. 1994. Effect of a null mutation of the insulin-like growth factor I receptor gene on growth and transformation of mouse embryo fibroblasts. Mol Cell Biol 14:3604–3612.
80. Baserga, R., Hongo, A., Rubini, M., Prisco, M., and Valentinis, B. 1997. The IGF-I receptor in cell growth, transformation and apoptosis. Biochim Biophys Acta 1332:105-126.
81. Valentinis, B., Romano, G., Peruzzi, F., Morrione, A., Prisco, M., Soddu, S., Cristofanelli, B., Sacchi, A., and Baserga, R. 1999. Growth and differentiation signals by the insulin-like growth factor 1 receptor in hemopoietic cells are mediated through different pathways. J Biol Chem 274:12423–12430.
82. Renehan, A.G., Zwahlen, M., Minder, C., O'Dwyer, S.T., Shalet S.M., and Egger, M. 2004. Insulin-like growth factor (IGF)-I, IGF binding protein-3, and cancer risk: systematic review and meta-regression analysis Nature Reviews Cancer 4:417.
83. Guler, H.P., Zapf, J., and Froesch, E.R. 1987. Short-term metabolic effects of recombinant human insulin-like growth factor I in healthy adults. NEngl J Med; 317:137–140.
84. Zenobi, P.D., Graf, S., Ursprung, H., and Froesch E.R. 1992. Effects of insulin-like growth factor-I on glucose tolerance, insulin levels, and insulin secretion. J Clin Invest 89:1908–1913.
85. Frystyk, J., Skjaerbaek, C.,Vestbo, E., Fisker, S., and Orskov, H. 1999. Circulating levels of free insulin-like growth factors in obese subjects: the impact of type 2 diabetes. Diabetes Metab Res Rev 15:314–322.
86. Frick, F., Oscarsson, J., Vikman-Adolfsson, K., Ottosson, M., Yoshida, N., and Eden, S. 2000 Different effects of IGF-I on insulin-stimulated glucose uptake in adipose tissue and skeletal muscle. Am. J Physiol Endocrinol Metab 278:729-737.
87. Fernandez, A.M., Kim, J.K., Yakar, S., Dupont, J., Hernandez-Sanchez, C., Castle, A.L., Filmore, J., Shulman, G.I., and Le Roith, D. 2001. Functional inactivation of the IGF-I and insulin receptors in skeletal muscle causes type 2 diabetes. Genes Dev 15:1926-1934.
88. Pratipanawatr, T., Pratipanawatr, W., Rosen, C.R., Bajaj, M., Cusi, K., Mandarino, L., Kashyap, S., Belfort, R., and De Fronzo, R. A. 2002. Effect of IGF-I on FFA and glucose metabolism in control and type 2 diabetic subjects. Am J Physiol Endocrinol Metab 282:1360-1368.

89. Simpson, H.L., Jackson, N.C., Shojaee-Moradie, F., Jones, R.H., Russell-Jones, D.L., Sonksen, P.H., Dunger, D.B., Umpleby, A.M. 2004. Insulin-like growth factor I has a direct effect on glucose and protein metabolism, but no effect on lipid metabolism in type 1 diabetes. J Clin Endocrinol Metab 89:425-432.
90. Rosen, C.J. and Pollak, M. 1999. Circulating IGF-I: new perspectives for a new century. Trends Endocrinol. Metab., 10:136-141.
91. Clemmons, D.R., Moses, A.C., Mc Kay, M.J., Sommer, A., Rosen, D.M., and Ruckle, J. 2000. The combination of insulin-like growth factor I and insulin-like growth factor-binding protein-3 reduces insulin requirements in insulin-dependent type 1 diabetes: Evidence for in vivo biological activity. J Clin Endocrinol Metab 85:1518-1524.
92. Baxter, R.C., Holman, S.R., Corbould, A., Stranks, S., Ho, P.J., and Braund, W. 1995. Regulation of the insulin-like growth factors and their binding proteins by glucocorticoid and growth hormone in nonislet cell tumor hypoglycemia. Journal of Clinical Endocrinology and Metabolism 80:2700-2708.
93. Firth, S.M., Ganeshprasad, U., and Baxter, R.C. 1998. Structural determinants of ligand and cell surface binding of insulin-like growth factor-binding protein-3. J Biol Chem 273:2631-2638.
94. Rosenfeld, R.G., Hwa, V., Wilson, E., Plymate, S.R., and Oh, Y. 2000. The insulin-like growth factor-binding protein superfamily. Growth Horm. IGF Res 10:16–17.
95. Zapf, J. 1995. Physiological role of the insulin-like growth factor binding proteins. Europ J Endocrinol. 132:645-654.
96. Rajah, R., Khare, A., Lee, P.D., and Cohen, P. 1999. Insulin-like growth factor-binding protein-3 is partially responsible for high-serum-induced apoptosis in PC-3 prostate cancer cells. Journal of Endocrinology 163:487-494.
97. Le Roith, D., Bondy, C., Yakar, S., Liu, J. L., and Butler, A. 2001. The somatomedin hypothesis: 2001. Endocr Rev 22:53-74.
98. Steele-Perkins, G., Turner, J., Edman, J.C., Hari, J., Pierce, S.B., Stover, C., Rutter, W.J., and Roth, R.A. 1988. Expression and characterization of a functional human insulinlike growth factor I receptor. J Biol Chem 263:11486-11492.
99. Chernausek, S.D., Jacobs, S., and Van Wyk, J. J, 1981. Structural similarities between human receptors for somatomedin-C and insulin: analysis by affinity labeling. Biochemistry 20:7345-7350.
100. Bhaumick, B., Bala, R.M., and Hollenberg, M.D. 1981. Somatomedin receptor of human placenta: solubilization, photolabeling, partial purification, and comparison with insulin receptor. Proc Natl Acad Sci USA 78:4279-4283.
101. Jacobs, S., Kull, F.C., Earp, H.S., Svoboda, M.E., Van Wyk J.J., and Cuatrecasas P. 1983. Somatomedin-C stimulates the phosphorylation of the beta-subunit of its own receptor. J Biol Chem 258(16):9581-4.
102. Blakesley, V.A., Kalebic, T., Helman, L.J., Stannard, B., Faria, T.N., Roberts, C.T., Jr. & LeRoith, D. 1996. Tumorigenic and mitogenic capacities are reduced in transfected fibroblasts expressing mutant insulin-like growth factor (IGF)-I

receptors, the role of tyrosine residues 1250, 1251, and 1316 in the carboxy-terminu of the IGF-I receptor. Endocrinology 137:410–417.
103. Riedemann, J., and Macaulay, V.M. 2006. IGF1R signalling and its inhibition. Endocr. Relat. Cancer 13(1):33–43.
104. Liu, J.P., Baker, J., Perkins, A.S., Robertson, E.J., and Efstratiadis, A. 1993. Mice carrying null mutations of the genes encoding insulin-like growth factor I (Igf-1) and type 1 IGF receptor (Igf1r). Cell 75:59-72.
105. Pollak, M.N., Schernhammer, E.S., and Hankinson S.E. 2004. Insulin-like growth factors and neoplasia. Nature Reviews. Cancer 4:505-518.
106. Peruzzi, F., Prisco, M., Dews, M., Salomoni, P., Grassilli, E., Romano, G., Calabretta, B., and Baserga, R., 1999. Multiple signaling pathways of insulin-like growth factor 1 receptor in protection from apoptosis. Mol Cel Biol 19:7203-7215.
107. Brazil, D.P., Yang, Z.Z., and Hemmings, B.A. 2004. Advances in protein kinase B signalling: AKTion on multiple fronts. Trends in Biochemical Sciences 29:233-242.
108. Mora, A., Sakamoto, K., Mc Manus, E.J., and Alessi, D.R. 2005. Role of the PDK1-PKB-GSK3 pathway in regulating glycogen synthase and glucose uptake in the heart. FEBS Lett 579(17):3632-8.
109. Senthil, D., Choudhury, G., Bhandari, B.K., and Kasinath, B.S. 2002. The type 2 vascular endothelial growth factor receptor recruits insulin receptor substrate-1 in its signalling pathway. Biochem J 368:49-56.
110. Kuemmerle, J. F. 2003. IGF-I elicits growth of human intestinal smooth muscle cells by activation of PI3K, PDK-1, and p70S6 kinase. Am. J. Physiol. Gastrointest. Liver Physiol. 284:411-422.
111. Galvan, V., Logvinova, A., Sperandio, S., Ichijo, H., and Bredesen, D.E. 2003. Type 1 insulin-like growth factor receptor (IGF-1R) signaling inhibits apoptosis signal-regulating kinase 1 (ASK1). J Biol Chem 278:13325-13332.
112. Pandini, G., Frasca, F., Mineo, R., Sciacca, L., Vigneri, R., and Belfiore, A. 2002. Insulin/insulin-like growth factor I hybrid receptors have different biological characteristics depending on the insulin receptor isoform involved. J Biol Chem 277:39684-39695.
113. Sasaoka, T., Ishiki, M., Sawa, T., Ishihara, H., Takata, Y., Imamura, T., Usui, I., Olefsky, J.M., and Kobayashi, M. 1996. Comparison of the insulin and insulinlike growth factor 1 mitogenic intracellular signaling pathways. Endocrinology 137:4427-4434.
114. Biedi, C., Panetta, D., Segat, D., Cordera, R., and Maggi, D. 2003. Specificity of insulin-like growth factor I and insulin on Shc phosphorylation and Grb2 recruitment in caveolae. Endocrinology 144:5497-5503.
115. Boucher, J., Tseng, Y.H., and Kahn C.R. 2010. Insulin and insulin-like growth factor-1 receptors act as ligand-specific amplitude modulators of a common pathway regulating gene transcription. J Biol Chem 285:17235-17245.

116. Jensen, M., and De Meyts, P. 2009. Molecular mechanisms of differential intracellular signaling from the insulin receptor. Vitamins and Hormones 80:51-75.
117. Mynarcik, D.C., Paul, F.W., Schaffer, L., Yu, G.Q., and Whittaker, J. 1997. Identification of common ligand binding determinants of the insulin and insulin-like growth factor 1 receptors. J Biol Chem 272:18650-18655.
118. Frederici, M., Porcio, O., Zucaro, L., Fuso, A., Borboni, P., Lauro, D., Sesti, G. 1997. Distribution of insulin/insulin-like growth factor-I hybrid receptors in human tissues. Mol Cell Endocrinol 129:121-126.
119. Zelobowska, K., Gumprecht, J., and Grzeszczak, W. 2009. Mitogenic potency of insulin glargine. Endokrynol Pol 60(1):34-39.
120. Rajpathak, S.N., Gunter, M.J., Wylie-Rosett, J., Ho, G.Y., Kaplan, R.C., Muzumdar, R., Rohan, T.E., and Strickler, H.D. 2009.The role of insulin-like growth factor-I and its binding proteins in glucose homeostasis and type 2 diabetes. Diabetes Metab Res Rev 25:3.
121. Kasuga, M., Fujita-Yamaguchi, Y., Blithe, D.L., and Kahn, C.R. (1983). Tyrosine-specific protein kinase activity is associated with the purified insulin receptor. Proc Natl Acad Sci USA 80:2137-2141.
122. Soos, M.A., and Siddle, K. 1989. Immunological relationships between receptors for insulin and insulin-like growth factor i. Evidence for structural heterogeneity of insulin-like growthfactor i receptors involving hybrids with insulin receptors. Biochem J 263(2):553–563.
123. Soos, M.A., Field, C.E., and Siddle, K. 1993. Purified hybrid insulin/insulin-like growth factor-i receptors bind insulin-like growth factor-i, but not insulin, with high affinity. Biochem J 290(2):419-426.
124. Sakai, K., Lowman, H.B., Clemmons, D.R. 2002. Increases in free, unbound insulin-like growth factor i enhance insulin responsiveness in human hepatoma g2 cells in culture. J Biol Chem 277(16):13620-13627.
125. Slaaby, R., Schäffer, L., Lautrup-Larsen, I., Andersen, A.S., Shaw, A.C., Mathiasen I.S., and Brandt, J. 2006. Hybrid receptors formed by insulin receptor (IR) and insulin-like growth factor I receptor (IGF-IR) have low insulin and high IGF-1 affinity irrespective of the IR splice variant. J Biol Chem 281(36):25869-74.
126. Belfiore, A., Frasca, F., Pandini, G., Sciacca, L., and Vigneri, R. 2009. Insulin receptor isoforms and insulin receptor/insulin-like growth factor receptor hybrids in physiology and disease. Endocr Rev 30:586-623.
127. Tan, K., and Baxter, R.C. 1986. Serum insulin-like growth factor I levels in adult diabetic patients: the effect of age. J Clin Endocrinol Metab 63:651-655.
128. Boulware, S.D., Tamborlane, W.V., Rennert, N.J., Gesundheit, N., and Sherwin, R.S. 1994. Comparison of the metabolic effects of recombinant human insulin-like growth factor-I and insulin. Dose-response relationships in healthy young and middle-aged adults. J Clin Invest; 93:1131-1139.
129. Carroll P.V., Umpleby, M., and Alexander, E.L. 1998. Recombinant human insulin-like growth factor-I (rhIGF-I) therapy in adults with type 1 diabetes

mellitus: effects on IGFs, IGF-binding proteins, glucose levels and insulin treatment. Clin Endocrinol (Oxf); 49:739-746.

130. Saukkonen, T., Amin, R., Williams, R.M., Fox, C., Yuen, K.C., White, M.A., Umpleby, A.M., Acerini, C.L., and Dunger, D.B. 2004. Dose-dependent effects of recombinant human insulin-like growth factor (IGF)-I/IGF binding protein-3 complex on overnight growth hormone secretion and insulin sensitivity in type 1 diabetes. J Clin Endocrinol Metab 89:4634-4641.
131. Schmid, C., Bianda, T., Zwimpfer, C., Zapf, J., and Wiesli, P. 2005. Changes in insulin sensitivity induced by short-term growth hormone (GH) and insulin-like growth factor I (IGF-I) treatment in GH- deficient adults are not associated with changes in adiponectin levels. Growth Horm IGF Res 15:300-303.
132. Lewitt, M.S., Denyer, G.S., Cooney, G.J., Baxter, R.C. 1991. Insulin-like growth factor-binding protein-1 modulates blood glucose levels. Endocrinology 129:2254-2256.
133. Katz, L.E., De Leon, D.D., Zhao, H., and Jawad, A.F. 2002. Free and total insulin-like growth factor (IGF)-I levels decline during fasting: relationships with insulin and IGF-binding protein-1. J Clin Endocrinol Metab 87:2978-2983.
134. Modric, T., Silha, J.V., Shi, Z., Gui, Y., Suwanichkul, A., Durham, S.K., Powell, D.R., Murphy, L.J. 2001. Phenotypic manifestations of insulin-like growth factor-binding protein-3 overexpression in transgenic mice. Endocrinology 142:1958-1967.
135. Silha, J. V., Gui, Y., and Murphy, L. J. 2002. Impaired glucose homeostasis in insulin-like growth factor binding protein-3 transgenic mice. Am, J. Physiol., 283:937-945.
136. Chang, P.Y., Benecke, H., Le Marchand-Brustel, Y., Lawitts, J., and Moller, D.E. 1994. Expression of a dominant-negative mutant human insulin receptor in the muscle of transgenic mice. J Biol Chem 269:16034-16040.
137. Lamothe, B., Baudry, A., Desbois, P., Lamotte, L., Bucchini, D., De Meyts, P., and Joshi, R.L. 1998. Genetic engineering in mice: impact on insulin signalling and action. Biochemical Journal 335:193-204.
138. Baudry, A., Lamothe, B., Bucchini, D., Jami, J., Montarras, D., Pinset, C., Joshi, R.L. 2001. IGF-1 receptor as an alternative receptor for metabolic signaling in insulin receptor-deficient muscle cells. FEBS Lett 488:174-8.
139. Poggi, C., Le Marchand-Brustel, Y., Zapf, J., Froesch, E.R., and Freychet, P. 1979. Effects and binding of insulin-like growth factor 1 in the isolated soleus muscle of lean and obese mice: comparison with insulin. Endocrinology 105:723-730.
140. Dimitriadis, G., Parry-Billings, M., Dunger, D., Bevan, S., Colquhoun, A., Taylor, A., Calder, P., Krause, U., Wegener, G., and Newsholme, E.A. 1992. Effects of in-vivo administration of insulin-like growth factor-1 on the rate of glucose utilization in the soleus muscle of the rat. J Endocrinol 133:37-43.
141. Hussain, M.A., Schmitz, O., Mengel A., Glatz Y., Christiansen J.S., Zapf J., and Froesch E.R. 1994. Comparison of the effects of growth hormone and insulin-like

growth factor I on substrate oxidation and on insulin sensitivity in growth hormone-deficient humans. J Clin Invest 94:1126-1133.

142. Le Roith, D., Werner, H., Beitner-Johnson, D., and Roberts, Jr., C.T. 1995. Molecular and cellular aspects of the insulin-like growth factor I receptor. Endocr Rev 16:143-163.
143. Seibler, J., Kuter-Luks, B., Kern, H., Streu, S., Plum, L., Mauer, J., Kuhn, R., Brüning, J.C., and Schwenk, F. 2005. Single copy shRNA configuration for ubiquitous gene knockdown in mice. Nucleic Acids Res 33:e67.
144. Seibler, J., Kleinridders, A., Küter-Luks, B., Niehaves, S., Brüning, J. C., and Schwenk, F. 2007. Reversible gene knockdown in mice using a tight, inducible shRNA expression system. Nucleic Acids Res 35(7):e54.
145. Fire, A., Xu, S., Montgomery, M.K., Kostas, S.A., Driver, S.E., and Mello, C.C. 1998. Potent and specific genetic interference by double-stranded RNA in Caenorhabditis elegans. Nature 391:806-811.
146. Hutvagner, G., and Zamore, P.D. 2002. RNAi: nature abhors a double-strand. Curr Opin Genet Dev 12:225-232.
147. Ketting, R.F., Haverkamp, T.H., van Luenen, H.G., Plasterk, R.H. 1999. Mut-7 of C. elegans, required for transposon silencing and RNA interference, is a homolog of Werner syndrome helicase and RNase D. Cell 99:133-141.
148. Tabara, H., Sarkissian, M., Kelly, W.G., Fleenor, J., Grishok, A., Timmons, L., Fire A., and Mello C.C. 1999. The rde-1 gene, RNA interference, and transposon silencing in C. elegans. Cell 99:123-132.
149. Plasterk, R.H.A. 2002. RNA Silencing: The Genome's Immune System. Science 296:1263-1265.
150. Chen, C.Z., Li, L., Lodish, H.F., and Bartel, D.P. 2004. MicroRNAs modulate hematopoietic lineage differentiation. Science 303:83-86.
151. Krichevsky, A.M., Sonntag, K.C., Isacson, O., and Kosik, K.S. 2006. Specific microRNAs modulate embryonic stem cell-derived neurogenesis. Stem Cells, 24(4):857-64.
152. Thai, T.H., Calado, D.P., Casola, S., Ansel, K.M., Xiao, C., Xue, Y., Murphy, A., Frendewey, D., Valenzuela, D., Kutok, J.L., Schmidt-Supprian, M., Rajewsky, N., Yancopoulus, G., Rao A., and Rajewsky K. (2007) Regulation of the Germinal Center Response by MicroRNA-155. Science 316:604-608.
153. Lee, Y., Ahn, C., Han, J., Choi, H., Kim, J., Yim, J. 2003. The nuclear RNaseIII Drosha initiates micro RNA processing. Nature 425:415–419.
154. Gwizdek, C., Ossareh-Nazari, B., Brownawell, A.M., Doglio, A., Bertrand, E., Macara, I.G., and Dargemont, C. 2003. Exportin-5 mediates nuclear export of minihelix-containing RNAs. J Biol Chem 278:5505–5508.
155. Khvorova, A., Reynolds, A., and Jayasena, S.D. 2003. Functional siRNAs and miRNAs exhibit strand bias. Cell 115:209-216.
156. Schwarz, D.S., Hutvagner, G., Du, T., Xu, Z., Aronin, N., and Zamore, P.D. 2003. Asymmetry in the assembly of the RNAi enzyme complex. Cell 115:199-208.
157. Denli, A.M., Tops, B., Plasterk, R.H.A., Ketting, R.F., and Hannon, G.J. 2004.

Processing of primary microRNAs by the microprocessor complex. Nature 432:231-235.
158. Sandy, P., Ventura, A., Jacks, T. 2005. Mammalian RNAi: A practical guide. Biotechniques. 39:215-224.
159. Tuschl, T. 2002. Expanding small RNA interference. Nat Biotechnol 20:446-448.
160. Brummelkamp, T.R., Bernards, R., and Agami, R. 2002. A system for stable expression of short interfering RNAs in mammalian cells. Science 296:550-553.
161. Zheng, L., Liu, J., Batalov, S., Zhou, D., Orth, A., Ding, S., and Schultz, P.G. 2004. An approach to genomewide screens of expressed small interfering RNAs in mammalian cells. Proc Natl Acad Sci USA 101:135-140.
162. Xia, X.G., Zhou, H., Samper, E., Melov, S. and Xu, Z. 2006. Pol II-expressed shRNA knocks down Sod2 gene expression and causes phenotypes of the gene knockout in mice. PLoS Genetics, 2:e10.
163. Chung, K.H., Hart, C.C., Al-Bassam, S., Avery, A., Taylor, J., Patel, P.D., Vojtek, A.B., and Turner, D.L. 2006. Polycistronic RNA polymerase II expression vectors for RNA interference based on BIC/miR-155. Nucleic Acids Res 34(7):e53.
164. Paddison, P.J., Caudy, A.A., Bernstein, E., Hannon, G.J., and Conklin, D.S. 2002. Short hairpin RNAs (shRNAs) induce sequence-specific silencing in mammalian cells. Genes Dev 16:948-958.
165. Pham, C.T.N., Mac Ivor, D.M., Hug, B.A., Heusel, J.W., and Ley, T.J. 1996. Long range distuption of gene expression by a selectable marker cassette. PNAS, 93:13090-13095.
166. Zhang, H., Kolbe, F.A., Jaskiewicz, L. Westhof, E., and Filipowicz, W. (2004) Single Processing Center Models for Human Dicer and Bekterial RNAse III. Cell 118: 57-68.
167. Hammond, S.M., Bernstein, E., Beach, D., and Hannon, G.J. (2000) An RNA-directed nuclease mediates post-transcriptional gene silencing in Drosophila cells. Nature 404:293-296.
168. Sijen, T., Vijn, I., Rebocho, A., van Blokland, R., Roelofs, D., Mol, J.N., Kooter, J.M. 2001. Transcriptional and posttranscriptional gene silencing are mechanistically related. Current Biology 11:436-440.
169. Paule, M.R., and White, R.J. 2000. Survey and summary: transcription by RNA polymerases I and III. Nucleic Acids Res 28:1283-1298.
170. Mc Bride, J.L., Boudreau, R.L., Harper, S.Q., Staber, P.D., Monteys, A.M., Martins, I., Gilmore, B.L., Burstein, H., Peluso, R.W., Polisky, B., Carter, B.J., and Davidson, B.L. 2008. Artificial miRNAs mitigate shRNA-mediated toxicity in the brain, Implications for the therapeutic development of RNAi. PNAS 105:5868-5873.
171. Czauderna, F., Santel, A., Hinz, M., Fechter, M., Direux, B., Fisch, G., Leeders, F., Arnold, W., Giese, K., Klippel, A., and Kaufman, J., 2003. Inducible shRNA expression for application in a prostate cancer mouse model. Nucleic Acid Research, 31(21):10887-10890.
172. Christoph, T., Bahrenberg, G., De Vry, J., Englberger, W., Erdmann, V.A., Frech, M., Kögel, B., Röhl, T., Schiene, K., Schröder, W., Seibler, J., and Kurreck, J.

2008. Investigation of TRPV1 loss-of-function phenotypes in transgenic shRNA expressing and knockout mice. Mol Cell Neurosci 37:579–589.

173. Oberdoerffer, P., Kanellopoulou, C., Heissmeyer, V., Paeper, C., Borowski, C., Aifantis, I., Rao, A., and Rajewsky, K. 2005. Efficiency of RNA interference in the mouse ematopoietic system varies between cell types and developmental stages. Mol Cell. Biol 25:3896-3905.
174. Collins, R.E., and Cheng, X. 2005. Structural domains in RNAi. FEBS Lett 579:5841-5849.
175. Lee, S.K., and Kumar, P. 2009. Conditional RNAi: towards a silent gene therapy. Adv Drug Deliv Rev 61:650-664.
176. Beglopoulos, V., and Shen, J. 2004. Gene-targeting technologies for the study of neurological disorders. Neuromolecular medicine 1:13-30.
177. Birmingham, A., Anderson, E.M., Reynolds, A., Ilsley-Tyree, D., Leake, D., Fedorov, Y., Baskerville, S., Maksimova, E., Robinson, K., Karpilow, J., Marshall, W.S, Khvorova, A. 2006. 3' UTR seed matches, but not overall identity, are associated with RNAi off-targets. Nat Methods 3:199-204.
178. Jackson, A.L., Bartz, S.R., Schelter, J., Kobayashi, S.V., Burchard, J., Mao, M., Li, B., Cavet, G., and Linsley, P.S. 2003. Expression profiling reveals off-target gene regulation by RNAi. Nat Biotechnol 21:635-637.
179. Lin, X., Ruan, X., Anderson, M.G., Mc Dowell, J.A., Kroeger, P.E., Fesik, S.W., and Shen, Y. 2005. siRNA-mediated off-target gene silencing triggered by a 7 nt complementation. Nucleic Acids Res 33:4527-4535.
180. Kleinman, M.E., Yamada, K., Takeda, A., Chandrasekaran, V., Nozaki, M., Baffi, J.Z., Albuquerque, R.J., Yamasaki, S., Itaya, M., Pan, Y., Appukuttan, B., Gibbs, D., Yang, Z., Karikó, K., Ambati, B.K., Wilgus, T.A., DiPietro, L.A., Sakurai, E., Zhang, K., Smith, J.R., Taylor, E.W., and Ambati, J. 2008. Sequence- and target-independent angiogenesis suppression by siRNA via TLR3. Nature 452:591-597.
181. Kittler, R., Pelletier, L., Ma, C., Poser, I., Fischer, S., Hyman, A.A., and Buchholz, F. 2005. RNA interference rescue by bacterial artificial chromosome transgenesis in mammalian tissue culture cells. PNAS, 102(7):2396-2401.
182. Hochman, L., Segev, N., Sternberg, N., and Cohen, G. 1983. Site-specific recombinational circularization of bacteriophage P1 DNA. Virology, 131:11-17.
183. Abremski, K., Hoess, R., and Sternberg, N. 1983. Studies on the properties of P1 site-specific recombination: evidence for topologically unlinked products following recombination. Cell 32:1301-1311.
184. Seibler, J. and Bode, J. 1997. Double-reciprocal crossover mediated by FLP-recombinase: a concept and an assay. Biochemistry 36:1740-1747.
185. Seibler, J., Schübeler, D., Fiering, S., Groudine, M., and Bode, J. 1998. DNA Cassette Exchange in ES Cells Mediated by FLP Recombinase: An Efficient Strategy for Repeated Modification of Tagged Loci by Marker-Free Constructs. Biochemistry 37:6229-6234.

186. Schlake, T., and Bode, J. 1994. Use of mutated FLP recognition target (FRT) sites for the exchange of expression cassettes at defined chromosomal loci. Biochemistry 33:12746-12751.
187. Lauth, M., Sprearco, F., Dethleffsen, K., Meyer, M. 2002. Stable and efficient cassette exchange under non-selectable conditions by combined use of two site-specific recombinases. Nucleic Acids Res 30(21):e115.
188. Osterwalder, M., Galli, A., Rosen, B., Skarnes, W.C., Zeller, R., and Lopez-Rios, J. 2010. Dual RMCE for efficient re-engineering of mouse mutant alleles. Nature methods 8(2):103-4.
189. Zheng, J. M., He, Y., and Fu, J. L. 2001. The study of a HPRT locus-specific transgenic method based on FLP recombinase mediated cassette exchange. Shi yan sheng wu xue bao 34(4):279-282.
190. Sorrell, D.A., Robinson, C.J., Smith, J., and Kolb, A.F. 2010. Recombinase mediated cassette exchange into genomic targets using an adenovirus vector. Nucleic Acids Res 39(16): e107.
191. Turan, S., Kuehle, J., Schambach, A., Baum, C., and Bode, J. 2010 Multiplexing RMCE: Versatile Extensions of the Flp-Recombinase-Mediated Cassette-Exchange Technology. J Mol Biol. 402(1):52-69.
192. Soriano, P. 1999. Generalized lacZ expression with the ROSA26 Cre reporter strain. Nature Genetics 21: 70-71.
193. Muyrers, J.P.P., Zhang, Y., Testa, G., Stewart, A.F. 1999. Rapid modification of bacterial artificial chromosomes by ET-recombination. Nucleic Acids Res 17(6):1555-1557.
194. Chomczynski, P., and Qasba, P.K. 1984. Alkaline transfer of DNA to plastic membrane. Biochem Biophys Res Commun 122:340-344.
195. Schaft, J., Ashery-Padan, R., van der Hoeven, F., Gruss, P., and Stewart, A.F. 2001. Efficient FLP recombination in mouse ES cells and oocytes. Genesis 31:6-10.
196. Hogan, B., Beddington, R., Costantini, F. and Lacey, E. 1994. Manipulating the Mouse Embryo: A Laboratory Manual. CSHL Press.
197. Koch, L., Wunderlich, F.T., Seibler, J., Könner, A.C., Hampel, B., Irlenbusch, S., Brabant, G., Kahn, C.R., Schwenk, F., and Brüning J.C. 2008. Central insulin action regulates peripheral glucose and fat metabolism in mice. J Clin Invest., 118(6):2132-47.
198. McCreath, K.J., Howcroft, J., Champbell, K.H.S., Colman, A., Schnieke, A.E., and Kind, A.J. 2000. Production of gene-targeted sheep by nuclear transfer from cultured somatic cells. Natur 405:1066-1069.
199. Beard, C., Hochedlinger, K., Plath, K., Wutz, A., and Jaenish. R. 2006. Efficient Method to Generate Single-Copy transgenic Mice by Site-Specific Integration in Embryonic Stem Cells. Genesis 44:23-28.
200. Morgan, D., Jarnagin, K., and Roth, R. 1986. Purification and characterization of t he receptor for insulin-like growth factor 1. Biochemistry 25:556-5564.
201. Caro, J.F., J. Poulos, Ittoop, O., Pories, W.J., Flickinger, E.G. and Sinha, M.K. 1988. Insulin-like growth factor I binding in hepatocytes from human liver,

human hepatoma, and normal, regenerating, and fetal rat liver. J Clin Invest 81:976-981.
202. Chung, J.H., Whiteley, M. and Felsenfeld, G. 1993. A 5' element of the chicken P-globin domain serves as an insulator in human erythroid cells and protects against position effect in Drosophilu. Cell 74:505-514.
203. Jägle, U., Gasser, J.A., Müller, M. and Kinzel, B. 2007. Conditional transgene expression mediated by the mouse β-actin locus. Genesis 45:(11)659–666.
204. Palais, G., Nguyen Dinh Cat, A., Friedman, H., Panek-Huet, N., Millet, A., Tronche, F., Gellen, B., Mercadier, J.J., Peterson, A. and Jaisser, F. 2009. Targeted transgenesis at the HPRT locus: an efficient strategy to achieve tightly controlled in vivo conditional expression with the tet system. Physiol Genomics 37(2):140-6.
205. Turan, S., Kuehle, J., Schambach, A., Baum, C. and Bode, J. 2010. Multiplexing RMCE: Versatile Extensions of the Flp-Recombinase-Mediated Cassette-Exchange Technology. J Mol Biol 10:(1)52-69.
206. Anderson, J. and Akkina, R. 2005. HIV-1 resistance conferred by siRNA cosuppression of CXCR4 and CCR5 coreceptors by a bispecific lentiviral vector. AIDS Res Ther 2(1):1.
207. Hinton, T.M. and Doran, T.J. 2008. Inhibition of chicken anaemia virus replication using multiple short-hairpin RNAs. Antiviral Res 80(2):143-149.
208. terBrake, O., tHooft, K., Liu, Y.P., Centlivre, M., von Eije, K.J. and Berkhout, B. 2008. Lentiviral vector design for multiple shRNA expression and durable HIV-1 inhibition. Mol Ther 16(3):557-564.
209. Caro, J.F., Sinha, M.K., Raju, S.M., Ittoop, O., Pories, W.J., Flickinger, E.G., Meelheim, D. and Dohm, G.L. 1987. Insulin receptor kinase in human skeletal muscle from obese subjects with and without non-insulin dependent diabetes. J Clin Invest 79(5):1330-7.
210. Caro, J.F., Ittoop, O., Pories, W.J., Meelheim, D., Flickinger, E.G. , Thomas, F., Jenquin M., Silverman, J.F., Khazanie, P.G. and Sinha, M.K. 1986 Studies on the mechanism of insulin resistance in the liver from humans with non-insulin-dependent diabetes. Insulin action and binding in isolated hepatocytes, insulin receptor structure, and kinase activity. J Clin Invest 78(1):249–258.
211. Kashiwagi, A., Verso, M.A., Andrews, J., Vasquez, B., Reaven, G. and Foley, J.E. 1983. In vitro insulin resistance of human adipocytes isolated from subjects with non-insulin-dependent diabetes mellitus. J Clin Invest 72(4):1246–1254.
212. Nolan, J.J., Friedenberg, G., Henry, R., Reichart, D. and Olefsky J. M. 1994. Role of human skeletal muscle insulin receptor kinase in the in vivo insulin resistance of noninsulin-dependent diabetes and obesity. J Clin Endocrinol Metab 78(2):471-7.
213. Cusi, K., Maezono, K., Osman, A., Pendergrass, M., Patti, M.E., Pratipanawatr, T., DeFronzo, R.A., Kahn, C.R., and Mandarino, L.J. 2000. Insulin resistance differentially affects the PI 3-kinase and MAP kinase-mediated signaling in human muscle. J Clin Invest 105(3):311-20.

214. Plum, L., Wunderlich, F.T., Baudler, S., Krone, W. And Brüning, J,C. 2005. Transgenic and knockout mice in diabetes research: novel insights into pathophysiology, limitations, and perspectives. Physiology 20:152-61.
215. Kulkarni, R.N., Holzenberger, M., Shih, D.Q., Ozcan, U., Stoffel, M., Magnuson, M.A. and Kahn, C.R. 2002. β-Cell-specific deletion of the Igf1 receptor leads to hyperinsulinemia and glucose intolerance but does not alter β-cell mass. Nat Genet 31: 111–115.
216. Xuan, S., Kitamura, T., Nakae, J., Politi, K., Kido, Y., Fisher, P.E., Morroni, M., Cinti, S., White, M.F., Herrera, P.L., Accili, D. and Efstratiadis, A. 2002. Defective insulin secretion in pancreatic beta cells lacking type 1 IGF receptor. J Clin Invest 110(7):1011-9.
217. Da Silva Xavier, G., Qian, Q., Cullen, P.J. and Rutter, G.A. 2004. Distinct roles for insulin and insulin-like growth factor-1 receptors in pancreatic beta-cell glucose sensing revealed by RNA silencing. Biochem J 377(1):149-58.
218. Koch, L., Wunderlich, F.T., Seibler, J., Könner, A.C., Hampel, B., Irlenbusch, S., Brabant, G., Kahn, C.R., Schwenk, F. and Brüning, J.C. 2008. Central insulin action regulates peripheral glucose and fat metabolism in mice. J Clin Invest 118(6):2132-47.
219. Klöting, N., Koch, L., Wunderlich, T., Kern, M., Ruschke, K., Krone, W., Brüning, J.C. and Blüher, M. 2008. Autocrine IGF-1 action in adipocytes controls systemic IGF-1 concentrations and growth. Diabetes. 57(8):2074-82.
220. Kappeler, L., De Magalhaes Filho, C., Dupont, J., Leneuve, P., Cervera, P., Périn, L., Loudes, C., Blaise, A., Klein, R., Epelbaum, J., Le Bouc, Y., Holzenberger, M. 2008. Brain IGF-1 receptors control mammalian growth and lifespan through a neuroendocrine mechanism. PLoS Biol 28;6(10):e254.
221. Berryman, D.E., List, E.O., Coschigano, K.T., Behar, K., Kim, J.K. and Kopchick, J.J. 2004. Comparing adiposity profiles in three mouse models with altered GH signaling. Growth Hormone and IGF Research 14: 309–318.
222. Meyer, C.W., Korthaus, D., Jagla, W., Cornali, E., Grosse, J., Fuchs, H., Klingenspor, M., Roemheld, S., Tschöp, M., Heldmaier, G., De Angelis, M.H. and Nehls, M. 2004. A novel missense mutation in the mouse growth hormone gene causes semidominant dwarfism, hyperghrelinemia, and obesity. Endocrinology 145:2531–2541.
223. Berryman, D.E., List, E.O., Kohn, D.T., Coschigano, K.T., Seeley, R.J. and Kopchick, J.J. 2006. Effect of growth hormone on susceptibility to diet-induced obesity. Endocrinology 147:2801–2808.
224. Todd, B.J., Fraley, G.S., Peck, A.C., Schwartz, G.J. and Etgen, A.M. 2007. Central insulin-like growth factor 1 receptors play distinct roles in the control of reproduction, food intake, and body weight in female rats. Biol Reprod 77(3):492-503.
225. Schwartz, M.W., Seeley, R.J., Campfield, L.A., Burn, P. and Baskin, D.G. 1996. Identification of targets of leptin action in rat hypothalamus. J Clin Invest 98: 1101-1106.

226. Sahu, A. 1998. Evidence suggesting that galanin (GAL), melanin-concentrating hormone (MCH), neurotensin (NT), proopiomelanocortin (POMC) and neuropeptide Y (NPY) are targets of leptin signaling in the hypothalamus. Endocrinology 139: 795-798.
227. Lopez, M., Seoane, L., Garcia, M.C., Lago, F., Casanueva, F.F., Senaris, R. and Dieguez, C. 2000. Leptin regulation of prepro-orexin and orexin receptor mRNA levels in the hypothalamus. Biochem Bio phys Res Commun 269:41-45.
228. Meister, B. (2000) Control of food intake via leptin receptors in the hypothalamus. Vitam Horm 59: 265-304.
229. Arvaniti, K., Huang, Q. and Richard, D. 2001. Effects of leptin and corticosterone on the expression of corticotropin-releasing hormone, agouti-related protein, and proopiomelanocortin in the brain of ob/ob mouse. Neuroendocrinology 73: 227-236.
230. Kumano, S., Matsumoto, H., Takatsu, Y., Noguchi, J., Kitada, C. and Ohtaki, T. 2003. Changes in hypothalamic expression levels of galanin-like peptide in rat and mouse models support that it is a leptin-target peptide. Endocrinology 144: 2634–2643.
231. Shillabeer, G., S. Vydelingum, G. Hatch, J. C. Russell, and D. C. Lau. 1998. Long-term regulation of leptin expression is correlated with adipocyte number in obese rats. Clin. Investig. Med. 21:54-62.
232. Couillard, C., Gagnon, J., Bergeron, J., Leon, A.S., Rao, D.C., Skinner, J.S., Wilmore, J.H., Despres, J.P. and Bouchard C. 2000. Contribution of body fatness and adipose tissue distribution to the age variation in plasma steroid hormone concentrations in men: the Heritage Family Study. J Clin Endocrinol Metab 85:1026-1031.
233. Guo, K. Y., P. Halo, R. L. Leibel, and Y. Zhang. *2004*. Effects of obesity on the relationship of leptin mRNA expression and adipocyte size in anatomically distinct fat depots in mice. Am. J. Physiol. Regul. Integr. Comp. Physiol. 287:112119.
234. Balthasar, N., Coppari, R., McMinn, J., Liu, S.M., Lee, C.E., Tang, V., Kenny C.D., McGovern R.A., Chua, S.C.Jr., Elmquist, J.K. and Lowell, B.B. 2004. Leptin receptor signaling in POMC neurons is required for normal body weight homeostasis. Neuron. 42:983–991.
235. Dhillon, H., Zigman, J.M., Ye, C., Lee, C.E. McGovern, R.A., Tang, V., Kenny, C.D., Christiansen, L.M., White, R.D., Edelstein, E.A., Coppari, R., Balthasar, N., Cowley, M.A., Chua, S. Jr., Elmquist, J.K. and Lowell, B.B. 2006. Leptin directly activates SF1 neurons in the VMH, and this action by leptin is required for normal body-weight homeostasis. Neuron 49:191–203.
236. Grill, H.J. 2010. Leptin and the systems neuroscience of meal size control. Front. Neuroendocrinol. 31:61–78.
237. Huo, L.,Maeng, L., Bjorbaek, C. and Grill, H.J. 2007. Leptin and the control of food intake: neurons in the nucleus of the solitary tract are activated by both gastric distension and leptin. Endocrinology 148:2189–2197.

238. Hayes, M.R., Skibicka, K.P., Bence, K.K., and Grill, H.J. 2009. Dorsa hindbrain 50-adenosine monophosphate-activated protein kinase as an intracellular mediator of energy balance. Endocrinology 150:2175–2182.
239. Bokov, A.F., Garg, N., Ikeno, Y., Thakur, S., Musi, N., DeFronzo, R.A., Zhang, N., Erickson, R.C., Gelfond, J., Hubbard, G.B., Adamo, M.L., Richardson, A. 2011. Does reduced IGF-1R signaling in Igf1r+/- mice alter aging? PLoS One 6(11):e26891.
240. Holzenberger, M., Dupont, J., Ducos, B., Leneuve, P., Géloën, A., Even, P.C., Cervera, P. and Le Bouc, Y. 2003. IGF-1 receptor regulates lifespan and resistance to oxidative stress in mice. Nature 421(6919):182-7.
241. Steil, G.M., Trivedi, N., Jonas, J.C., Hasenkamp, W.M., Sharma, A., Bonner-Weir, S. and Weir, G.C. 2001. Adaptation of beta-cell mass to substrate oversupply: enhanced function with normal gene expression. Am J Physiol Endocrinol Metab 280:788–796.
242. Jetton, T.L., Lausier, J., LaRock, K., Trotman, W.E., Larmie, B., Habibovic, A., Peshavaria, M., Leahy, J.L. 2005. Mechanisms of compensatory beta-cell growth in insulin-resistant rats: roles of Akt kinase. Diabetes 54:2294–2304.
243. Liu, Y.Q., Jetton, T.L., and Leahy, J.L. 2002. Beta-cell adaptation to insulin resistance. Increased pyruvate carboxylase and malate-pyruvate shuttle activity in islets of nondiabetic Zucker fatty rats. J Biol Chem 277:39163–39168.
244. Chen, C., Hosokawa, H., Bumbalo, L.M., and Leahy, J.L. 1994. Mechanism of compensatory hyperinsulinemia in normoglycemic insulin-resistant spontaneously hypertensive rats. Augmented enzymatic activity of glucokinase in b-cells. J Clin Invest 94:399–404.

8 Acknowledgements

Die Durchführung dieser Arbeit erfolgte in einer Forschungskooperation zwischen der Universität zu Köln (AG Prof. Dr. Jens Brüning) und der TaconicArtemis GmbH in Köln.
Mein Dank geht an Prof. Dr. Jens Brüning für seine Unterstützung und Diskussionsbereitschaft bei dieser Arbeit. Prof. Dr. Frieder Schwenk und Dr. Jost Seibler danke ich für die Möglichkeit an diesem interessanten Thema zu arbeiten und ihrer ständigen Hilfestellung und Diskussionsbereitschaft.
Ich möchte Prof. Peter Kloppenburg, Prof. Thomas Wunderlich und Dr. Ursula Lichtenberg dafür danken, dass sie sich dazu bereit erklärt haben, mein Prüfungskomitee zu bilden.
Bei Dr. Jan Mauer möchte ich mich für seine Hilfe und Unterstützung bei der Durchführung der Phänotypisierungsexperimente bedanken.
Mein besonderer Dank gilt meinen Kollegen Sonja Ortmann, Simone Janzen und Martina Reiss, für eine einmalige und unterhaltsame Laborzeit. Allen weiteren Mitarbeitern der Firma TaconicArtemis, insbesondere der Tierhaltung sowie der Zellkultur, die zum Gelingen dieser Arbeit beigetragen haben, danke ich für ihre Unterstützung.
Danke an Dr. Jost Seibler und Dr. Jan Mauer für ihre exzellente Korrekturarbeit.

9 Erklärung

Ich versichere, daß ich die von mir vorgelegte Dissertation selbständig angefertigt, die benutzten Quellen und Hilfsmittel vollständig angegeben und die Stellen der Arbeit einschließlich Tabellen, Karten und Abbildungen, die anderen Werken im Wortlaut oder dem Sinn nach entnommen sind, in jedem Einzelfall als Entlehnung kenntlich gemacht habe; dass diese Dissertation noch keiner anderen Fakultät oder Universität zur Prüfung vorgelegen hat; dass sie – abgesehen von unten angegebenen Teilpublikationen – noch nicht veröffentlicht worden ist sowie, dass ich eine solche Veröffentlichung vor Abschluß des Promotionsverfahren nicht vornehmen werde. Die Bestimmungen dieser Promotionsordnung sind mir bekannt. Die von mir vorgelegte Dissertation ist von Prof. Dr. Jens C. Brüning betreut worden.

Köln, März 2012 Fabian Schütte